STRUCTURE AND GROWTH OF ANISOTROPIC METAL COLLOIDS

By

CHARLES MARTIN LOFTON

A DISSERTATION PRESENTED TO THE GRADUATE SCHOOL
OF THE UNIVERSITY OF FLORIDA IN PARTIAL FULFILLMENT
OF THE REQUIREMENTS FOR THE DEGREE OF
DOCTOR OF PHILOSOPHY

UNIVERSITY OF FLORIDA

2003

TABLE OF CONTENTS

page

LIST OF FIGURES

Abstract of Dissertation Presented to the Graduate School
of the University of Florida in Partial Fulfillment of the
Requirements for the Degree of Doctor of Philosophy

STRUCTURE AND GROWTH OF ANISOTROPIC METAL COLLOIDS

By

Charles Martin Lofton

December 2003

Chair: Wolfgang Sigmund
Major Department: Materials Science and Engineering

The synthesis of noble metal colloids is of importance to a number of technological applications, most often taking advantage of the optical properties of these materials. The size and shape of metal colloids dominate their optical absorbance and non-linear optical properties. Of particular interest for several applications are anisotropic particles such as platelets and rods. These particles have been reported in literature for approximately seventy years using a wide variety of synthesis techniques, although the reproducibility and yield of these schemes are low. Furthermore, the mechanistic explanations for these techniques are inadequate to explain the appearance of similar structure in different reaction environments. In this dissertation, several synthesis techniques from the literature, along with modified and original techniques, were used to synthesize anisotropic colloids of copper, silver and gold. The particles were characterized using scanning and transmission electron microscopy to determine their crystal habit and internal crystallographic structure. It was found that similar structures were observed to be synthesized in different schemes. These similarities were used to

make a mechanistic description that did not depend on a unique reaction environment. Two dimensional particles in the shape of triangular or hexagonal prisms were found to have a constant (111) main face and contained one or more twin planes parallel to this face. The anisotropy of these particles was attributed to the formation of reentrant grooves, sites of preferential metal adatom attachment where a twin plane intersects two surface planes. One dimensional particles in the form of rods or wires were also observed in multiple schemes, and had a consistent pentagonal cross-section. The internal structure of these particles was found to consist of five crystal variants bounded by five (111) type twin planes along a [110] direction. It is proposed that this structural arrangement creates a radial stress which restricts the growth of the particle perpendicular to the axis. In order to relieve this stress, edge dislocations form, emerging at the end faces and creating self-perpetuating steps that accelerate axial growth. Other particle types, such as ribbons, tetrahedra and decahedra, were also characterized and their growth was described using the mechanisms developed for the prism and rods.

CHAPTER 1
INTRODUCTION

Properties and Applications of Transition Metal Nanoparticles

The fabrication of noble metal nanoparticles has at least a 2000 year history, starting as far back as the Roman cassian purple dye made from gold nanoparticles, while the scientific investigation of these particles goes back to Faraday in the nineteenth century. The most distinguishing feature of metal colloids are their optical properties, which, unlike in bulk metal, are dominated by surface plasmon absorption. This optical phenomenon, producing the strong color of cassian purple, is a result of the distinct conduction bands in the metal nanoparticle. Unlike the continuous conduction bands in bulk metals, the restricted size of electronic oscillations in metal nanoparticles produces distinct electronic transitions. These electronic transitions lie in the ultraviolet (UV)-visible range for some metals, including copper, silver and gold, leading to distinct colors. The electronic transitions can be altered by the particle size, shape, the dielectric medium surrounding the particle and the presence of any species that can complex with the surface. The single absorption band of silver nanoparticles splits into a transverse and longitudinal band when the shape is rod-like [1]. Silver spheres have a strong yellow color, while triangular prisms have a green color [2]. Surface plasmon adsorption for silver and gold is far more intense and stable than the absorption of any organic dye. While organic dyes are bleached over time due to oxidation, metal nanoparticles do not undergo degradation with exposure to light. In addition, metal nanoparticles have been found in certain instances to have non-linear optical properties, a change in the refractive

index with the intensity of incident light. Anisotropic nanoparticles appear to have this property on a more pronounced scale, possibly due to the splitting of electronic oscillations along different axes.

Numerous applications of metal nanoparticles take advantage of their optical properties. Most employ gold and silver, due to their ease of fabrication and high chemical stability against oxidation. In surface enhanced Raman scattering (SERS), the strong plasmon absorption is used to enhance the Raman signal of organic molecules on a metal surface by an order of $10^{14} – 10^{15}$ [3]. This allows the nature and amount of organic molecules to be determined at concentrations far below normal detection limits, even to the point of single molecule detection [3]. Gold nanoparticles strongly bond to deoxyribonucleic acid (DNA), which provides colloidal stability through electric double-layer repulsion. When gold colloids of a few nanometers diameter are made with specific single strands of DNA, they act as highly reliable assays for DNA identification: only the conjugate DNA to that on the particle will bind to the surface, leading to a reduction in the electric double layer stabilizing the particle suspension. The agglomeration of the colloids into larger aggregates causes a size-dependant shift in the plasmon absorption that changes the assay color from red to blue. The ability of gold to absorb specific molecules on its surface allows for nanoparticles injected into tissue to accumulate in certain regions that contain conjugate molecules. This technique has been used in biological transmission electron microscopy (TEM) sample preparation to identify the location of molecules in cells. The binding of nanoparticle to tissue can be used on a larger scale to identify the location of cancerous tumors or other diseases through their distinct optical absorption. The localization of the nanoparticles can also be used to

adsorb UV light, leading to local heating of the tissue to kill cancerous growth with minimal damage to surrounding tissue. The binding of gold nanoparticles to photoactive or fluorophore molecules such as pyrene renders the hybrid particle suitable for light-harvesting and optoelectronic applications with efficiencies far in excess of organic dyes [3]. Metal nanoparticles can enhance light induced charge separation by forming favorable heterojunctions with optically active molecules and semiconductors, forming Schottky barriers that allow the metal to act as an electron sink that prevents electron/hole recombination [4]. These heterojunctions are important for enhancing efficiency in solar cells and photocatalytic devices based on semiconducting oxides. The non-linear optical properties hold interest for their potential application in optical limiting devices. These devices use the change in refractive index that occurs at higher intensities to direct or block light. Optical limiting will be essential for optical computing and for protecting sensitive equipment from damaging light pulses.

Metal nanoparticles have numerous current and potential applications besides optical applications. They are used as catalysts for numerous organic reactions, the efficiency of which is generally controlled not only by the surface area of the metal but by particular crystal faces present on the surface. Platinum nanoparticles, as well as other noble metals, attached to inert alumina substrates are widely used for catalyses of hydrocarbons. Metal nanoparticles, particularly highly anisotropic particles, have been used as building blocks for very small scale electronic devices fabricated with laboratory techniques such as atomic force microscopy (AFM).

Synthesis of Transition Metal Nanoparticles

Many of the transition metals have been synthesized as colloids, although the oxidative instability of most metals has restricted their usefulness. The nobler face

centered cubic (FCC) metals, nickel, palladium, platinum, copper, silver and gold, dominate in literature and applications due to their stability and low reduction potential. Numerous means exist for making metal colloids, most of which involve the reduction of a metal cation in a solvent to a neutral metal species in the presence of some surface active organic molecule such as a binding ligand or a polymer [5]. The neutral metal species generally has a very low solubility, and when the concentration exceeds the solubility limit, the metal atoms rapidly aggregate into particle nuclei. After the agglomeration of the initial atoms into nuclei, the surface agent adsorbs to the surface of the metal, through either a metal-ligand interaction, such as the strong attachment of a thiol to gold through the metal-sulfur bond, or through physical adsorption caused by entropic effects in large molecules. These compounds prevent adhesion between two free metal surfaces through steric or electrostatic repulsion. Depending on the nature of the surface active agent, additional adatoms of neutral metal may or may not be able to attach to the particle, allowing the size of the particles to be controlled. The nature of the molecular monolayer also controls the ability of the particles to be dispersed in a particular solvent. Through the controlled nucleation and growth of the metal colloids, the size and size-distribution of the particles can be controlled.

Although crystals are expected to form into Wulff shapes due to surface energy minimization, anisotropic crystals have been observed in many metals and through many synthesis techniques [6]. In fact, highly anisotropic prisms and wires have been produced, generating speculation on the mechanism of their growth [2, 7-11]. Clearly, wires of one hundred to one aspect ratio are not thermodynamically the most stable structures, but their fabrication indicates that there was some local thermodynamic or

kinetic phenomenon arising that facilitates their formation. Understanding the nature of this mechanism is the purpose of this dissertation.

A number of explanations for the formation of these anisotropic particles have been put forward in the literature, but no rigorous models have been described. The explanations presented are generally empirical and restricted to explaining the results of a single synthesis technique. The explanations tend to fall into two general categories, which will be referred to as the "crystal face poisoning" and "physical restriction" explanations. In the crystal face poisoning model, the anisotropic shapes are explained by the adsorbing organic monolayer energetically affecting different crystal faces to different degrees [12, 13]. This alteration in the energy of the different faces expresses itself through preferential attachment of metal adatoms to certain faces during growth, altering the crystal habit of the particles into anisotropic shapes [14]. In addition, the variable strength of organic binding to different crystal faces could alter the rate of adatom attachment by blocking diffusion to the surface. These postulates have been used to explain the observation that particles of a particular shape in a given synthesis technique all appear to have the same crystallographic orientation, with the same crystal faces making up the particle surface. This type of explanation has proven successful in numerous other systems, such as the precipitation of organic molecules, oxides, phosphates and carbonates, and semiconductors from aqueous solutions. In these cases, the presence of small amounts of surface active molecules or ions has had a dramatic effect on crystal habit, including creating anisotropic shapes.

The problem with using this explanation for noble metal colloids lies in the symmetry of the FCC metal system. Anisotropic crystal growth in systems with high

complexity and low crystal symmetry is more easily explained than a single component crystal with a high symmetry. For an FCC crystal, the major crystal faces, {100}, {110} and {111}, have different surface energies that lead to predictable crystal habits. The domination of the {111} faces will lead to an octahedraon, while the {110} faces produce a rhombic dodecahedron and the {100} faces produce a cube. Intermediate crystal shapes can result from two types of faces being present. In the case of the surface energy of the faces being altered by an adsorbing species, the crystal can change in shape but will remain isotropic. Only the presence of some symmetry breaking defect can disrupt the symmetry enough to yield anisotropic growth. Although defects such as twin planes have been reported in the literature for anisotropic noble metal crystals, no attempt has yet been made to link their presence with the anisotropic growth. Furthermore, no studies have been performed on the strengths of adsorption of molecules to different faces or their effect on surface energy or diffusion of metal adatoms. Together, this makes the crystal face poisoning explanation questionable.

The second explanation that appears in literature is referred to here as the "physical restriction" explanation. In some of the synthesis methods for copper, silver and gold rods, cationic surfactants such as a tetraalkyl ammonium compounds or anionic surfactants such as Aerosol OT (AOT) are used as the surface active agent to prevent colloid agglomeration [8-11]. These surfactants can form liquid crystals in aqueous solutions at high concentrations, including rod-like micelles at the concentrations used in metal rod synthesis. The rod-shaped micelles have been linked to the formation of the rod-shaped particles by means of creating a physical template in which the adatoms can attach to a nucleus. This mechanism is purely speculative and has not been substantiated

by any evidence. For a number of reasons it is difficult to imagine that it could occur. The domain size and stability of the rod-shaped micelles are very limited. These micelles are constantly breaking and reforming on a time scale shorter than the growth time of the particles and on a length scale smaller than the length of the rods. The residence time for the commonly used cetyl triammonium bromide (CTAB) is on the order of hundreds of microseconds, while these particles form over seconds to minutes [15]. The metal rods are approximately 5 times larger in diameter than the micelles and it is unlikely that the micelles could stretch to accommodate the particles. Finally, evidence points to the surfactant head groups attaching to the surface of the metal, but these groups would be oriented towards the outside of a micelle and not the inside. These factors make this mechanism unreasonable.

An additional observation of metal nanoparticle growth is that every synthesis method reported for anisotropic colloids produces a mixture of particle shapes, including a wide variety of spherical or isotropic shapes. Many of these synthesis methods involve stirred and homogeneous reaction environments in which nucleation is a rapid and singular event. In addition, different particle shapes have been characterized as having the same crystal faces in nearly the same ratios. The diverse mixture of particle shapes in a highly uniform synthesis system leads to the question of why these different types of particles appear together if one shape is favored. If the local reaction environment was determining particle growth, one would expect uniformity of crystal habit with a uniform reaction environment. The presence of identical particle shapes and crystal habits in different reaction schemes with different solvents, metal salts, capping agents and

temperatures makes the reliance on the reaction environment to explain shape difficult to believe.

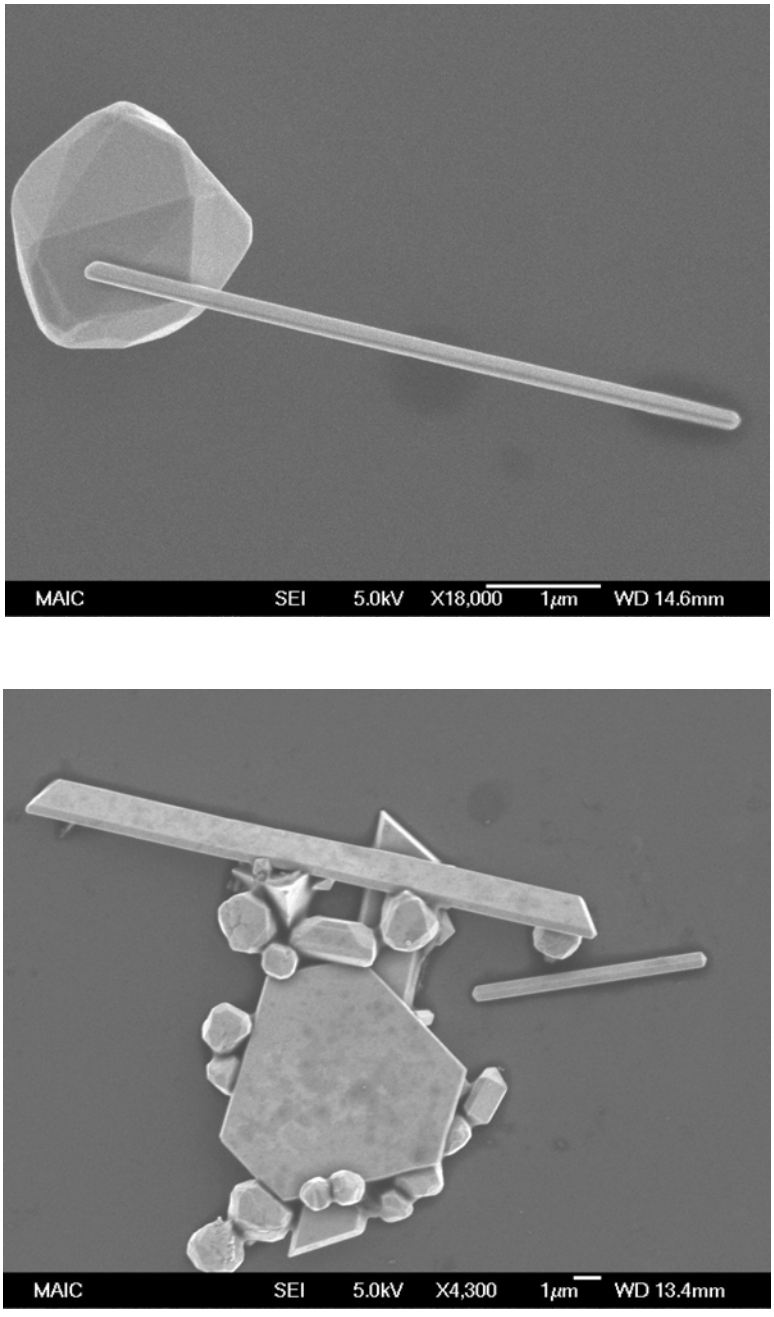

Figure 1-1: Examples of different colloid morphologies formed simultaneously in a well homogenized reaction. On top is an isotropic gold particle formed with a high aspect ratio wire. On the bottom is a mixture of one rod, two ribbons, a truncated hexagonal platelet, a tetrahedron and numerous other isotropic particles with various degrees of faceting.

The expectation would be that different chemical conditions would favor different crystal faces, and that the particle shapes would vary accordingly. The commonalities in morphologies and ratios of crystal facets, however, are difficult to ignore. Instead of the reaction environment, the nature of the nucleation event generally appears to determine the final product. Because no effort has been given towards explaining metal colloid growth across crystal systems and synthesis methods, this report will compare a number of common systems and attempt to draw conclusions on a growth mechanism that could explain them all.

Purpose and Thesis

While numerous papers have described the synthesis of anisotropic noble metal colloids and many of them have offered explanations on growth mechanisms, no attempt has been made to link the similarities in colloid structure across synthesis methods. If such similarities in the structure of the colloids exist for different synthesis methods, a common growth mechanism should be considered. The primary purpose of this research was to use a variety of both previously used and original synthesis methods to produce anisotropic metal colloids and to obtain structural data through microscopy to evaluate similarities in the crystal habits across these synthesis schemes. Furthermore, the structural data obtained were used to develop a common growth model for the colloids. The author will demonstrate in this dissertation that the diverse synthesis methods did produce structurally similar colloids. The author will also propose a growth model in which the presence of twin planes in the colloids determines the morphology of metal colloids. During the nucleation of metal nanoparticles or shortly afterwards, twin planes will form in a certain percentage of particles. These twin planes create reentrant grooves, sites of kinetic advantage for the addition of adatoms, which leads to rapid growth of the

particle parallel to these planes in the presence of a supply of reduced metal atoms. Furthermore, the number and relative orientation of these twins determine the final shape of the particle as a rod, platelet, tetrahedra, decahedra, ribbon or cube. Furthermore, in an environment where metal dissolution and reattachment can cause particle ripening, the kinetic advantage offered by twin planes to certain particles can lead to increased uniformity of particle shape and size. This method can be used to produce high yields of nanoparticles by creating a competitive growth stage where only particles of a certain shape will survive. The increased understanding of metal colloid formation will allow for superior control over particle shape and synthesis reproducibility.

CHAPTER 2
LITERATURE REVIEW

Review of Crystal Habit and Anisotropic Growth

The factors that govern the shape of growing crystals are numerous, interdependent in complex and difficult to separate ways, and often impossible to observe directly. As such, scientific attempts to describe and predict crystal growth by combining elementary principles often meet with difficulty. Factors such as natural and forced convection, solute partitioning, and the effects of thermal, compositional and mechanical stresses can all contribute to the size, shape, and growth rate of a crystal. Often times numerous assumptions have to be made and certain factors have to be entirely ignored to simplify the problem to a reasonable level. This, however, does not stop the application of elementary principles and theoretical models to new systems. In this report, a series of compositionally similar systems with similar crystal habits formed by widely differing synthesis methods will be considered. In this chapter, the explanations offered by other scientists making these particle systems will be presented, as well as other data and models considered relevant. This will lay a basis for comparison to the data presented in this report.

The nucleation and growth of crystals have been studied for more than a thousand years, with Geber (720-813) first mentioning the purification of salts by recrystallization [16]. Much of what is currently known of crystallization was recognized on an empirical level by the chemists and alchemists of the Renaissance, including separation, purification and the ability to control crystal habit. The scientific revolution led to the

advancement of the understanding of crystallization through more quantitative methods in the 19th century. Wilhelm Ostwald is widely recognized for creating many of the terms and concepts currently used in this field. Among them are the concepts of supersolubility and critical nucleus size, the Law of Stages, his interpretation of Liesegang rings and the relationship between particle size and solubility [16]. The concepts of supersolubility and critical nucleus size were systematic representations of older, but less generalized, observations. Ostwald recognized that the driving force for nucleation and growth related to the degree to which a solution was cooled or concentrated beyond its solubility limit. He furthermore recognized that a critical size of nucleus was necessary before the new phase was stable. In the Law of Stages, he described metastability by pointing out that an unstable system does not transform to the most stable state, but to a state most resembling its own, the state that requires the smallest loss of free energy. Another way of saying this is that systems tend to go through intermediate substances or allotropic forms on their way to the most stable form. Liesegang discovered in 1896 that rings appeared in crystals of silver nitrate when silver chromate was added in small amounts. Ostwald interpreted this by recognizing the importance of diffusion kinetics and the possibility of local supersaturation of individual phases. He reasoned that a supersaturated solution of silver chromate was formed in the advancing wave front of the counter-diffusing ions during silver nitrate crystallization. The silver chromate reached the supersolubility limit and precipitated until saturation was attained. The process repeated itself periodically as the reacting ions were replenished and the wave front became enriched by silver nitrate precipitation. The relationship between particle size and solubility explains Ostwald ripening. This describes the greater

stability of larger particles with lower curvature and the growth of large particles at the expense of smaller ones.

The mechanisms of crystal growth have received much attention and description since Ostwald, including the Gibbs-Curie thermodynamic criterion of the equilibrium form of crystals, the Bravais-Donnay-Harker law of the relationship between the faces of a crystal and the Nernst-Noyes-Whitney theory of the rate of heterogeneous reactions [16]. Essential to these descriptions was the recognition that crystals will try to lower their surface energy by presenting faces with the lowest energy and that growth is expected to occur on the faces with the highest reticular density where attaching species can make the greatest attachment to the crystal. Due to this, crystals develop with the slowest growing planes as the preferred habit. Because the faces with the highest growth rates are bound on each side by slower growth faces, they grow themselves out of existence, leaving only slow growing faces. According to the Wulff-Curie rule, the equilibrium habit of a crystal contains the closest packed crystallographic planes with small Miller indices. This leads to so called Wulff shapes and the Wulff construction. Wulff represented the growth of crystals geometrically, relating the shape of a crystal to the specific surface energy [6]. From this proceeds certain crystal shapes that are common to specific crystal structures. These include cubes, octahedron and rhombic dodecahedron for {100}, {111} and {110} dominant planes, respectively. La Mer and others contributed to the kinetics of crystal nucleation and growth as summarized in reference 6. La Mer and Dinegar described the growth of monodisperse particles by dividing their formation into three stages [17]. In stage one, the supersaturation of a system is increased until a critical concentration, c_N, is reached where nucleation is

extremely rapid. In stage two, the precipitation of particles reduces the supersaturation below a point, c_O, where further nucleation is unlikely. In stage three, the growth on the existing nuclei continues until the concentration is reduced to the equilibrium solubility. This allows for the size and size distribution of crystals to be controlled by controlling the length of the nucleation step.

The growth of crystals has been divided into three main types: continuous growth, nucleation-mediated growth and spiral growth [18]. In continuous growth, the surface of the crystal is rough and every site is a possible growth site and is equivalent to the others in the attachment and detachment of molecules. A more widely observed mode of growth is the nucleation mediated mode, in which the surface is molecularly flat and different sites have different likelihoods of the addition or detachment of molecules. This mode recognizes that an attaching molecule increases in stability with a greater number of nearest neighbors. Sites such as edges and kinks in the surface have greater stability, and thus an attaching molecule is less likely to detach. The exhaustion of these surface sites leads to a molecularly smooth surface where attachment of molecules is unfavorable. This will arrest the growth of the surface until a nucleating layer of a critical size forms on the surface. The rate of the formation of these two-dimensional nuclei is critical to the overall rate of crystal growth. In the third mode, spiral growth, the presence of screw dislocations controls the rate of growth. Dislocations such as screw dislocation create self-perpetuating steps that are not exhausted. This avoids the necessity of nucleating a new molecular layer after each layer meets a bounding surface. Ming has identified two other mechanisms for the formation of self-perpetuating grow steps: edge dislocations emerge at crystal surfaces producing a step on all planes except

those belonging to the zone of the Burgers vector of the dislocation [19]. Stacking faults, like those formed by twin planes in cubic structures, form sub-steps on surfaces they intercept [20,21]. A single stacking fault creates a sub-step with one third the height of a molecular plane, while two parallel faults create a sub-step with two thirds the height of a molecular plane. Monte-Carlo simulations demonstrate that these provided additional stabilizing energy to an attaching molecule. A molecule adsorbing to a full step has five nearest neighbors in a FCC structure, while a molecule only has three nearest neighbors. A molecule on a sub-step has four nearest neighbors, making attachment and retention more favorable. An additional mechanism for the acceleration of crystal growth, known as reentrant grooves, will be described in the next section.

Twin Plane Growth Mechanism in Silver Halide Crystals

Twin planes can affect the growth of crystals by the formation of reentrant grooves. At such a site, the twin causes two surface planes to form an obtuse angle where the number of nearest neighbors for an adsorbing molecule is increased. Berriman and Herz were the first to suggest that twin planes could explain the formation of tabular or plate-like silver halide particles in spite of the uniform growth environment and highly symmetric sodium chloride type crystal structure [22]. They observed that identical growth conditions could produce either isotropic particles or tabular particles depending on the method of nucleation. Silver bromide tabular particles were observed in the TEM, and evidence of twin planes parallel to the main crystal face was found. Hamilton and Brady expanded this work and speculated that the crystal growth was almost non-existent at low levels of supersaturation on defect-free crystals [23]. They recognized that the large size and high aspect ratio of some of the particles arise from a factor accelerating the nucleation of atomic layers. Using an explanation derived from Hamilton and

Seidensticker's work [24] on germanium dendrites grown in supercooled germanium melts, they proposed that if a new (111) layer nucleates with a stacking fault, a twin plane will expand over the crystal surface. The intersection of this internal twin plan with a {111} face can be at a 70.5 ^{o} or 109.5^{o} angle.

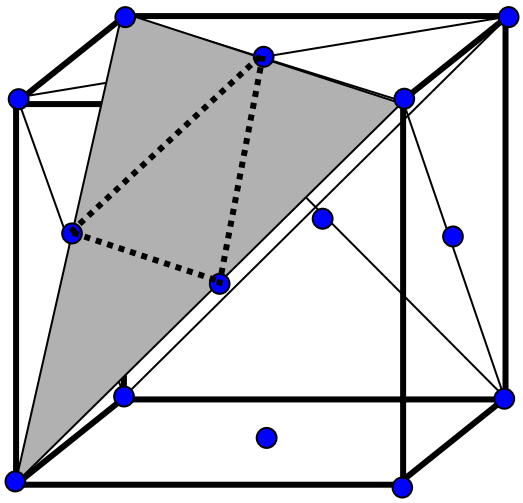

Figure 2-1: Relative orientations of {111} planes in a FCC lattice. Planes my be oriented 70.5 ^{o} apart, such as the grey and red planes, or 109.5^{o} apart, such as the grey and blue planes.

If the twin plane intersects two {111} faces at the acute angle, an area called a reentrant groove will form. At this groove, an adatom will be always able to attach to multiple neighbors, making dissolution unlikely and the nucleation of a new atom layer more rapid. The more rapid layer nucleation at the reentrant groove leads to rapid growth parallel to the twin plane. They showed scanning electron microscopy (SEM) images of reentrant grooves on the sides of silver halide particles to support their proposal. Hamilton and Brady proposed that the presence of a single twin plane would lead to the formation of a triangular tabular crystal, and that two parallel twin planes would lead to regenerating reentrant grooves that would lead to highly anisotropic growth. Furthermore, they suggested that if two or more non-parallel twin planes were to

intersect, crystal shapes other than tabular would grow, explaining the presence of wires and tetrahedra in their silver halide samples.

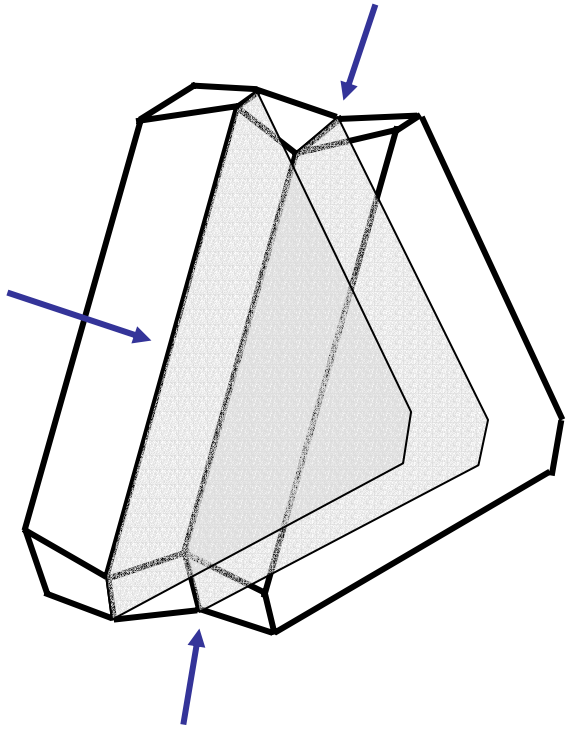

Figure 2-2: The formation of reentrant grooves (blue arrows) by twin planes. Twin planes (grey) cause represent a mirror plane in a crystal that can cause surface faces to form obtuse angle with one another. These obtuse angles are sites where an adatom will have a number of nearest neighbors similar to one attaching to an atomic edge.

The technology of silver halide crystal growth has been heavily characterized because of its photoreduction behavior, which is of great importance to photographic technology. The fabrication of AgCl, AgBr and AgI crystals has been refined to a high degree, such that tabular platelet, wire, tetrahedral, and numerous other morphologies can be fabricated. All the crystal habits represented are dominated by {111} and {100} type faces. These materials are FCC systems where {111} planes were the preferred location of twins. The microstructure of these materials has been characterized extensively, and the formation and preferential growth along reentrant grooves have been proven to

generate the anisotropic growth observed in synthesis. The similarities in crystal habit and morphology of this system with metal colloids are striking. This section will describe the silver halide system in order to compare it to that data collected for this report.

Goessens et al. used TEM and electron diffraction to characterize the crystal habit and internal structure of AgBr crystal formed in a solution in which the components were in a slight supersaturation with respect to AgBr [25-27]. For wire or needle shaped crystals, the internal structure was found to contain three crystals extending down the length of the wire, each of which was twinned with respect to one another. There were two (111) type twin planes and one (221) type twin plane. The twins radiated out from the center of the wire diameter and were thus not parallel to one another. The (111) type twins made a 109.5^{o} angle relative to one another. For tabular crystals, two (111) twin planes were observed parallel to the large face of the crystal. Tetrahedral particles were found to contain two (111) twin planes with a 70.5^{o} angle between them.

Given the presence of twin planes and the kinetic advantage they give to growth, Goessens et al. developed a model to explain the morphology of AgBr particles. In the case of a twin plane forming in a particle, three reentrant grooves form on faces oriented 120^{o} from one another, leading to rapid growth in three directions. Because the adjacent faces will not grow as quickly, the face growing faces will grow themselves out, leaving a triangular prism whose thickness was determined by the size of the particle at the time of twin formation. If another twin forms parallel to the first on one of the large, triangular faces, the particle will again grow parallel to the twin plane, but the growth direction will be rotated 60^{o} from the first due to the misorientation of the crystal in the

[211] direction [28]. These will then grow out, leaving an hexagonal platelet. Further parallel twins will lead to alternating triangular and hexagonal shapes with the width of the particle growing with each new reentrant groove. Bögels et al. found that if the rapidly growing side faces contained {100} faces bound by {111} faces, instead of strictly {111} faces, then the presence of only two parallel twin planes created reentrant grooves that did not grow out, such that a platelet could grow laterally without additional twining [29]. If the second twin plane were oriented at a 70.5 degree angle, the particle will form a tetrahedral. If the second twin plane is oriented at a 109.5^{o} angle, a particle containing three crystallites will be formed, with a central crystal and two others joining together at a common line. The open area between the two crystals on the outside will grow together, forming a (221) twin interface that gives the particle a deformed hexagonal cross-section. The intersection of the three twins at the center of the particle produces reentrant grooves on both sides that allow growth parallel to them. This allows for one dimensional growth of the particle into a rod. Furthermore, the nature of the reentrant grooves and their orientation to one another make them self-perpetuating so that the groove never grows itself out, making very large aspect ratio wires possible.

Review of Anisotropic Silver and Gold Nanoparticles

In this section, a review of the morphology and synthesis techniques of silver and gold nanoparticles with anisotropic shapes will be presented. The intent is not to exhaustively present all the examples of these particles in the literature, but to give an overview of the diversity of chemical methods to produce these particles. A number of techniques will be explained in greater detail. These are the same or similar to techniques used to produce the nanoparticles analyzed in this report.

Zsigmondy was the first to observe plate-like gold colloids using light microscopy in 1906 [30]. Beischer and Krause were the first to examine the shape of gold colloids using an electron microscope in 1937, finding the particles to be in shape of octahedrons [31]. Triangular and hexagonal platelets have been observed in gold colloid samples since Turkevich et al. began using citric acid to reduce and stabilize gold chloride in 1951 [32]. They found that the size distribution and morphology of these colloids varied with the method of preparation. Milligan and Morriss confirmed the formation of platelets with widths on the order of a few hundred nanometers, and also used numerous other methods of reduction and stabilization to form particles, none of which produced a similar morphology to the citric acid method [33].

Since that time, examples of plate-like morphologies in colloidal gold and other FCC transition metals have appeared periodically. Zhou et al. found this morphology when photoreducing gold chloride in a PVA aqueous solution [34]. Malikova et al. found a limited number of gold platelets with smaller spherical particles when gold chloride was reduced with salicylic acid [35]. Bradley et al. found triangular nanoparticles in the size range of 5 nm in palladium and nickel samples reduced in the presence of tetraoctyl ammonium glycolate [36]. The tetraoctyl ammonium molecule was found to bond to the metal surface and stabilize the particles. When the ammonium surfactant was used as a halide salt, however, only spherical particles were observed. Only when the glycolate salt or another α-hydroxy carboxylate containing molecules such as lactic, tartratic, or gluconic acid were used, did the triangular particles form. Through Raman spectroscopy, it was observed that the surface of the particles retained some of the glycolic acid in some type of monodentate or bridging bonding through the carboxylic acid group. The effect

of the α -hydroxy group could not be determined, but molecules with carboxylic acid groups not containing α -hydroxy groups were not found to produce triangular particles.

TEM Investigations of the internal structure of platelets revealed similarities between particles of different FCC metals. Barbara Brüche produced large gold hexagonal platelets by reducing gold chloride with salicylic acid [37]. She attributed their highly anisotropic shape to screw dislocations creating a continuous ledge for gold adatom attachment. The work of Curtis et al. produced copper colloids with hexagonal platelet shapes [38]. High resolution TEM showed that the main face was a (111) face and that there were two sets of [110] fringes across the entire platelet. This type of forbidden structure could only be explained by crystal flaws or by non-zero Laue zone effects. Kirkland et al. found that the triangular or hexagonal faces of gold platelets were {111} planes, and imaged twin planes inside the particle, parallel to this main face [39]. Diffraction patterns taken perpendicular to the main face contained forbidden 1/3[422] spots not normally allowed for a single FCC crystal. Three possible explanations were proposed for these spots: The existence of fractional FCC unit cells, the presence of stacking faults/twins on the (111) planes, or the elongation of the [111] reciprocal lattice points due to the extreme thinness of the particles along the [111]. Due to the observation of twins parallel to the main face, these were suggested as the cause of the forbidden spots. They proposed that the presence of twin planes could favor growth of platelets by creating reentrant grooves for the favorable addition of gold adatoms. Jin et al. found that spherical silver nanoparticles converted to triangular prisms after exposure to a conventional fluorescent light for 70 hours [40].

The triangular prisms morphology of silver, gold and copper nanoparticles has been observed in non-liquid processing as well. Evaporation techniques in argon atmospheres have been used to make nanoparticles with sharp triangular profiles [41,42]. Evidence of twining parallel to the triangular face was reported. Takanori Tomita proposed that these particles morphologies were driven by twin planes, and that these twin planes were formed in the nucleus through the motion of the surrounding medium [43]. He suggested that motion of the medium cause bending or twisting in the nucleus taking advantage of elastic anisotropy in the FCC crystal. If the strain causes a sufficient displacement in the atom spacing on the surface, the addition of an adatom will create a stacking fault, leading to a twin boundary. Twin planes are relatively easy to form in noble metals because of low stacking fault energies. The stacking fault energy of gold is 50 mJ/m^2, for silver, 25 50 mJ/m^2 and for copper, 80 50 mJ/m^2 [44]. This compares to 150 and 200 mJ/m^2 for nickel and aluminum, respectively.

The polyol technique was first used in 1992 to produce silver nanowires by reducing silver nitrate in ethylene glycol in the presence polyvinyl pyrrolidone at 160^{o}C [45]. The silver nitrate and the polymer were separately dissolved in the solvent and were then added drop wise to the hot reaction vessel and were allowed to react in the reducing environment of the heated ethylene glycol. At lower reaction temperatures, wires were found in low yield. With the addition of a small quantity of platinum hexachlorate to the reaction solution and under certain polymer to silver concentrations, higher yields of wires were obtained. The addition of the platinum salt forms platinum seeds on which the silver grew. The concentration of platinum was one thousand times

less than the silver, but the presence of the platinum seeds dramatically increased wire yields.

This technique was again used to produce silver nanowires of 30-40 nm and up to 50 μm in length by Sun et al., who more fully characterized their structure and synthesis [46-48]. They found that the rate and order of addition of the reactants to the hot reaction vessel was critical to producing a large yield of wires. The temperature and ratio of polymer to silver could be more broadly controlled. The polyvinyl pyrrolidone even be exchanged with polyethylene glycol to produce a low yield of wires, while polyvinyl alcohol only yielded spheres. Interestingly, wide variations in the synthesis conditions produced almost identical wires, while the nucleation step required careful control. The platinum salt was added before the addition of the silver and polymer, and was found to produce 5 nm platinum particles upon which the silver would later nucleate. When the silver was added, large spheres initially formed on the platinum seeds, with small silver spheres homogeneously nucleating. Through ripening, the smaller spheres dissolved, and a portion of the larger spheres began to elongate, eventually forming wires. The final product was about 70% wires and the remainder spherical particles with diameters equal or slightly larger than the wire diameters. The wires where characterized as containing a single (111) twin plane down their axis, with one twin oriented in a [011] direction and the other in a [211] direction. The group further advanced the technique by removing the Pt salt and using a "self-seeding" process, where a specific addition rate for the reactants produced wires without Pt seeds [12]. The wires produced by all synthesis variations where characterized as being structurally similar. By increasing the concentration of silver and the ratio of PVP to silver and excluding Pt seeds, nanosize cubes with {100}

faces were made in a high yield [49]. Sun et al. made cross-sectional TEM samples of their nanowires and found that the wires contained five twin planes radiating out from the center [13]. They theorized that after nucleation, the silver particles formed decahedra containing five (111) twin planes and ten {111} faces, and that the {111} faces subsequently stopped growing larger, and that the particles grew parallel to the twin planes, forming {110} faces in a rod shape. The rod shape was explained by the preferential adsorption of PVP to {110} faces, although the change in crystal habit from all {111} faces to {110} faces could not be explained. Their mechanism was also unable to explain the mixed products of the synthesis scheme, how the wide variations in the processing variable that did not effect structure or why very precise nucleation procedures that had to be followed to produce wires.

The polyol method was also applied to making nanosize prisms of silver [7]. These particles were made by mixing silver nitrate and polyvinyl pyrrolidone in N, N-dimethylformamide (DMF) and then refluxing the mixture at 156^{o}C for 10 to 20 minutes. The results of the reaction were triangular prisms of silver in a yield over 50%. The ratio of reactants was almost identical to that of the silver wire synthesis, but no wires were observed. Interestingly, the most critical factor for prism formation was not the reactant ratio or the temperature, but the nucleation step [50]. The reactants needed to be mixed and left to nucleate nanosize silver seeds before being refluxed in order to produce prisms.

The effect of PVP on the reduction of silver was investigated by Zhang et al. using microscopy and spectroscopy [51] and by Huang et al. using photoelectron spectroscopy [52]. The PVP absorbed on a silver surface was found to be very difficult to remove,

even with multiple washings in various solvents. This indicated that the adsorption involved some chemical bonding. They observed that when the ratio of PVP monomeric units to silver ions in a reduction reaction was increased up to a ratio of 1.5, the size of the resulting silver nanoparticles consistently decreased. Above this ratio, no appreciable size decrease was observed. Comparing the ultraviolet spectra of silver nitrate in water to a PVP/silver nitrate solution, they found a shift in the absorption spectra. They theorized that the lone pairs of the nitrogen and oxygen atoms in PVP could donate to the two *sp* orbitals in the silver ion, coordinating the ion in solution. From photoreduction experiments, the presence of PVP in silver nitrate solutions increased the formation of silver particles, leading to the suggestion that the coordination of silver ions by PVP could catalyze the reduction of silver by donating electron density. IR spectroscopy of silver powders prepared with PVP showed a splitting of the C-N absorption band, with a higher wave number band forming. The C=O band also shifted to a lower wave number, interpreted as the coordination of these groups with the solid silver surface. These results would explain the strong adsorption of PVP to silver particles. Photoelectron spectroscopy of PVP covered silver surfaces shows a splitting in the oxygen photoemission spectrum while the nitrogen and carbon peaks remain unchanged [52]. The oxygen splitting is attributed to bonding of the oxygen to the silver surface.

A technique call seed-mediated growth has been used to fabricate silver and gold nanorods and nanowires [1, 53-59]. In this method, 4nm diameter, citric acid covered silver or gold were synthesized and then added to an aqueous solution of additional silver or gold salt, a mild reducing agent, and the cationic surfactant cetyl triammonium bromide (CTAB). In the solution, the metal salt cannot be reduced by the reducing agent

alone, but must be catalyzed by the presence of a seed, insuring that new new nuclei will form and only the preformed seeds will grow in size. The effect of the CTAB has been speculated on, but is not fully understood. The authors speculated that the CTAB, which takes on the form of cylindrical micelles at the concentration used, could act as a "soft template" where the seed is trapped in the micelle, and as the addition metal salt is reduced on the seed. The shape of the micelle constrains the growth of particle two dimensions to form an elongated structure. No data directly supporting this proposal was presented. According to other research into gold nanorods, thermal gravimetric analysis was used to characterize the nature of CTAB adsorbed on the metal as a double layer of molecules, with the ionic amine head group of one layer bonding to the surface of a metal and the second layer oriented so that their head groups projected from the surface [60]. This bilayer type surfactant structure is characteristic of high concentration lamellar CTAB and not the cylindrical micelles of the synthesis method.

The authors alternatively suggested that the CTAB preferential adsorbs on the long-axis crystal faces of the growing rod. It is undoubtedly correct to assume that the CTAB adsorbs on the growing crystal faces, however, no description of the crystal orientation or dominant faces was presented, nor was any thermodynamic evidence offered to suggest that the CTAB could cause the preferentially growth, and was not simply adsorbing on what ever face was presented to it. Z. L. Wang et al. performed crystallographic analysis on gold nanoparticles formed using electrochemical reduction [7]. This electrochemical synthesis used CTAB in conjunction with tetraoctyl or tetradodecyl ammonium bromide in an electrochemical cell where a gold plate acted as a sacrificial anode and a platinum plate acted as a cathode [61, 62]. In their sample they found a distinct mixture of short

aspect ratio nanorods, long aspect rods, and a variety of isotropic particles with truncated octahedral, icosahedral, and decahedral shapes. They found that while both the short and the long rods had uniform crystal habits with in their respective groups, each group's crystal habit was different. The short rods had {110} and {100} type faces and grew in the [001] direction, the long rods had {111} and {1-10} faces and a [11-2] growth direction, while the isotropic particles showed {111} and {100} type face. The presence of such diverse morphologies while maintaining uniformity with in specific subsets of these particles all produced in a single reaction indicates that the control of crystal habit cannot be primary attributed to CTAB or any other absorbed component. If the stabilization of a certain face is so advantageous as to allow the growth of high aspect ratio particles, then one would not expect other faces to dominate in particles exposed to the same chemical environment. In addition, Chen and Carroll used the same silver seeds and a higher concentration of CTAB to produce truncated triangular silver nanoprisms with {111} basal planes [8]. Silver nanowires were also produced through a surfactant-less chemical synthesis using only silver nitrate, sodium citrate and sodium hydroxide [63]. These wires were found to contain at least one twin plane, as well as, the superposition of [110] and [111] zones in their diffraction patterns. The growth mechanism was attributed to Ostwald type ripening and the binding action of citrate causing the reordering of the silver surfaces to a more stable wire morphology after the initial formation of spheres.

Copper nanorods were fabricated and extensively investigated by Pileni's group at the U.P.M.C. Laboratoire, Paris, France [64-67]. In their synthesis method, the industrial surfactant Aerosol-OT was converted from the sodium salt to a copper salt, and then

dissolved in a mixture of isooctane and water to form a reverse micro-emulsion containing interconnected cylindrical micelles. The addition of hydrazine lead to the formation of copper nanorods of a narrow diameter distribution around 25nm and lengths of approximately one micron. TEM investigation with selected area diffraction lead to the conclusion that the rods contained five (111) twin planes radiating out from the center axis of the rod with the rod axis being a [110] direction and the side faces being {110} types [9]. This arrangement is identical to that proposed by Sun et al. in reference 13. Copper nanorods formed by copper metal evaporation under vacuum were found to be oriented in the [110] direction [68], while copper nanorods formed by reducing copper chloride in air contained superimposed [111] and [110] patterns similar to those observed in solution growth copper, gold and silver nanorods [69].

The internal structure of gold nanoparticles and nanorods was investigated using TEM by a number of researchers. Z. L. Wang extensively investigated single crystal gold nanoparticles without defects with shapes with various degrees of truncation between cubes and octahedral, containing different ratios of {111} to {110} faces [70]. He also found crystals with an apparent five-fold symmetry, containing five twin planes about a central axis, forming a decahedron. The particles appeared to be an assembly of five tetrahedra, each sharing a side with two other tetrahedra. Each tetrahedra fills an angle of 70.5^{o}, a five of them fill a total angle of 354.6^{o}, leaving 7.4^{o} to be filled by strain in the crystal. C. J. Johnson et al. preformed diffraction on gold rods and found the superposition of [112] and [100] zones and [110] and [111] zones when patterns were taken perpendicular to the axis of the rod [10]. They attributed this superposition to an internal rod structure consisting of a five-fold symmetry of the rod down the axis

containing five twin planes. They described the long axis of the rod as being a [110] direction and the side faces as {100}. Gai et al. also suggested a five-fold axis joined by twins, but the long axis being a [100] direction and the side faces {110} types [71].

Gold nanorods have also been observed using other methods for the reduction of gold chloride in the presence of cationic amine surfactants. Kim et al. used 254 nm UV light to photochemically form gold rods with aspect ratios of 3-4 [11]. A small amount of gold nanorods and platelets were observed when gold chloride was reduced with hydrazine in the presence of Aerosol-OT and Span80, two industrial surfactants [72]. Nanosized structures with long, narrow, and very thin morphologies, so called nanobelts, nanoribbons, or nanotabes, have been seen frequently in vacuum grown oxides such as zinc oxide. They have also been identified as forming from silver colloids refluxed in water while being exposed to light [73]. The axis length was [110] like silver nanowires, but the cross-sections were clearly rectangular in shape. The ribbons were single-crystalline and easily twisted along their length. The yield and reproducibility of these structures was limited, however, and the mechanism for formation was not understood.

Two established methods for producing anisotropic colloids have been sited in the anisotropic metal colloid literature as techniques to follow. Several papers have claimed that the growth of metal colloids follows the same mechanism as in these techniques, although no experimental evidence was presented to support this claim. The first technique is to use the crystal anisotropy of some metals and semi-metals systems to create differential growth in different directions. Complex molybdenum chalcogenide wires have been produced in solution in organic solvents [74-76]. These materials consist of triangular molybdenum selenide or telluride units which naturally connect into

chains, and which can further aggregate into bundles. Similarly, the trigonal phase selenium and tellurium is formed of covalently bonded atoms forming polymeric, helical chains [77]. Perpendicular to these chains, weak van der Waals forces join chains together. Aging of amorphous selenium nanoparticles can produce 10-100 nm diameter wires by extending the polymeric chains, while minimizing inter-chain aggregation [78]. In each of these systems, the natural anisotropy of the crystals was directly linked to the anisotropy of the morphology. This mechanism cannot function for noble metal colloids due to the highly symmetric FCC system.

The second technique involves the formation of one-dimensional structures in solutions with a high content to two different surface active agents. These techniques were pioneered by Alivisatos, Peng and co-workers in a number of publications dealing with semiconductor nanorods [79,80]. They used hexylphosphonic acid (HPA) and trioctylphosphine oxide (TOPO) in various ratios in the synthesis of CdSe and other semiconductors. They concluded that the TOPO stabilized the crystal faces parallel to the c-axis of the wurtzite structure, while the HPA stabilized the faces perpendicular to this axis. This technique was refined to produce monodisperse samples, but the aspect ratio was limited to about ten to one. Cobalt nanorods were produced by the reduction of cobalt carbonyl in this surfactant mixture, but it is unclear as to whether they are in a hexagonal close packed crystal structure, or the less symmetric ε-Co structure [81]. Without the surfactant mixture, isotropic particles were obtained for both systems, and the rods gradually became spherical with aging. Like the first technique, this technique relies on the inherent anisotropy of certain materials, using adsorbing molecules to force the system to express this anisotropy in structural form.

CHAPTER 3
EXPERIMENTAL PROCEDURE

Reproducibility of Particle Shape and Yield

Similar shapes have been observed in copper, silver and gold particles grown in different chemical environments. In order to demonstrate the commonality of structure in these three metals, several synthesis methods have been used in this report. They include previously documented methods, as well as, original and modified methods. While attempting to replicate the products reported in the literature, it was found that the methods often did not work as described or produced irreproducible results. In most synthesis schemes employed, results were not consistent from batch to batch, even when great care was taken to replicate the conditions exactly. A scheme for producing silver wires could produce high yields for several trails in a row, only to produce large spheres in the next trail. As a consequence of this fact, the intention of this report is not to describe rigorous methods of particle synthesis, but to describe similarities in structure that could explain the difficulties in reproducible synthesis.

Visible observations early in particle growth were found to give an indication of the final products. As a consequence, the failure to reproduce results seems to indicate that very minor factors in the beginning of the reaction alter the growth of the nuclei, changing the final product shape. If the shape of the particles was due to a balance of thermodynamics between different crystal faces, one would not expect such large alterations in shape, as between high aspect ratio wires and spheres, but more subtle variations in size indicating slight changes in crystal growth on different faces. The

importance of the nucleation process on the final products supports the thesis that structural flaws, such as twin planes, are acting as the determining factor in growth, and that these flaws can form very early during growth.

Synthesis Schemes

A general description of the major synthesis methods will be presented here. Many modifications and variations, too many to enumerate, were used in the synthesis of the particles characterized in the later chapters. Only the most successful schemes of each method will be described in detail. For each scheme, the purity of the reactants was maintained at a high level by using 99.9% pure reactants and handling them with Teflon coated spatulas and glassware washed with deionized water. The reaction vessels where borosilicate glass, and were washed with aqua regia in order to remove any noble metal ions from the glass surface, followed by washing with deionized water and ethanol.

The primary method of producing silver and gold nanoparticles was through a modified version of the Polyol method. In this method, ethylene glycol (EG) or N,N dimethyl formamide (DMF) were heated to generate a reducing environment capable of converting silver and gold ions into their respective metallic forms. The polymer polyvinyl pyrrolidone (PVP) is soluble in both of these solvents and is used in the synthesis. PVP acts as both the dispersing agent, sterically separating the growing particle surfaces which would bond if they collided with each other, and as an assistant in the reduction process. The PVP increases the rate of reduction of the metal cations, especially when EG is used, possibly due to the electron donating characteristics of the double-bonded oxygen. While PVP separates the particles surfaces, it is apparent that it is mobile enough to allow for additional adatoms to diffuse to the surface and attach. It is

clear that while the PVP has a strong bond with silver and gold surfaces, it is mobile enough to rearrange during particle growth.

For the synthesis of silver wires, silver nitrate was reduced in EG with PVP at 160°C for one hour. The experimental procedure was similar to that in references 36, 37 and 39, although the procedures had to be modified extensively to observe silver wire formation. Separate solutions of 0.1 M silver nitrate in EG and 0.6 M PVP in EG were freshly made prior to heating. 3 mL of each solution were added into 5 mL of preheated EG in a round bottom borosilicate reaction vessel containing a Teflon coated stir bar and immersed in a silicone oil bath at 160°C. The best results were found when the reactant solutions were added using a syringe pump over 5 to 10 minutes at a constant rate. In some cases, 0.1mM $PtCl_2$ was added prior to the reactant addition so that Pt seeds formed on which the silver wires grew. Within a few minutes of the reactant addition being complete, the final product of this reaction could be predicted. If the solution was a transparent yellow, reflecting nanosize silver particles in low concentration, the final product was always a high yield of wires. The yellow color persisted for an additional 15 to 20 minutes after reactant addition, before the solution rapidly develops a simmering metallic appearance. The conversion from yellow to metallic can occur within one minute. The wires produced this simmering effect when ever stirred due to the alignment of the wires in the shear field of the liquid. Without stirring, the wires settled slowly, but were easily redispersed. If the color of the solution turned an opaque tan color early in the reaction, the final product was always dominated by spherical or slightly faceted particles of between 100-300 nm diameter. The rapid formation of large silver particles and the yield of silver after only a few minutes reaction time indicates that the heated EG

can reduce nearly all the silver nitrate in less than 10 minutes. The persistence of the yellow color in the wire-rich batches, indicating a low concentration of sub-100 nm particles, means that only a small amount of the silver reduced could actually attach to a nucleus. This leads to the conclusion that the nuclei that form wires have a kinetic disadvantage for adatom attachment for a long period of time, followed by an explosion of growth along one axis. The nature of the particles at different stages of wire formation are described further in Chapter 5. The centrifuged silver wires were washed and redispersed in ethanol for storage.

The silver wire synthesis was very difficult to reproduce. Often times, a silver film would develop on the inside of the reaction vessel, even if the glass was washed with aqua regia or a Teflon container was used. This film seemed to act as a sink for reduced silver, because the total silver particle yield was much reduced, and the particles were all spherical. Transferring the liquid to a fresh container generally lead to wire production. Preheating the EG for an hour sometimes improved the quality of the produces, although it is uncertain all the reactions that can take place in EG at these temperatures, many of the products being highly volatile and escaping the condenser.

Gold rods, prisms, ribbons and isotropic particles were produced when a similar procedure as for silver wires was used. 3 mL of 0.1 M gold chloride in EG and 3 mL of 0.6 M PVP in EG were added using a syringe pump over 5 minutes to 5 mL of EG at 160°C. The distinctive yellow color of gold chloride disappeared within a few minutes of heating, but the characteristic wine-color of gold nanoparticles was not observed. After one hour, the shimmering of metallic gold particles could be seen. These particles were

always a mixture of shapes, with about half of the particles being anisotropic wires or platelets.

Silver prisms were produced in high yield by reducing silver nitrate in DMF with PVP. 0.022 M silver nitrate in DMF and 0.066 M PVP in DMF were prepared while a reaction vessel and stirring rod were brought to 156°C in a silicone oil bath. A small portion of the silver nitrate was reduced at room temperature over about 10 minutes time, producing a light yellow color. After this, the two solutions were simultaneously added to the hot reaction vessel and a condenser apparatus was placed over the top of the vessel to prevent loss of solvent. After 20 minutes of reaction, the solution became a brown-blue color indicating silver prisms. This solution was mixed with five times excess acetone and centrifuged to sediment the prisms and remove the DMF and remaining reactants. The prisms were redispersed in ethanol and centrifuged repeatedly until pure. The product was highly reproducible, and had a high yield of prisms.

High aspect ratio gold prisms, refered to as platelets, where made in high yield by using a similar procedure as for silver prisms. Identical ratios and reaction procedures were used, with gold chloride replacing silver nitrate. The length of reaction time was increased to 17 hours, after which metallic gold particles could be seen circulating in the solution. This procedure produced high yield of the platelets.

A mixture of rods, prisms and other shapes was produced when silver nitrate or gold chloride was reduced in aqueous solutions in the presence of CTAB. In this procedure, developed by Murphy, gold or silver seeds of approximately 4nm where produced by reducing the metal salt with sodium borohydrate in an aqueous solution containing sodium citrate. The citrate strongly bonds to the metal surface and creates a

negative surface charge that provides colloidal stability. 0.25mM sodium citrate and 0.25mM silver nitrate or gold chloride were dissolved in water, followed by the rapid addition of enough sodium borohydrate to make a 3mM concentration. The metal seeds formed with in seconds, as seen from the color change. The nature of the seeds was very sensitive to the mixing of the components, as could be observed from the frequency of the plasmon absorption determined in a UV-vis spectrometer. In fact, reproducing the seeds was nearly impossible, as the silver dispersion would vary from yellow to yellow-brown to green, and the gold from a wine red color to purple. Furthermore, the solution had to be aged for the residual sodium borohydrate to decompose, while its color slowly continued to change. One part seed solution was added to nine parts 0.1M solution of CTAB containing 0.25mM additional metal salt, followed by 0.5mM of ascorbic acid, leading to reduction of the metal. Ascorbic acid is weak reducing agent (0.4-0.5 V) and will generally not reduce either metal salt (0.7996 V) unless a metal surface is available to catalyze the reaction. In reality, controlling the reduction of the metal salt was very difficult, and was highly dependant on pH and temperature of the solution. The metal nanoparticles were separated by centrifuging repeatedly to remove the CTAB, being redispersed in water each time.

Mixed gold particles were produced in an aqueous electrochemical cell containing CTAB and a secondary cationic surfactant through the oxidation of a sacrificial gold anode and the reduction of the cationic gold on a platinum cathode. The secondary surfactant was either tetraoctyl ammonium bromide or tetradodecyl ammonium bromide, both of which are not soluble in water. An aqueous solution of 0.1 M CTAB and 0.01M secondary surfactant was prepared in a borosilicate beaker, which was immersed in an

ultrasonic bath. The ultrasonic bath had effect of emulsifying the secondary surfactant in the CTAB. A gold and a platinum plate, each 2 cm square were placed in the solution 1 cm apart. A current of 5 mA was pulled through the solution using a power supply while the solution was subjected to sonication. A wine or purple color would slowly begin to develop around the cathode. After 20 minutes of sonication, the power supply was turned off and the nanoparticles were separated through centrifuging.

The copper particles were produced through the reduction of copper (I) oxide in a sugar solution at elevated temperature. 1 g of copper oxide, milled until submicron in size, was mixed with 15 g of powdered sucrose and 3 g of water. The solution was sealed in a Teflon container and heated to 85°C for 2 days before the reduced copper and copper oxide particles were separated by washing and centrifuging. The heated sugar undergoes a breakdown process in which simple reducing sugars are produced. Metals such as copper are known to catalyze this breakdown. The products were a mixture of large copper particles, including rods and prisms, with a significant amount of unreduced copper oxide.

CHAPTER 4
CRYSTAL HABIT OF TWO DIMENSIONAL METAL COLLOIDS

Application of the Silver Halide Platelet Growth Model

The two current explanations for anisotropic metal growth in solution, the crystal face poisoning and the physical restriction explanations, will be demonstrated to be incorrect in the results of this study. A more suitable explanation, the reentrant groove growth mechanism as described for silver halide solution growth will be presented and evaluated.

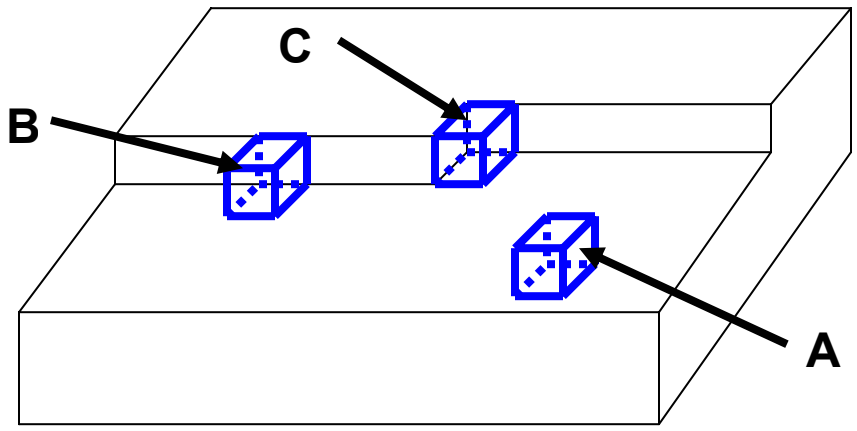

Figure 4-1: Possible ways an adatom can attach to a crystal surface. An adatom attaching to a flat crystal face, as in A, is more easily redissolved than one on a kink or corner site such as B and C.

Surface roughness is energetically unfavorable for materials, particularly those on the nanoscale, which leads to atomically smooth faces on nanoparticles. The addition of an adatom to the surface is often thermodynamically unfavorable, even in a supersaturated solution. A lone adatom on a crystal face, as in Figure 4-1 A, loses much of the stabilization it received from the solvent, while gaining little of the stabilizing

lattice energy. This makes the dissolution of this adatom likely, and requires that a nucleation event of a new atomic layer occur before continued growth on this face. Once a nuclei is present on the surface, kink and corner sites, as in Figure 4-1 B and C, provide greater stabilization to an adatom, leading to rapid completion of the atomic layer on the face. A rate limiting nucleation step is then required again. If a site, such as the intersection of a twin plane with a surface, exists, kink and corner sites may be continuously present for adatom attachment. As can be seen in Figure 4-2, the stacking fault at a (111) twin plane causes a concave joining of two {111} faces. At this reentrant groove, adatoms (blue) can always attach without a new nucleation event.

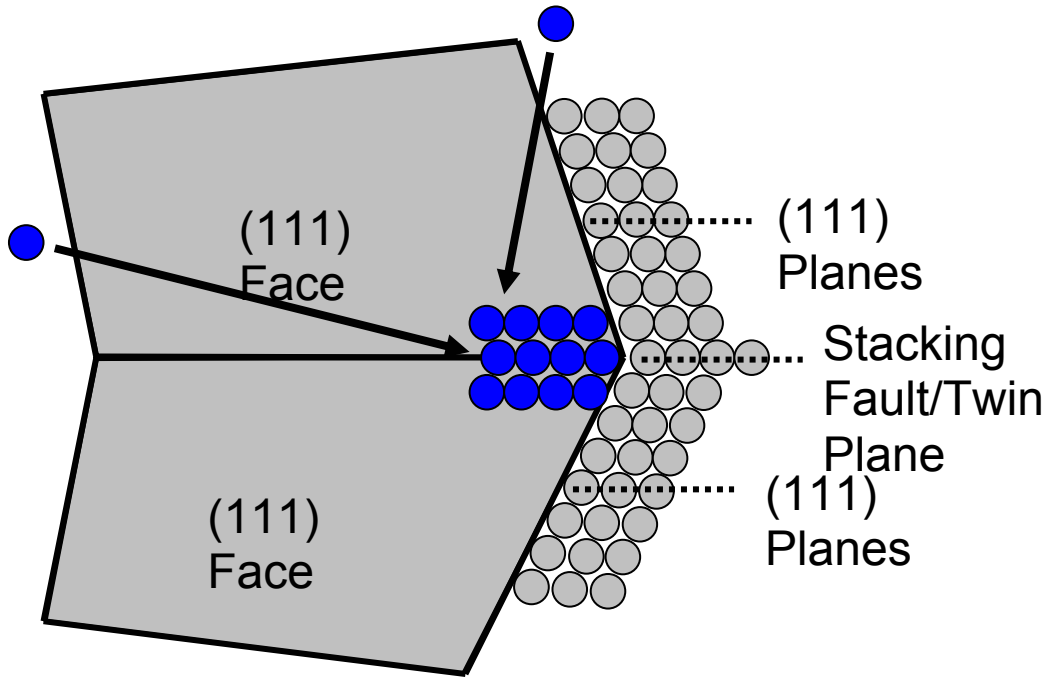

Figure 4-2: Concave joining or reentrant groove of two {111} faces at the stacking fault created by a twin plane. This creates a favorable location for adatoms (blue) to attach to the crystal.

In the reentrant groove model, the crystal habit for a nuclei of a FCC metal containing a (111) twin plane is assumed to be a hexagonal prism with {111} faces. The

prominence of the {111} type faces is reasonable due to the low surface energy of this densely packed crystal face. There will be two parallel {111} main crystal faces and twelve {111} planes intersecting the twin plane on six sides. Figure 4-3 shows that the {111} faces will form alternating concave and convex edges around the six edges, referred to as A and B type sides. It is the A sides that have the concave shape that forms the reentrant groove where adatom addition is favored and particle growth is rapid. Because each A side is bound by two B sides, this rapid growth leads to the A sides growing themselves out, transforming the original hexagonal prism to a triangular prism. Once the A sides run out, further growth is very slow. The dimensions of the platelet are determined by the size of the nuclei at the time of twinning.

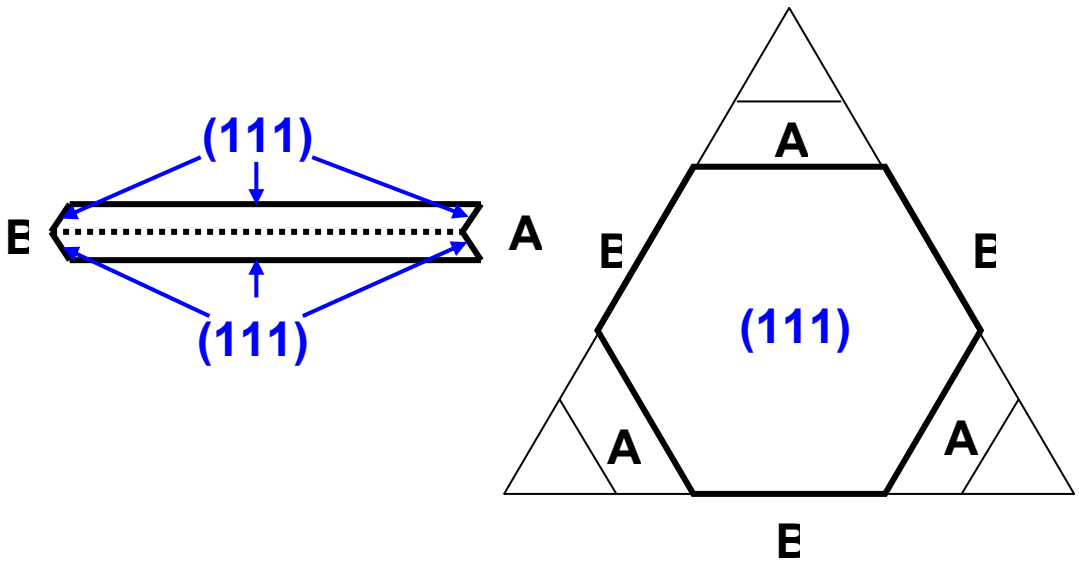

Figure 4-3: Effects of twinning on particle growth. When a twin forms in a particle (dashed line), the symmetry of the FCC system leads to a hexagonal prism with alternating sides containing reentrant grooves. Rapid growth of these A sides bounded by B sides leads to a triangular prism shape.

If a second twin plane forms parallel to the first, the symmetry of the FCC system will cause the grooves and ridges of the {111} side planes to be reversed from those of the

first twin, as seen in Figure 4-4. This causes all six sides to contain reentrant grooves, such that each side regenerates the others, leading to an expanding hexagonal crystal. Because the reentrant grooves do not grow out, one can expect very high aspect ratio particles to form in this situation.

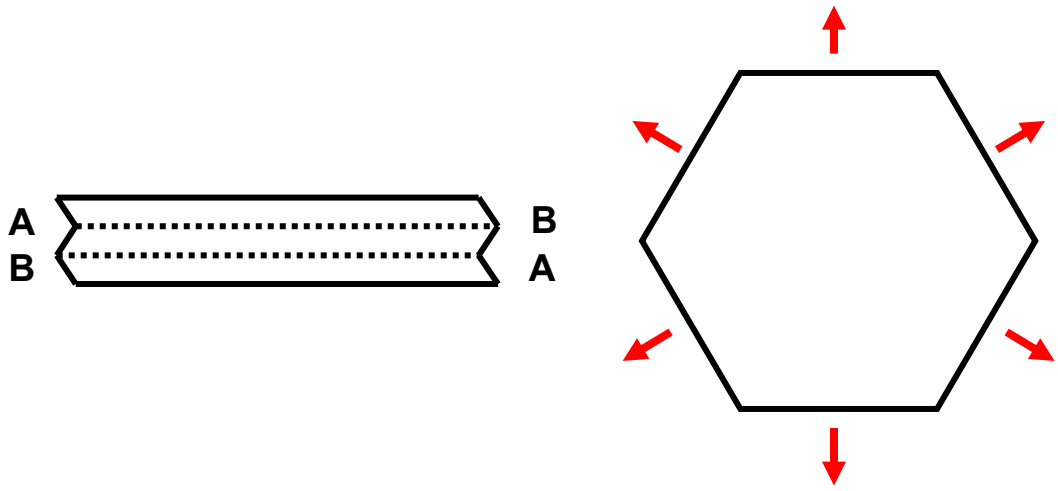

Figure 4-4: Growth of a particle with two parallel twins. The twin planes (dashed lines) create reentrant grooves on all six sides, leading to rapid growth on each side.

Silver Platelets Formed Through Reduction in DMF

When silver nitrate is dissolved in DMF containing PVP, a yellow color immediately appears in the solution, indicating the formation of spherical silver nanoparticles. This can be confirmed using the UV-vis spectra of the particles, which corresponds closely to that of a nanosize spherical silver particle.

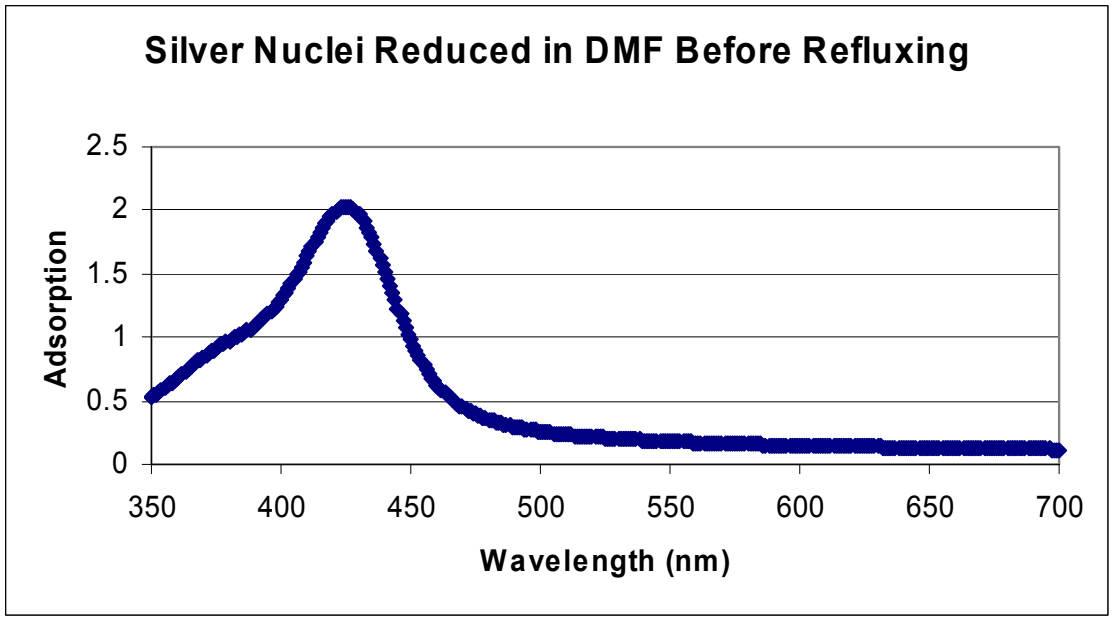

Figure 4-5: UV-visible spectrum of the silver seeds formed upon mixing of silver nitrate with DMF containing PVP. The spectrum corresponds closely to the expected plasmon absorption frequency of spherical silver particles.

HRTEM of the nuclei quenched in acetone after 20 minutes revealed spherical and isotropic particles on the order of 5-15 nm in diameter. No evidence of twinning or other defects was observed.

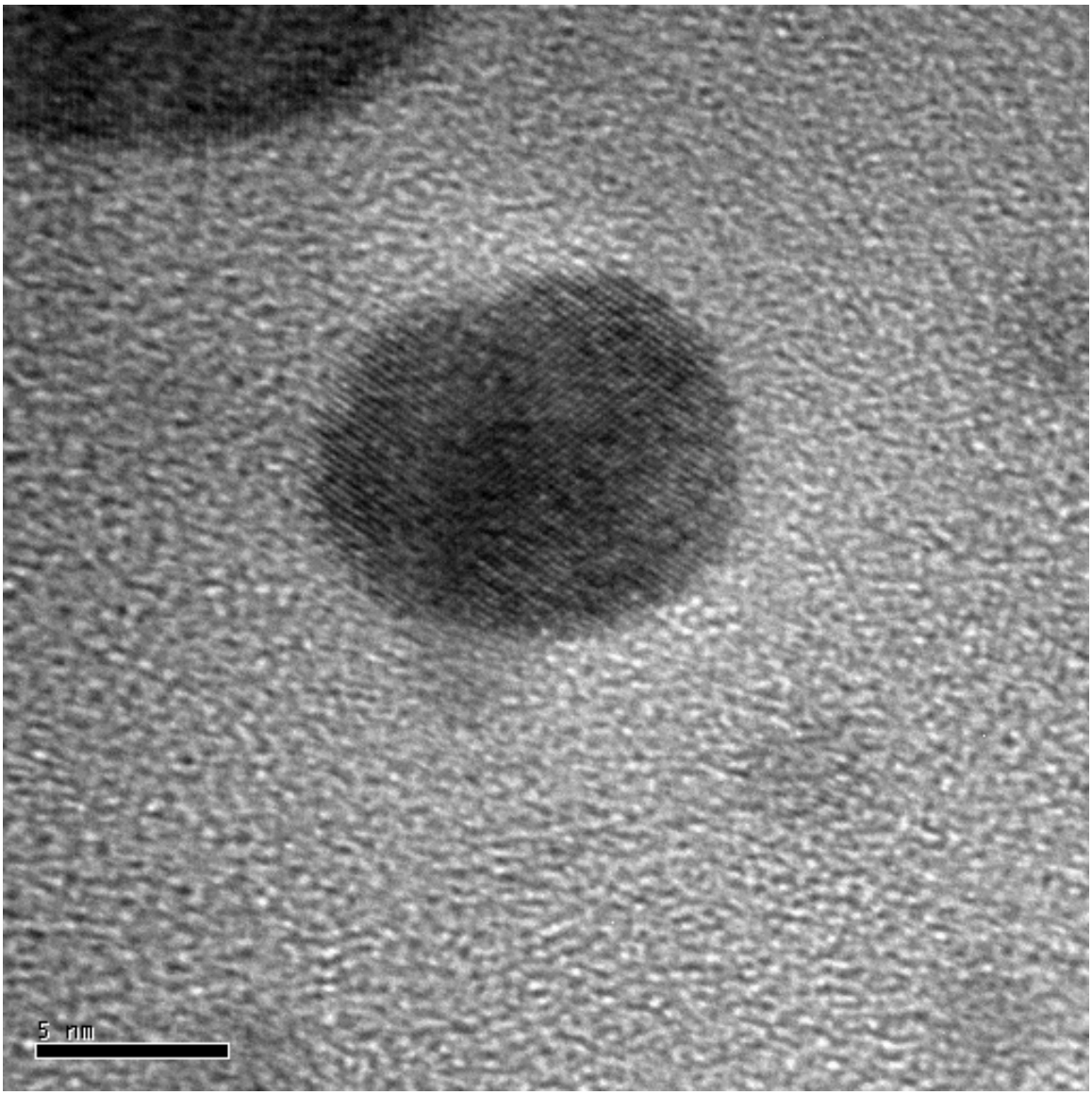

Figure 4-6: Seed particle from the addition of silver nitrate to a PVP containing solution of DMF, quenched with acetone after 20 minutes and separated for HRTEM analysis. As with this particle, the seeds showed no evidence of twinning or other dislocations.

When the solution is refluxed at 156^{o}C, the remainder of the silver nitrate is reduced, reproducibly producing a nearly 100% yield of thin silver prisms of largely triangular or truncated triangular shape. The non-triangular shaped particles are dominated by 60° and 120° angles. The prisms were on average 200nm in width when the system was refluxed for 30 min.

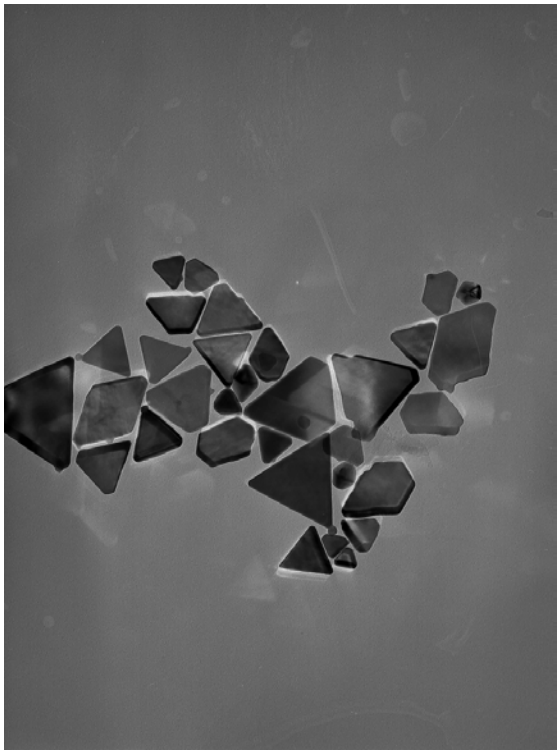

Figure 4-7: Silver nanoprisms grown in DMF for 30 minutes.

As the refluxing time is increased, the majority of the particles do not change in size or shape. When the refluxing time is 17 hours, the average prism size has increased to ~300nm, with some of the prisms being ~1μm in width. Most of the prisms in the 17 hour sample were in the same size range as the 30 min sample, with a minority of the prisms growing much larger. In addition, many of the small prisms had less defined edges and appeared to be partially dissolved.

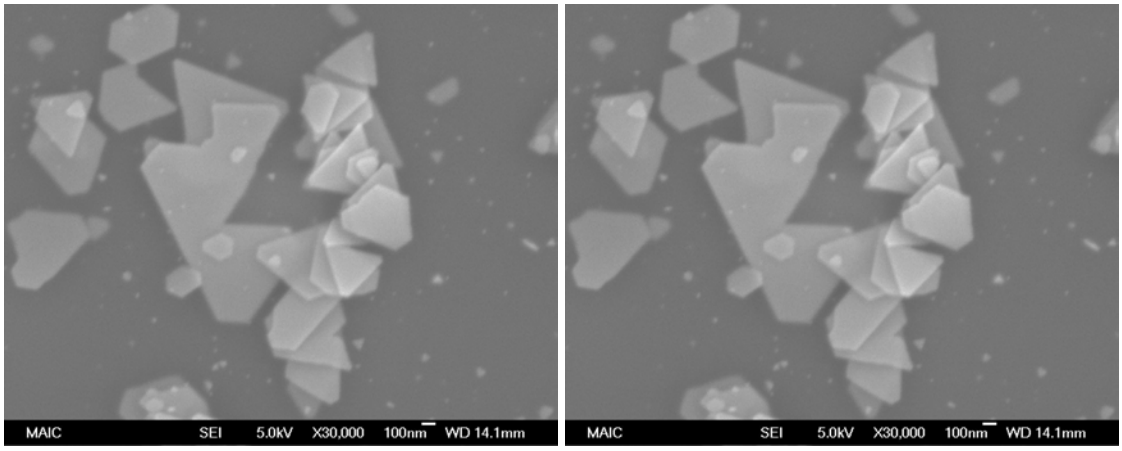

Figure 4-8: SEM images of silver nanoplatelets grown for 17 hours in DMF.

In this system, the conversion of the spherical particles to triangular without the expected faceted, low surface area cubes and octagons supports the proposition that the growth is being governed by a twin plane. After 30 minutes of reaction, the silver yield is approximately 100% of the silver nitrate addition, indicating that further changes in shape and size with refluxing must come from dissolution and reprecipitation of the reduced silver. Once a twin plane forms in a particle, the particle grows rapidly to form a triangular prism, the growth of which is arrested when the reentrant grooves grow out. During the twinning and growth of these particles, the silver nitrate is completely consumed, leading to the arrest of the growth of those particles whose reentrant grooves have not grown out. These two factors explain the two types of prisms observed at 30 minutes reaction time. Furthermore, the difference in size of the particles must be explained by the twinning event occurring after the initial nuclei form. Because the size of the particles at the time of twinning determines the final prism size, gradual formation of twins in this reaction leads to different prism sizes. The particles which twin early in their growth result in smaller prisms.

At 17 hours, a minority of the prisms have grown several times larger than the other, while the majority are the same size or smaller. This indicates that a second twinning event can take place, leading to further growth through the addition of dissolved silver from the small particles. As can be seen in Figure 4-8, small particles remain after 17 hours. This indicates that the kinetics for dissolution of reduced silver are slow, limiting the final size of the doubly twinned particles compared to the gold particles formed in DMF.

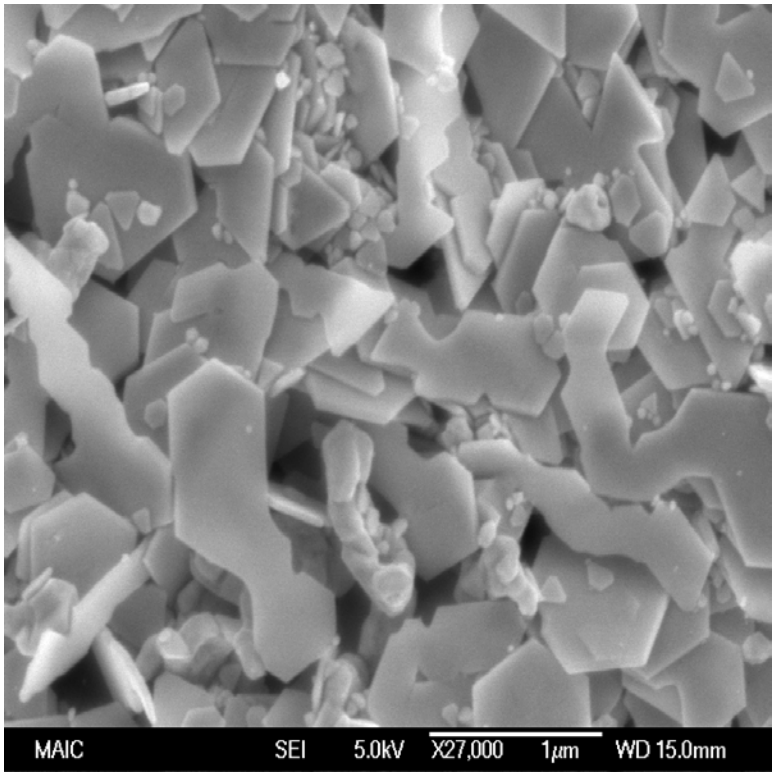

Figure 4-9: Silver prisms refluxed for 98 hours.

When the DMF/silver solution is refluxed for 98 hours, oddly shaped, plate-like particles form. These particles are again dominated by 60 and 120 degree angles, but appear to have randomly grown on different sides, often forming kinked or bent structures. It is not clear what is causing this, although it appears that some of the particles have fused together during refluxing, possibly due to desorbtion or breakdown

of the PVP dispersing agent. This morphology is similar to that seen in reference 72, where silver prisms were refluxed in water for 10 hours, and may be a similar phenomena.

Diffraction patterns were obtained from samples reacted for 30 minutes and 17 hours. Both indicate that the main faces of the prisms are {111} faces. Expected in this pattern were the (1/3)[422] forbidden reflections that can be generated by the stacking fault at a twin plane. The stacking fault breaks down the systematic absence rules for single crystals, leading to less intense forbidden spots. These forbidden reflections were not observed, although this does not necessarily mean that they don't exist. Only if a particle with a single twin has a number of planes that is not a factor of three does the systematic absence rule break down. For the 17 hour samples, clear diffraction near the undiffracted beam was difficult, possibly due to the increased thickness of the prisms blocking a large amount of the beam intensity or through operator inexperience.

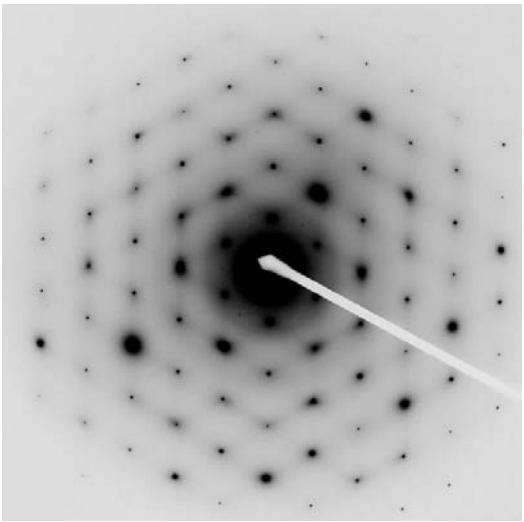

Figure 4-10: Diffraction patterns from silver prisms grown in DMF showing a <111> axis perpendicular to the top face. The image is from a sample reacted for 17 hours.

Silver Prisms Formed Through Reduction in Aqueous Solution

Silver nitrate reduced by ascorbic acid in the presence of CTAB and silver seed particles in aqueous solution produced a mixture of particle shapes. This synthesis scheme followed that of Murphy, where high aspect ratio silver wires were reported in small quantities of approximately 3%. Various samples produced under identical conditions produced various ratios of truncated triangular prisms, rods and isotropic particles containing one or more dislocations. In spite of rigorous attempts to reproduce results of this synthesis method, results varied widely, often with large numbers of isotropic particle. Samples were occasionally rich in prisms and rods, as in Figure 4-11.

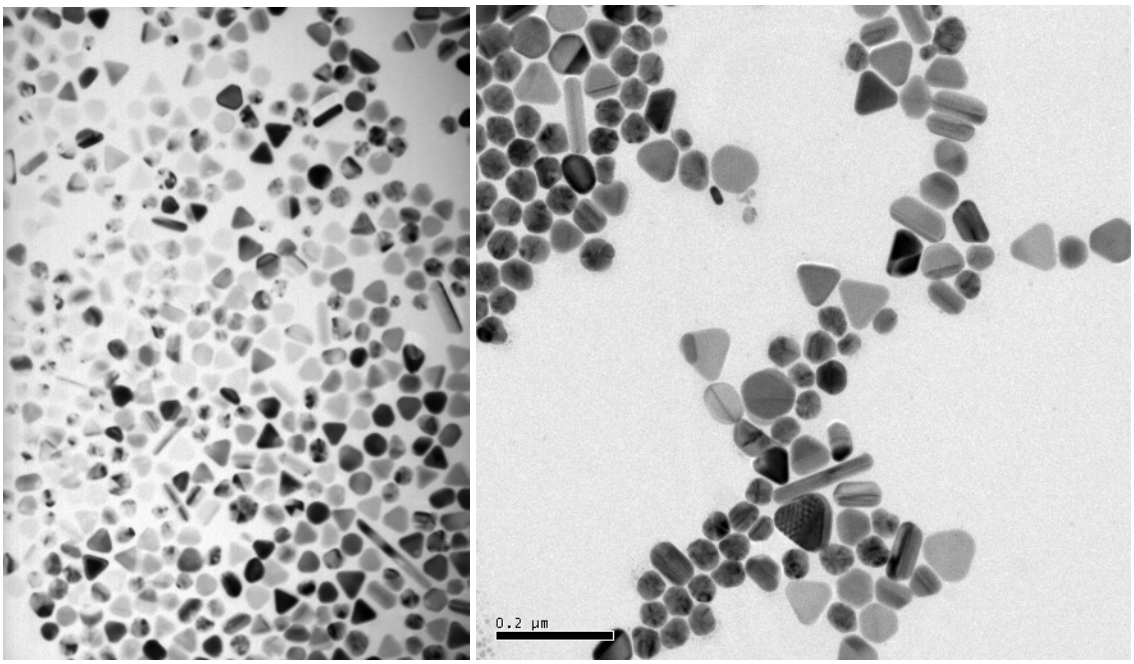

Figure 4-11: Silver nanoprisms made in an aqueous solution containing CTAB.

TEM investigation of the prisms showed that they had the same {111} main face as those formed in DMF. Clear evidence of forbidden (1/3)[422] reflections could be obtained on these prisms as seen in the left image of Figure 4-12. The first ring of low intensity spots, rotated 30° from the second ring of 220 reflections, are these forbidden

reflections. Interestingly, Moiré fringes were observed on some of the prisms. Tilting of the sample was not able to reveal the presence of a second particle below the one seen in the right image in Figure 4-12. The stacking of two prisms with their lattices offset by a small degree could cause this pattern. Alternatively, the presence of some additional flaw parallel to the twin plane may generate an offset in the stacking of the crystal planes. This feature was relatively rare in these particles.

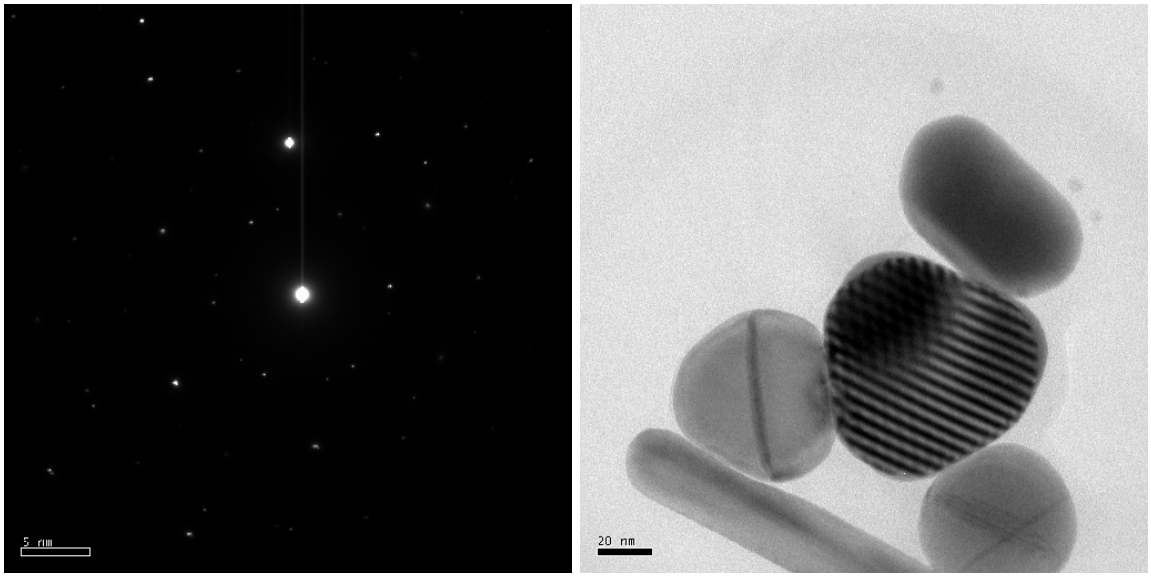

Figure 4-12: Left, diffraction pattern from a silver prism taken perpendicular to the top face, indicating a <111> direction, with forbidden reflections. Right, the prism in the center of this picture contains moiré fringes, possibly as a result of twinning.

Gold Platelets Formed Through Reduction in DMF

When the same concentration of gold chloride was used to replace silver nitrate in the DMF polyol process, prisms of much greater width and aspect ratio resulted after 17 hours. The average width was ~10μm while the thicknesses remained ~20nm. The profile of the particles was triangular, hexagonal, or a truncated version of these two. With an aspect ratio of ~500 to 1, these particles are unique in the literature. SEM images of gold nanoplatelets are shown in Figure 4-13.

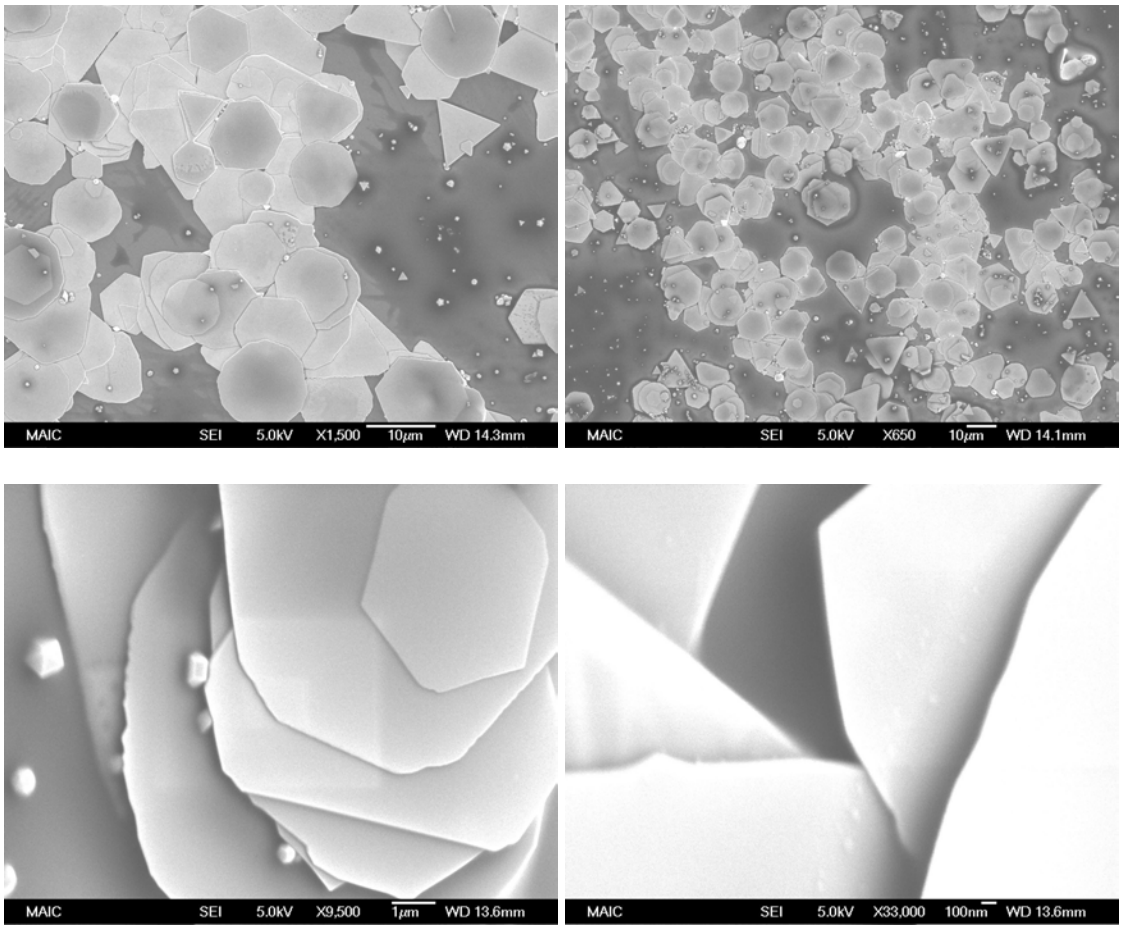

Figure 4-13: SEM images of gold platelets after 16 hours in DMF. Top images are taken perpendicular to the substrate. Bottom images where taken on the same sample at a 45 degree angle to the platelet normal in order to observe the edges.

The SEM images taken at a 45 degree tilt about the mount face show the very thin and uniform thickness of the platelets. TEM data also shows a very uniform thickness and Selected Area Diffraction (SAD) shows that the large faces are {111} planes as seen in the silver prisms.

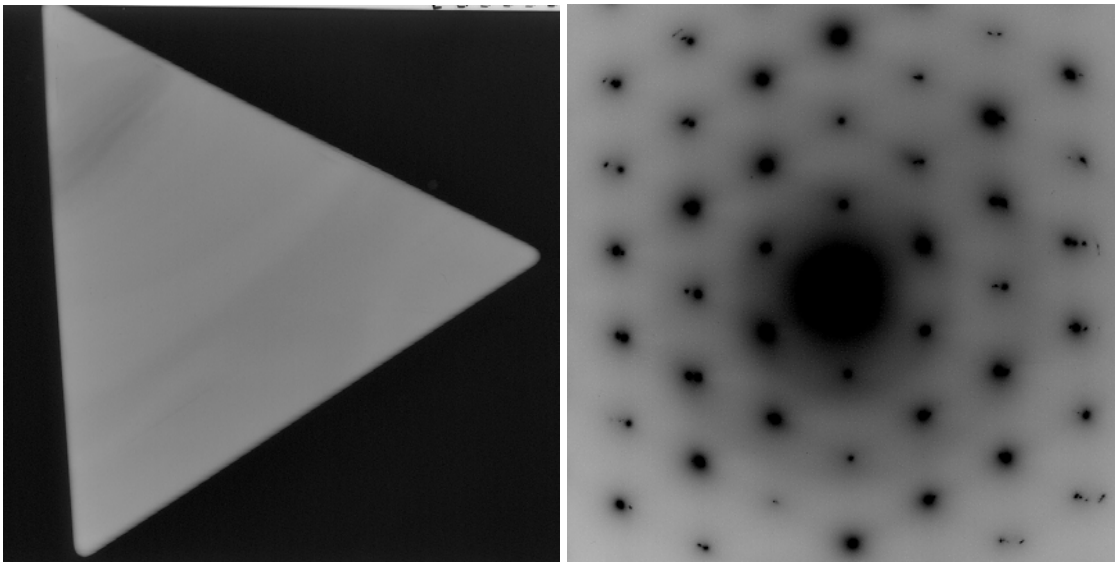

Figure 4-14: On the left, a TEM image of triangular nanoplatelet. On the right, a selected area diffraction pattern of platelet take perpendicular to primary face indicating a (111) main face.

When a high quality diffraction pattern is collected from a gold platelet, the forbidden (1/3)[422] reflections can clearly be seen. When two parallel twin planes are present in a particle, the systematic absence rule is always broken regardless of the number of lattice planes. Thus, this is further evidence of double twin structure of these platelets.

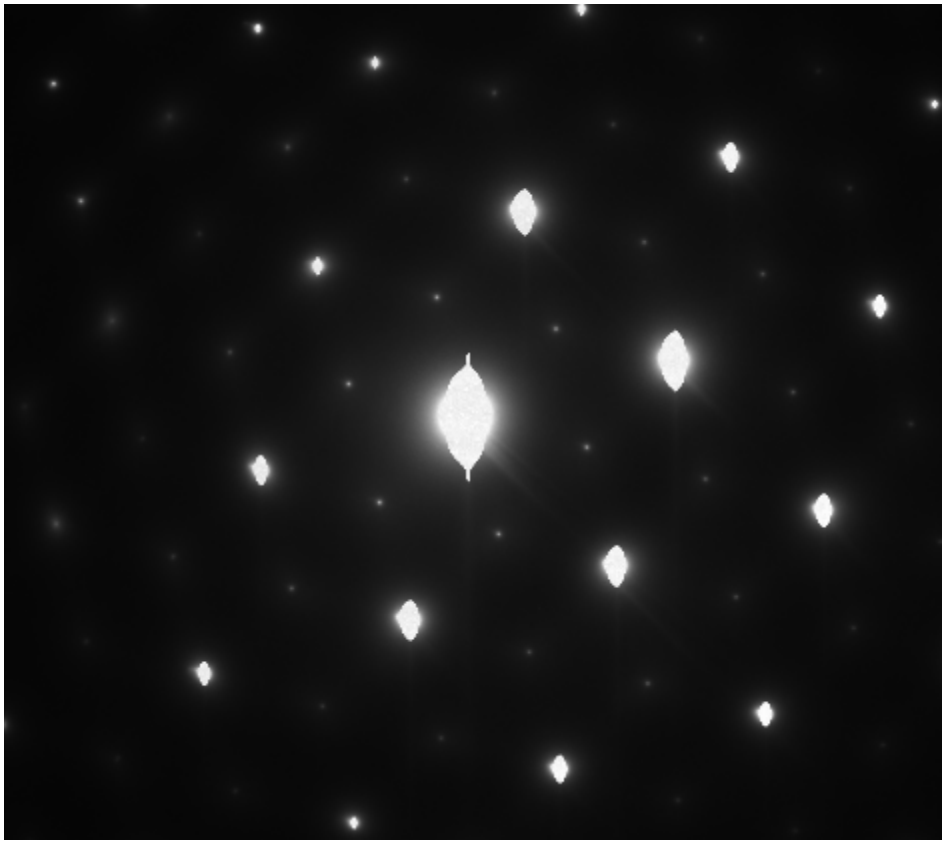

Figure 4-15: Diffraction pattern of a hexagonal gold platelet. The six bright spots around the central beam are the six-fold diffraction pattern of a [111] direction. The six dimmer spots within the bright spots are the forbidden (1/3)[422] reflections.

SEM and TEM were used in an attempt to directly observe twin planes parallel to the main faces. Figure 4-16 shows a high magnification SEM image of the side of a gold platelet. The reentrant groove is clearly visible.

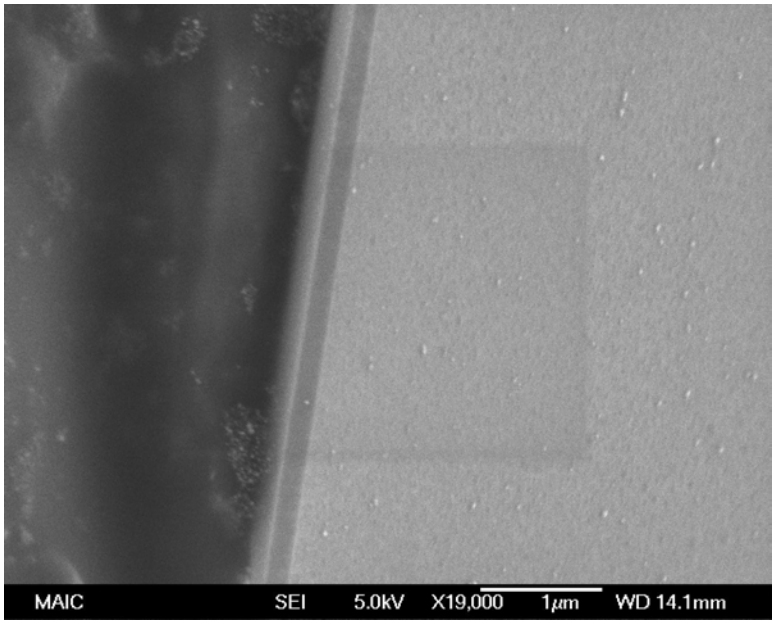

Figure 4-16: A high magnification SEM image of the edge of a gold platelet with a depression through the middle indicating the reentrant groove. The image is taken at a 45° angle with the main face (grey region on the right).

Gold platelets were embedded in epoxy and microtomed in an attempt to view the particles on edge. This technique did not prove successful, however, as can be seen in Figure 4-17. Although the platelets could be observed on their edge, they were heavily deformed by the microtoming process. This is not unexpected, due to the low yield stress of gold and the ease at which high purity metals form dislocations. No useful data could be obtained from these samples.

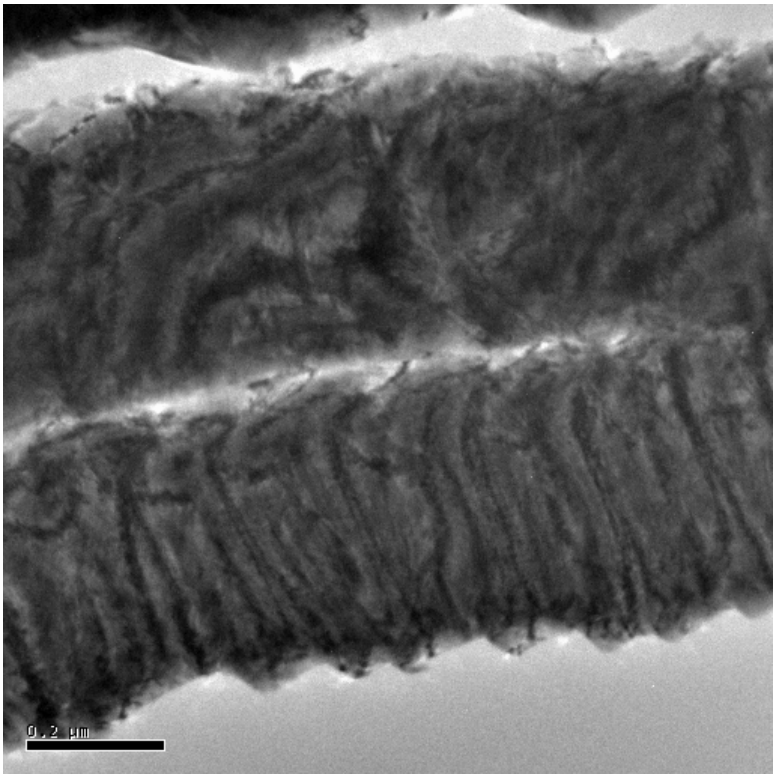

Figure 4-17: TEM image of gold platelets embedded in epoxy and cross-sectioned with a microtome. The cut surfaces of the platelets where heavily deformed, as seen by the wavy contrast in the image. No clear data could be obtained with this technique.

When the gold platelets were refluxed for an additional 24 hours in fresh DMF, evidence of dissolution of the metal is seen. Figure 4-18 shows platelets with pitting on the sides, unlike the freshly made platelets. This indicates that significant amounts of reduced gold can dissolve during refluxing and are available for ripening of particle shape.

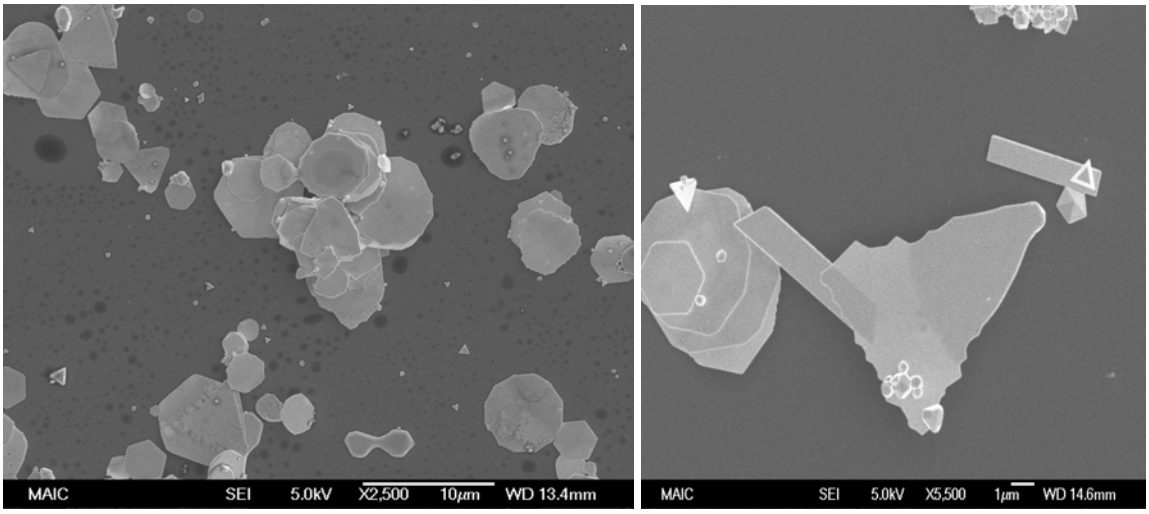

Figure 4-18: Dissolution of gold platelets after additional boiling. The sharp edges of the hexagonal gold platelets were found to etch away when the platelets were refluxed in fresh DMF.

Gold Prisms Formed Through Reduction in Aqueous Solution

Gold prisms were synthesized in aqueous solutions containing CTAB according to the method used to make silver prisms. The reproducibility and yield were nearly the same; only certain batches contained prisms, and they were mixed with rods and isotropic particles.

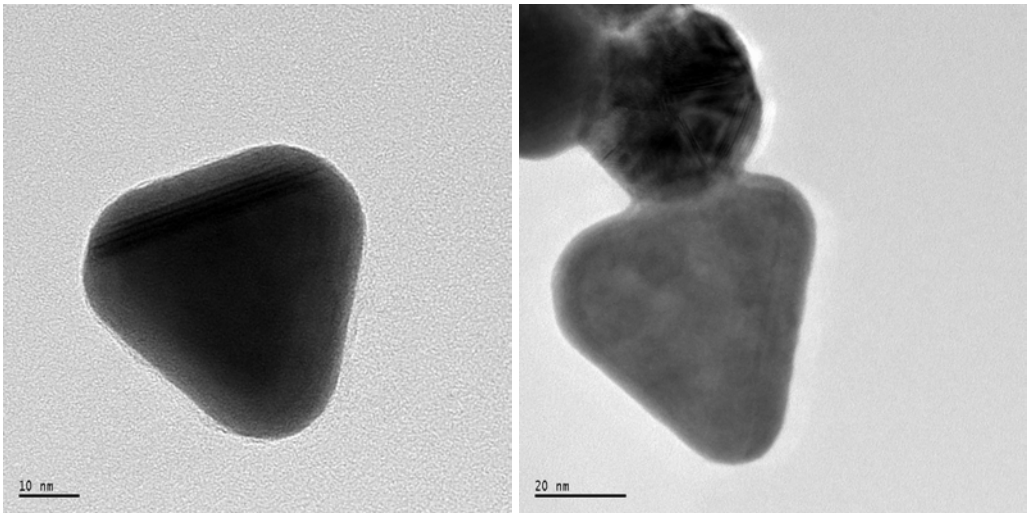

Figure 4-19: HRTEM images of gold prisms formed in aqueous solution. Contrast lines are seen in the upper edge of the left image on and the right edge of the right image.

The gold prisms were approximately the same size as the prisms obtained for silver. It was noticed that most of the prisms had a contrast line or Moiré fringe on one edge of the triangular face. This feature makes it appear that there is at least one additional twin plane on this edge. As will be seen in Chapter 6, a second twin plane forming on a B side of a hexagonal prism will form a 70.5° angle with the first twin plane, and will cause the formation of a tetrahedron. The uniform contrast over the surface of the particle, and the lack of a change in profile with tilting of the sample, indicates that there is no tetrahedron formation in these samples. This means that either there is a second twin plane and the particle has not had an opportunity to grow into this shape, or that the edge contrast represents some other type defect, perhaps the intersection of multiple twin planes. This last possibility will be revisited in Chapter 5.

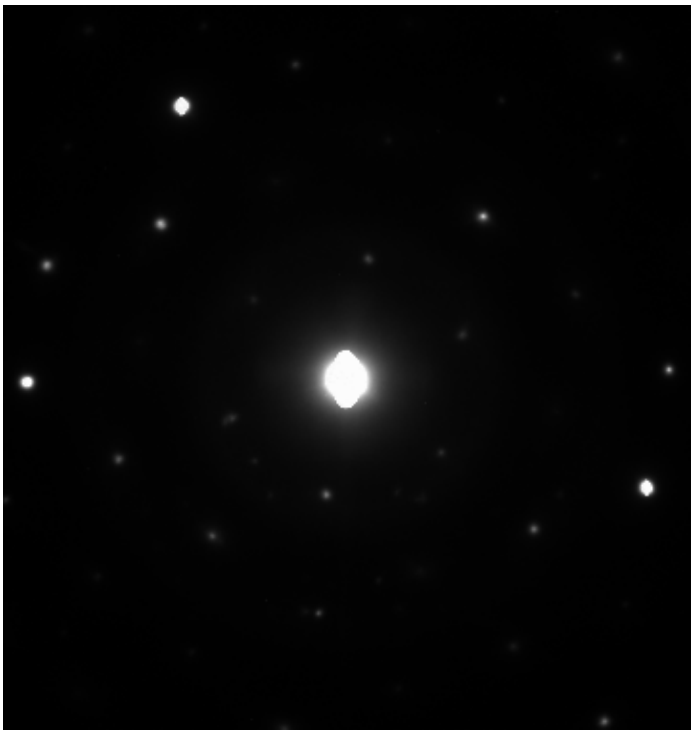

Figure 4-20: Diffraction pattern of gold prism grown in aqueous solution. The [111] pattern is visible.

Copper Platelets Grown in Aqueous Solutions

Copper platelets where one of the products of reducing copper (I) oxide in a heated sugar solution. The low aspect ratio and large size indicate that a twinning event occurred in a single crystal particle which had already grown to a large size.

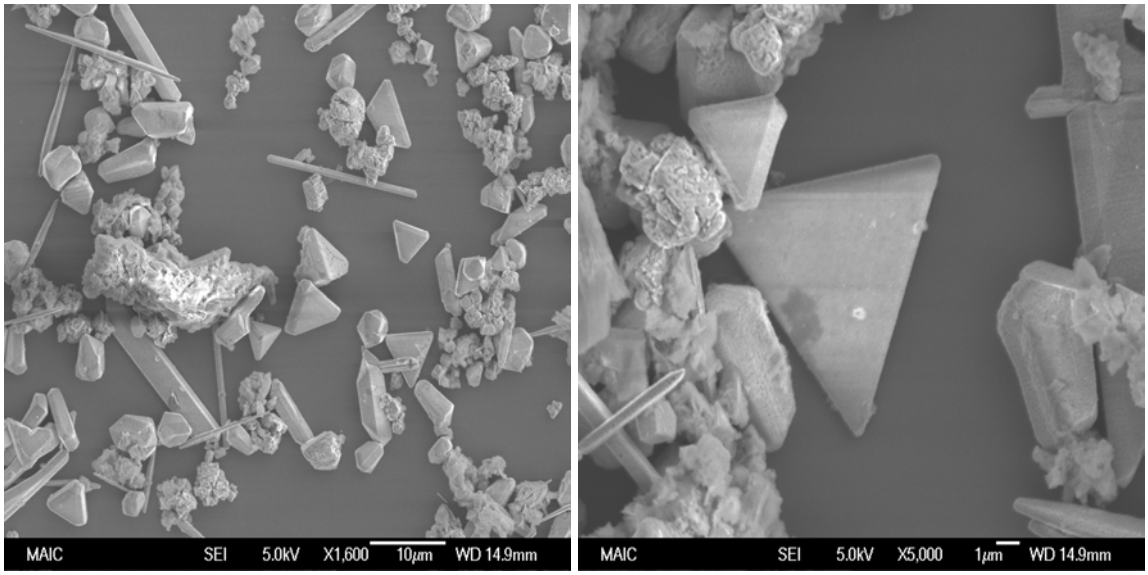

Figure 4-21: Copper platelets mixed with rods, tetrahedra and irregular particles made in a sugar solution.

The platelets were generally thicker than 1 μm and were difficult to analyze with diffraction due to being nearly electron opaque. Diffraction patterns obtained from the thinnest particles found were of fairly poor quantity due to the very long exposure times required to obtain spots from the diffracted beams. These patterns can still be recognized as a [111] axis perpendicular to the platelet face.

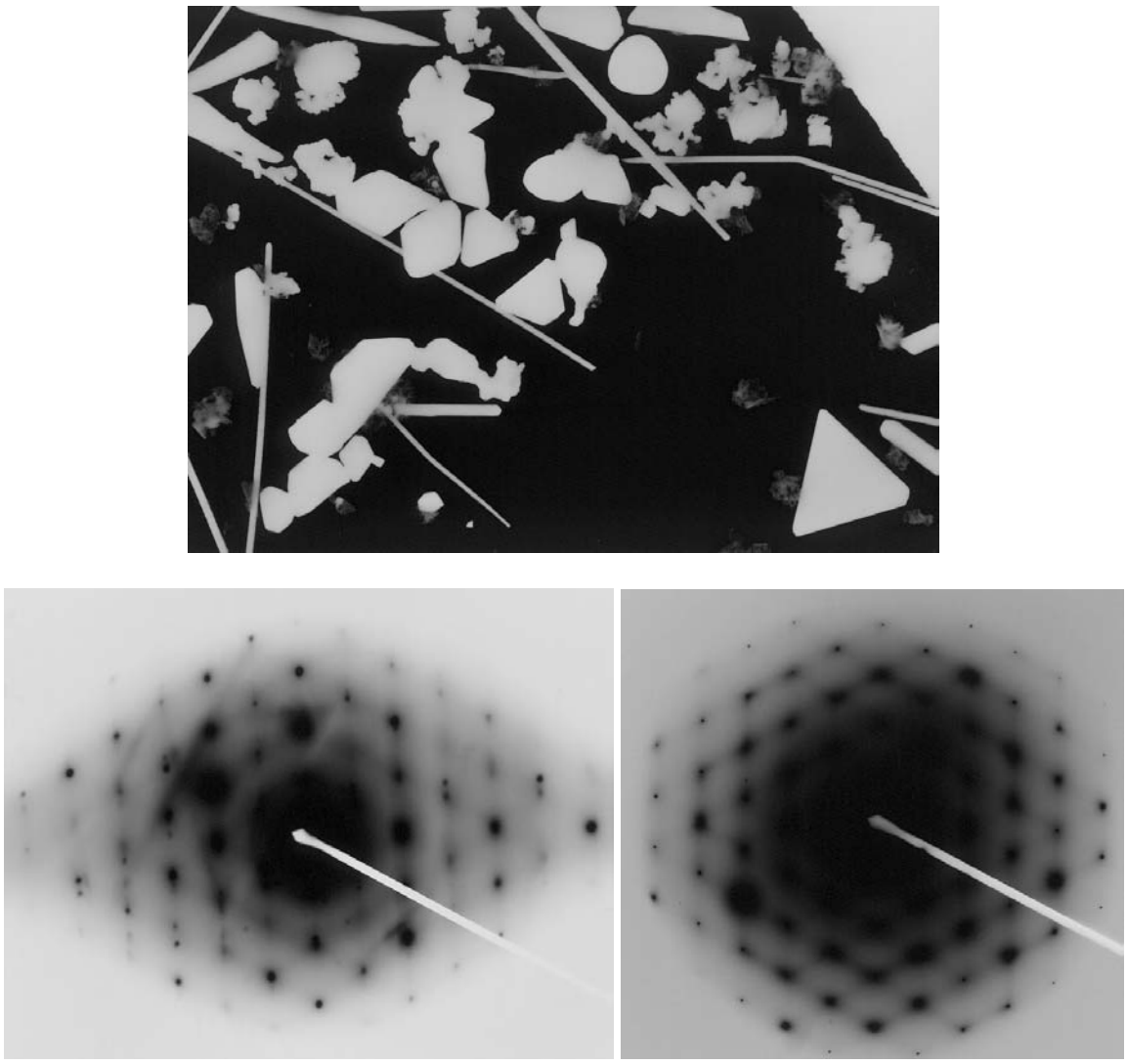

Figure 4-22: TEM data from copper platelets. The bright field negative (above) shows very sharp contrast due to the thickness of the particles. Diffraction patterns of copper platelets were obtained from the thinnest particles indicate a [111] axis when viewing the platelets from above (bottom).

Due to the difficulty in obtaining diffraction patterns, the presence of forbidden spots could not be evaluated. It is clear that all three metals develop prisms with the same crystal habit with very different processing methods.

CHAPTER 5
CRYSTAL HABIT OF ONE DIMENSIONAL METAL COLLOIDS

Application of the Silver Halide Wire Growth Model

Silver halide systems such as AgBr and AgCl have been observed to grow into wires in solution. Given the success in applying the reentrant groove growth mechanism of silver halide platelets to gold, silver, and copper platelets, the corresponding silver halide model for wires will be tested for the metal wires produced for this report [25-27]. The wires contain three crystal variants joined together by three intersecting twin planes. Figure 5-1 shows the internal structure of silver halide wires along with the type of twin plane joining each variant. Two of these twin planes are (111) type planes and one is a (221) type. The three planes radiate out from the axis of the wire, such that the twin planes are parallel to this long axis. The axis for all three variants is a {110} type.

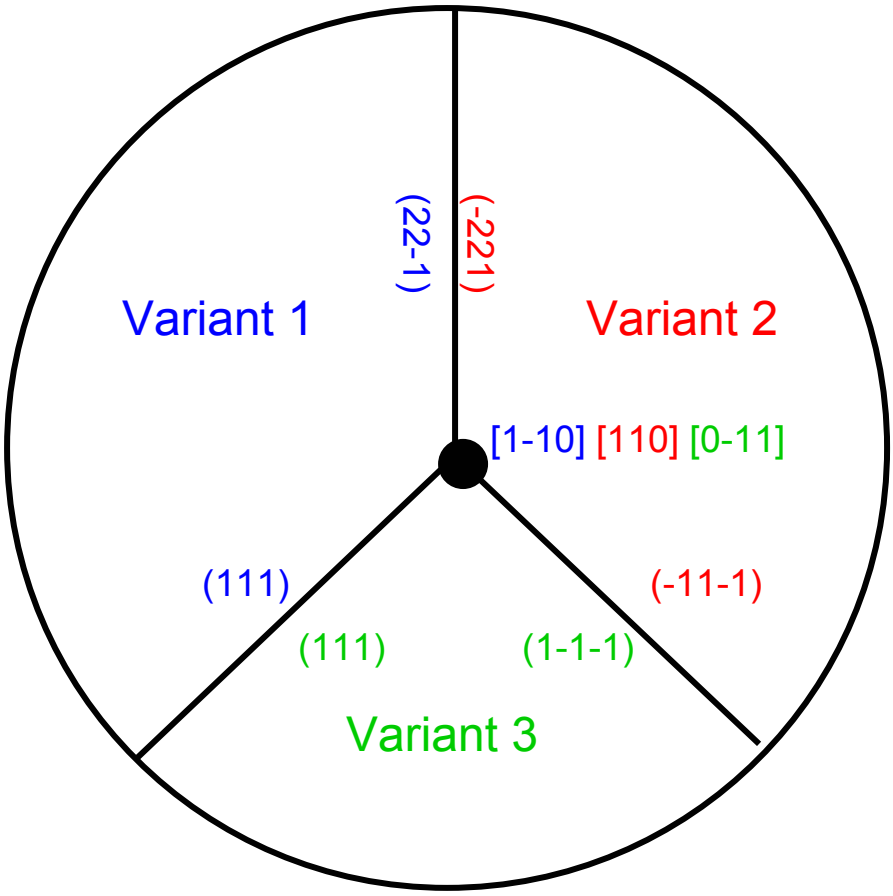

Figure 5-1: Internal structure of silver halide wires looking down the axis of the wire as described in references 25-27. The black lines represent the twin planes joining the variants. The three crystal variants are color coded with the indices of the common planes and directions.

According to reference 27, a wire begins as a hexagonal particle with a single twin, possessing six sides bound by {111} planes. As seen in Chapter 4, the particle has alternating "A" and "B" sides. The "A" sides contain the reentrant grooves where growth is rapid. If a second twin plane forms on one of the "A" sides before it grows outs, the two twin planes will make a 109.5° angle with one another. It is this junction that creates reentrant grooves that regenerate and allow for continuous growth in one dimension.

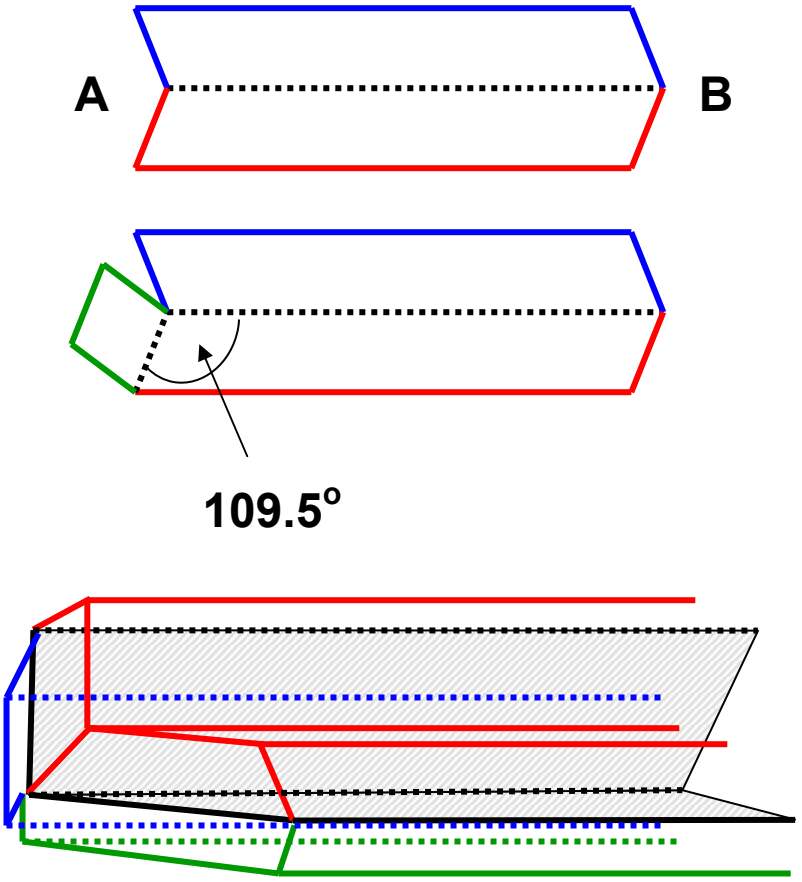

Figure 5-2: Formation of a nanowire. If a twinning event takes place on the fast growing "A" side of a previously twinned particle before the "A" side grows out of existence, a particle with two twins, 109.5° apart, will be formed. The presence of the two twins leads to regenerating reentrant grooves that leads to rapid growth in one direction.

The junction between the twin planes acts as a reentrant groove that causes the adjacent "B" sides, located on each end of the twin plane intersection, to grow out. At this point, two "A" sides meet on each end of the twin plane intersection. Because the attachment of adatoms to one face regenerates the adjacent face, the "A" and "B" sides regenerate one another and particle growth is not arrested. The "B" side across from the twin intersection grows slowly, limiting the lateral growth of the particle. This is demonstrated in Figure 5-3.

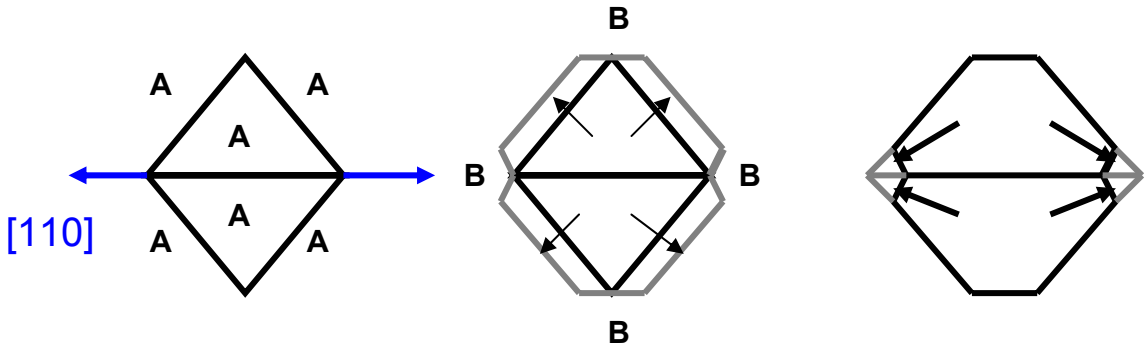

Figure 5-3: Regeneration of reentrant grooves on wire. Looking at two twin planes oriented 109.5^{o} apart, one can imagine two triangular prisms, each with one twin, bound to one another on an "A" side along the [110] direction. The fast growing "A" sides lead to the formation of the slower growing "B" sides. The contact between the two "B" sides along the joint between the twin planes acts as a reentrant groove itself. This regenerates the "A" face and leads to rapid growth parallel to the [110] direction. One of the "B" sides for each prism does not regenerate, and forms the side faces of the growing wire.

Another diagram explaining the mutual regeneration and one-dimensional growth is shown in Figure 5-4.

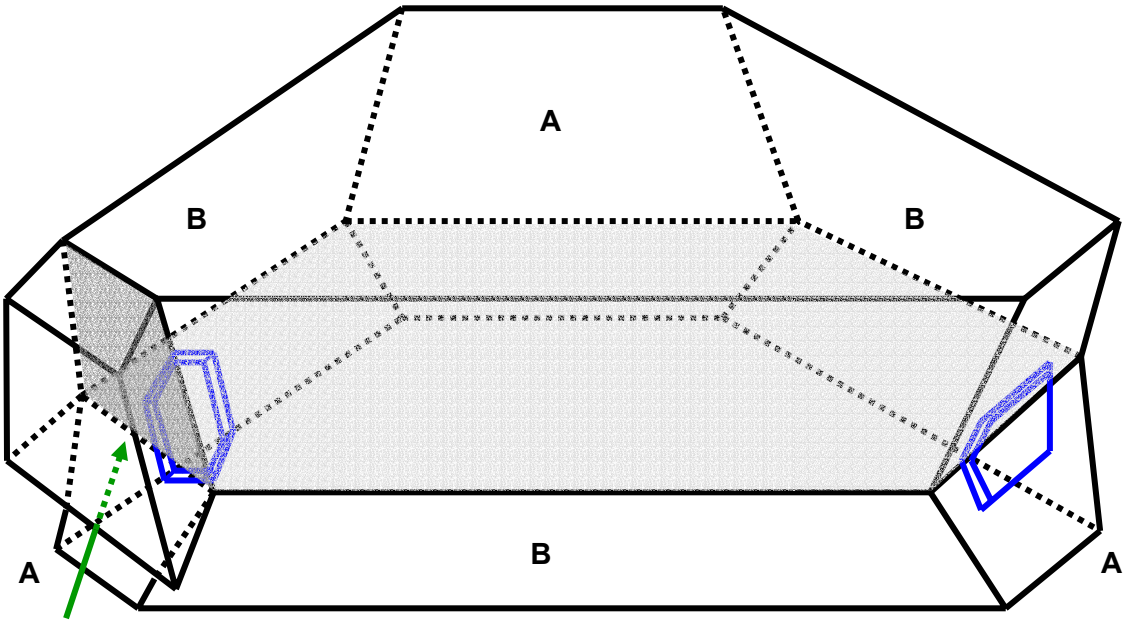

Figure 5-4: Another view of the growth of metal wires. Top; after the formation of a twin plane (light grey), a second twin plane (dark grey) forms on one of the (111) planes that makes up the three reentrant grooves, blocking one reentrant groove (an "A" side) and forming two new ones. The reentrant grooves are sites of rapid addition of material (blue planes).

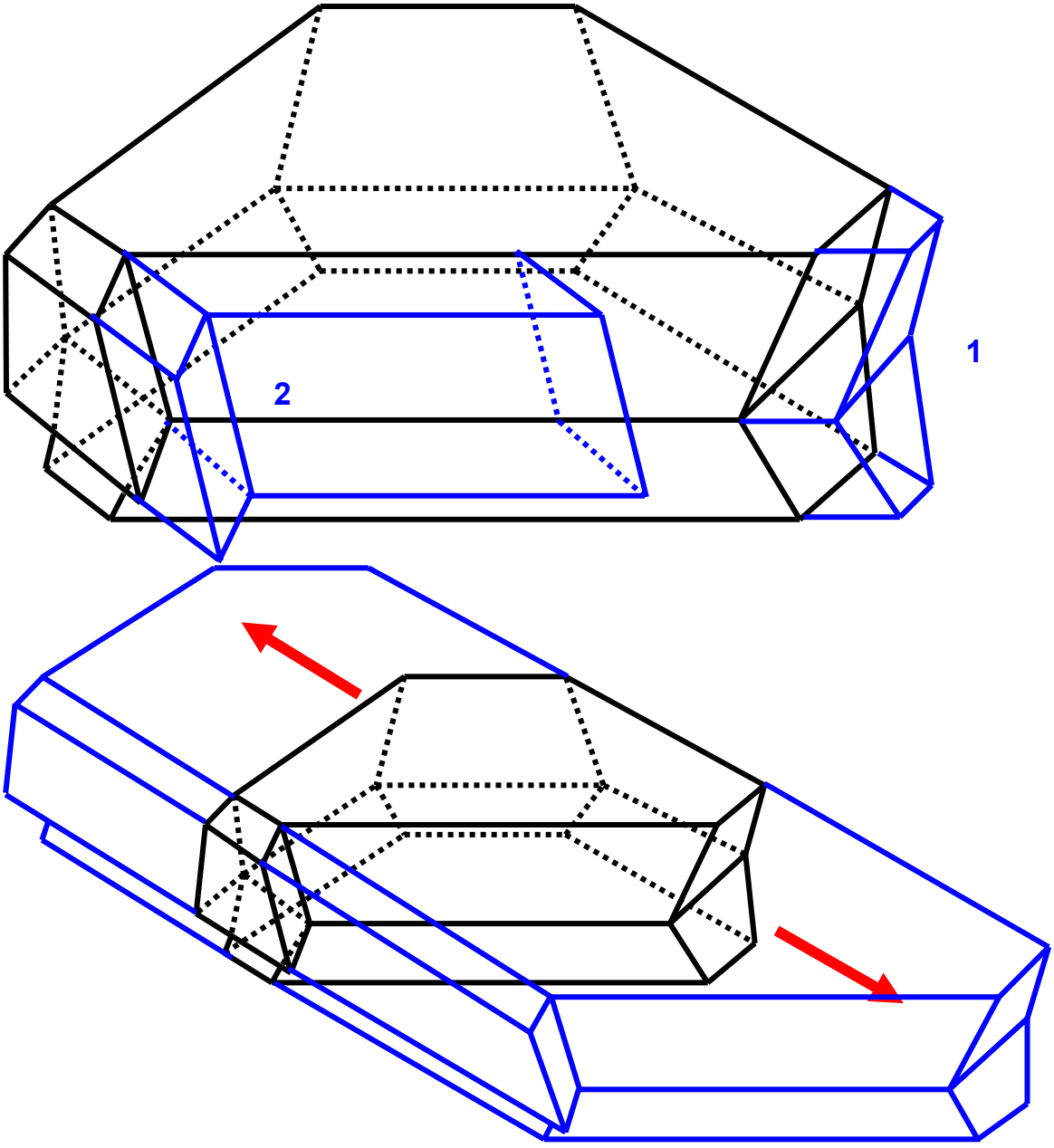

Figure 5-4 (Continue): The intersection of the two twin planes (green arrow) forms a slow growth groove that will later be closed by a (221) plane. Middle; two twin planes in this configuration will regenerate each other. As material is added to groove 1, the two sides bounding the reentrant groove shrink the groove until it vanishes. Material added to groove 2, however, expands one side bounding groove 1, regenerating it. Bottom; the uniaxial growth of a doubly twinned particle.

Created by the two twin planes is a gap designated by the green arrow in Figure 5-4, top image. The two variants on either side of this gap cannot exactly match due to their orientation, requiring the formation of a (221) twin plane. This higher energy twin plane usually grows more slowly than the others, often creating a gap or trench along the growing wire. Together, the two (111) and one (221) twin planes form the cross-section of the wire as it grows.

The faceting of silver halide wires was reported in reference 82. The fact that the two of the variants are larger than the third is caused by the larger angle between the (221) and (111) twin planes compared with the angle between the two (111) twins. This leads to two-fold symmetry down the axis of the wire. As seen in Figure 5-5, there are four {111} side faces, two {100} side faces, two {111} end faces and two {100} end faces. The (221) twin plane runs along the edge between the two {100} end faces.

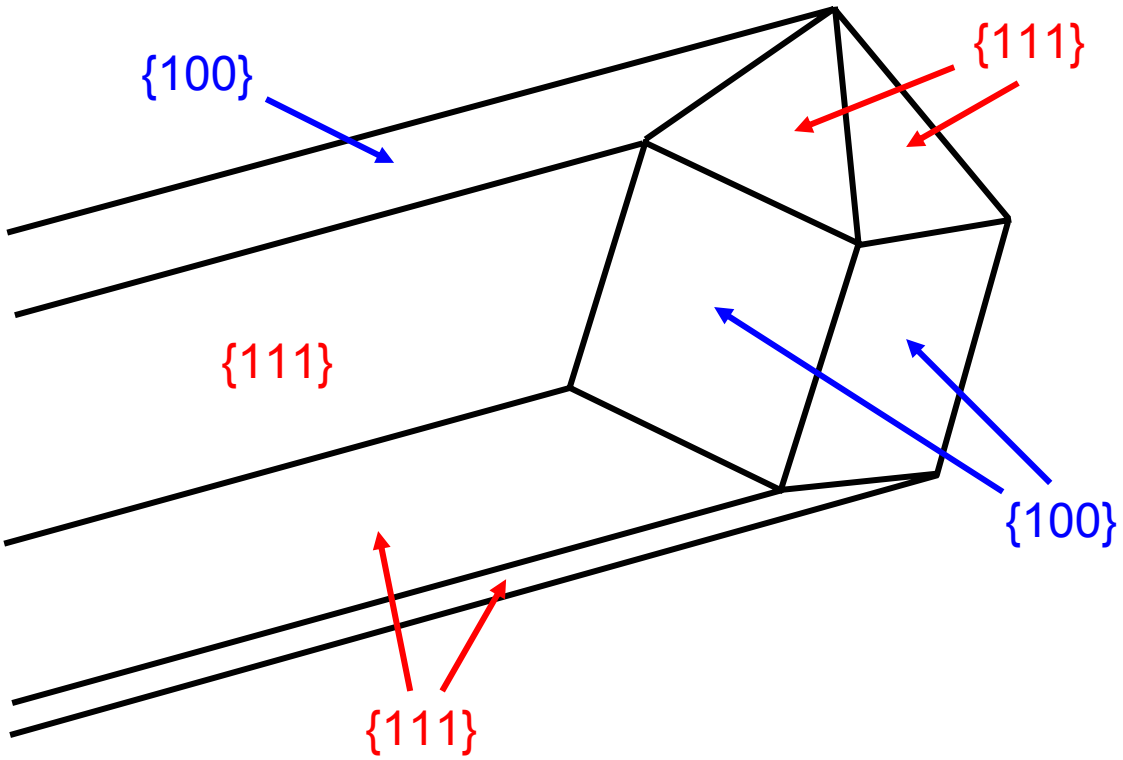

Figure 5-5: Faceting of silver halide wires according to reference 82.

To assist in determination of the validity of silver halide model for the metal rods, a stereographic projection was prepared using Desktop Microscopist for the cross-section of a rod. Because the rods will be primarily observed perpendicular to their axis, this will assist in identifying the location of twin interfaces and the crystallographic directions associated with them. This projection is shown in Figure 5-6. The three variants are distinguished using blue, red and green indices, and the twin planes are identified by the variants they separate. All three variants are oriented with a [110] type direction projecting out of the page. Of particular interest will be the overlapping [114] and [011] zones along the [221] twin planes, the [112], [001], and [122] zones nearly overlapping and the [114] zone nearly overlapping the [111] twin planes.

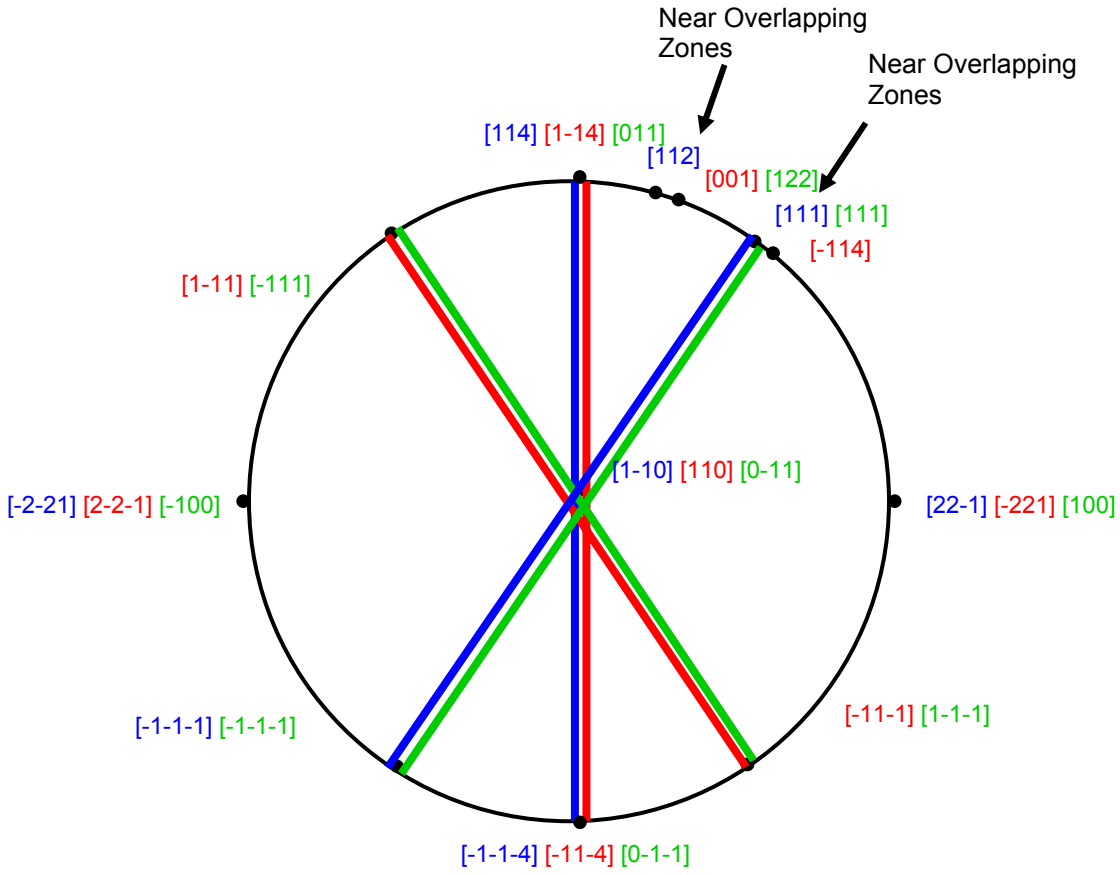

Figure 5-6: Superpositioned crystallographic projections of the three proposed crystal variants present in the wire. Blue denotes variant 1, red variant 2, and green

denotes variant 3. The direction of the three twin planes and the variant they separate are designated by the colored lines.

Silver Nanowires from the Polyol Method

Silver nanowires prepared by the polyol process in EG were observed in the SEM and are shown in Figure 5-7.

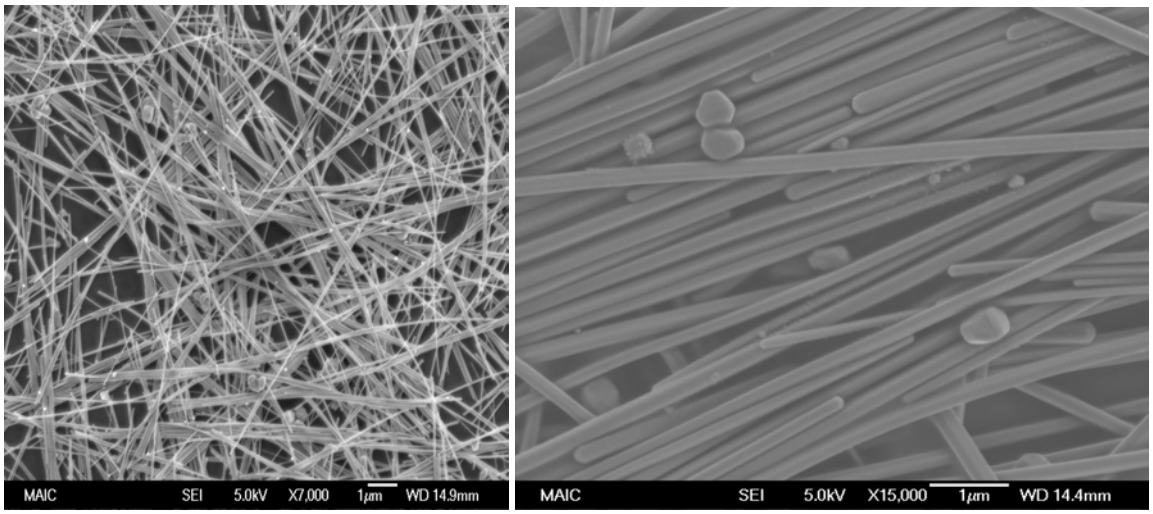

Figure 5-7: SEM of silver wires made by the polyol process.

The nanowires were found to range in diameter from 100 to 300 nm and were largely longer than 10 μm. Although the diameter of the wires varied from batch to batch, the diameter of wires within a batch was highly uniform. The yield of wires was high, although a small percentage of the material consisted of faceted, but fairly isotropic particles. Depending on the processing of the wires, more or less faceted structures were seen. Generally, the wires appeared circular in cross-section, but if sample's growth was rapidly quenched by pouring the hot sample directly out of the reaction vessel into acetone, more faceted wires were observed. It is believed that the sudden termination of silver addition by cooling and by the addition of a solvent in which PVP is insoluble, preserves the wire facets present during growth. If the suspension of wires is allowed to slowly cool in the mother liquor containing soluble silver species, much more rounded

cross-sections were observed. Longer reaction times also seem to improve faceting. Silver wires with a high degree of faceting are shown in Figure 5-8.

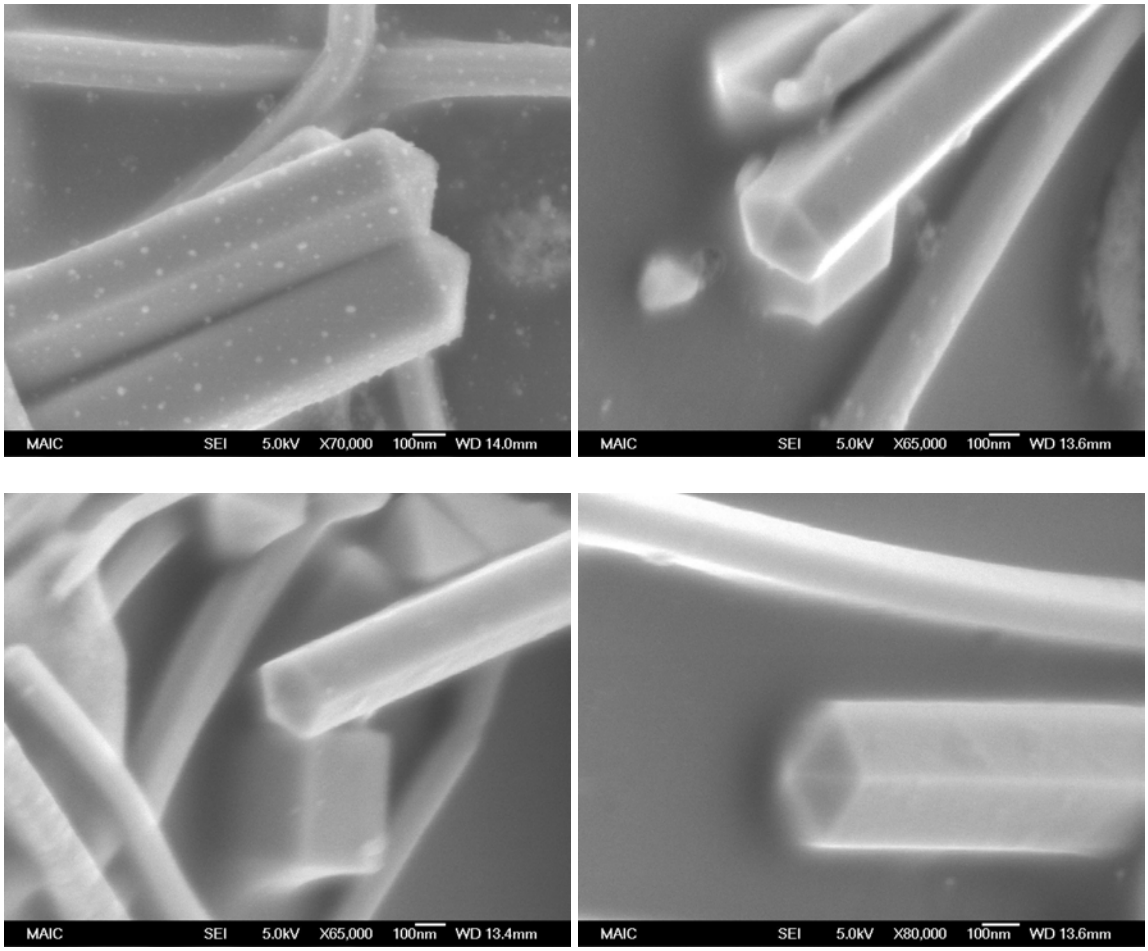

Figure 5-8: SEM images of silver wires showing faceting at the tip. Pentagonal cross-sections were observed for a majority of the wires.

Instead of the expected two-fold symmetry of the wire cross-section, with six side faces, the wires consistently had five-fold, pentagonal cross-sections. The end facets cut out identical angles and the side faces were of identical shape and size.

A single silver nanowire was observed under TEM in order to determine its internal structure. Contrast lines due to twin planes were frequently observed along the length of the wires. Figure 5-9 shows the wire and two diffraction patterns obtained after rotation of the wire about the long axis in order to find an identifiable zone axis.

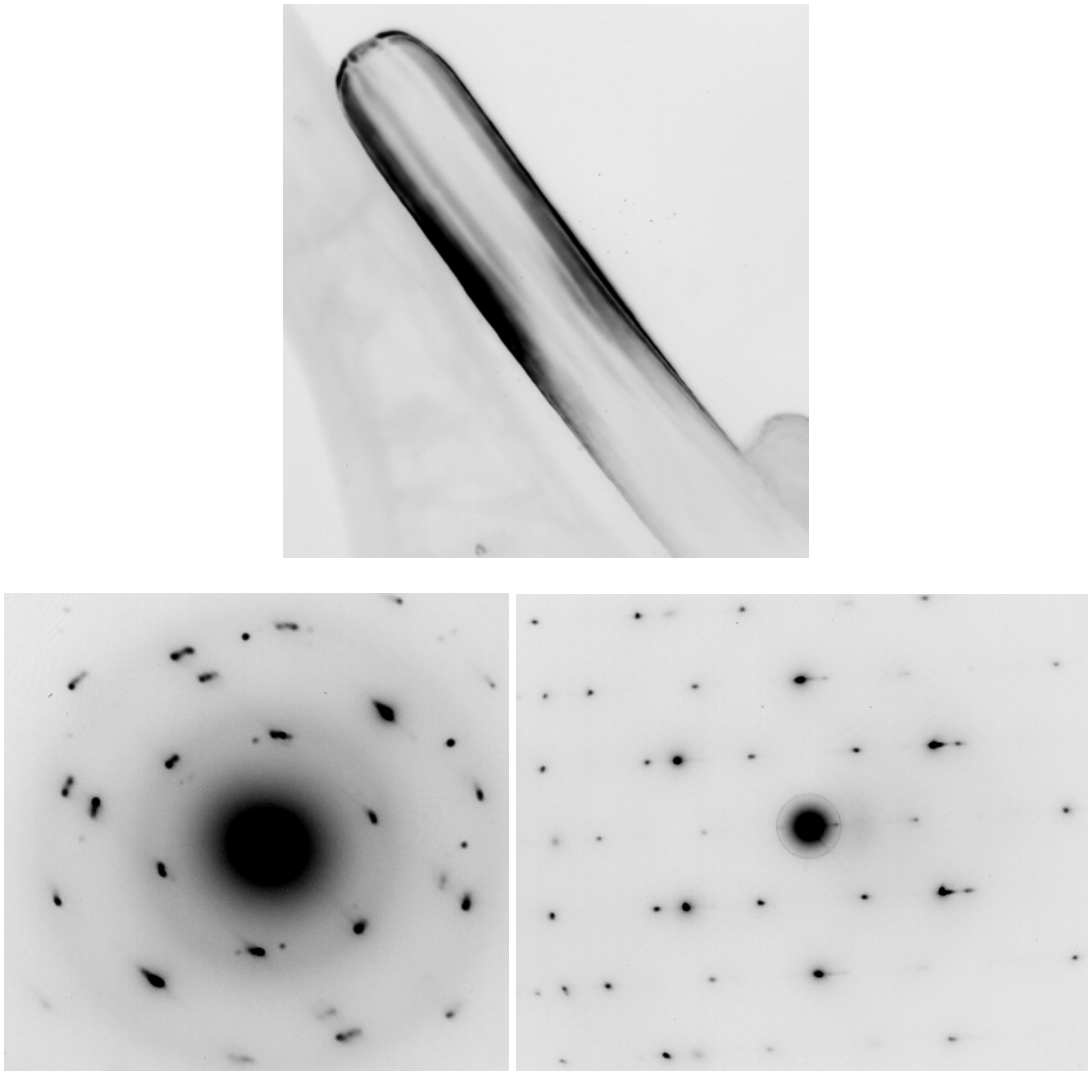

Figure 5-9: At the top is a bright field TEM image of a silver wire. Diffraction patterns at the bottom were generated by rotation about the long axis of this wire. Each was taken at a slightly different angle. The two diffraction patterns are superimposed [111] and [110] type patterns.

As can be seen by the bright field image, no twin plane is aligned with this zone axis. The diffraction patterns can be indexed as a [111] type pattern superimposed on [110]. In both patterns, the 220 spots at the top and bottom of the image overlap for the superimposed axes, indicating that a twin with a common [110] type direction exists in the wire. Accounting for the rotation of the image relative to the diffraction pattern at the camera length used, this pair of overlapping spots lies parallel to the axis of the wire.

The superimposed pair could not be generated from the stereographic data generated from the silver halide model, and thus appears to indicate two or more variants oriented in some different manner.

Tilting the wire approximately 18 degrees from the axis in Figure 5-9, revealed a contrast line down the axis of the wire that appears to be a twin plane. Figure 5-10 shows a bright field image of this angle, with a dark field image where the diffracted beam of one half of the wire is observed. In addition, the diffraction pattern from this angle is shown.

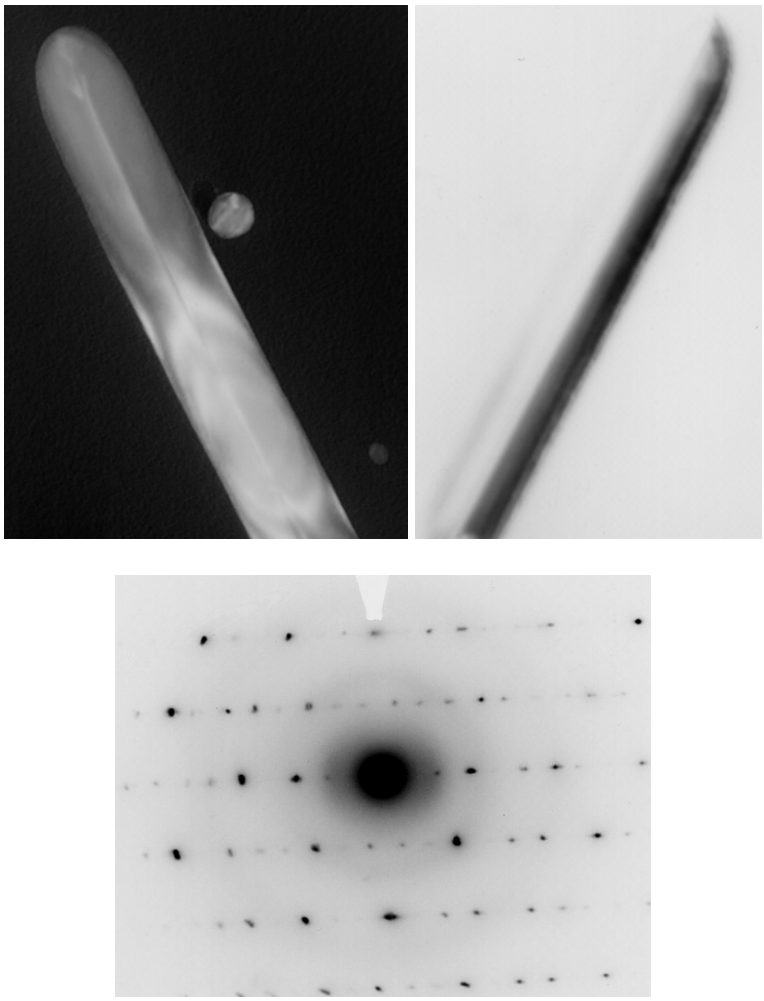

Figures 5-10: At the top are bright and dark field images of the silver wire rotated to maximize the appearance of the contrast line seen along the length of the wire. At the bottom is the corresponding diffraction pattern at this rotation.

The diffraction pattern indicates the superposition of a [100] and a [211] pattern with one pair of 220 spots overlapping (at the top and bottom of the image). These overlapping spots again indicate that the [110] type direction is held in common between two twins. Again rotating the image and diffraction pattern, the overlapping spots are found to lie parallel to the contrast line running down the axis, further indicating that the line observed in the images is a twin plane. Furthermore, as the contrast line is found to extend the entire length of the wire, which means that the wire's crystallographic growth direction is of a [110] type. If the twin plane is assumed to be a (111) plane, and if the direction of the wire is a [110] type direction, then a [211] type direction must lie in the twin plane and point perpendicular to the axis length. Thus, the [211] pattern can be expected for diffraction from both crystals on either side of the twin plane. The [100] type pattern cannot be accounted for by using the silver halide model.

Although the silver wires clearly have twin planes down their long axes and their long axes are a [110] type direction, the rest of the data does not support the silver halide model. Both diffraction data and faceting of the wires indicates a different orientation and internal structure of the wires. These features will reappear, however, in other one-dimensional metal samples.

Silver Nanorods from Aqueous Reduction on Seeds

Silver particles formed using the Murphy method were investigated using high-resolution TEM. The particles had a wide variety of morphologies, falling in to three general types; rod and wire like, truncated triangular and hexagonal platelets, and isotropic particles.

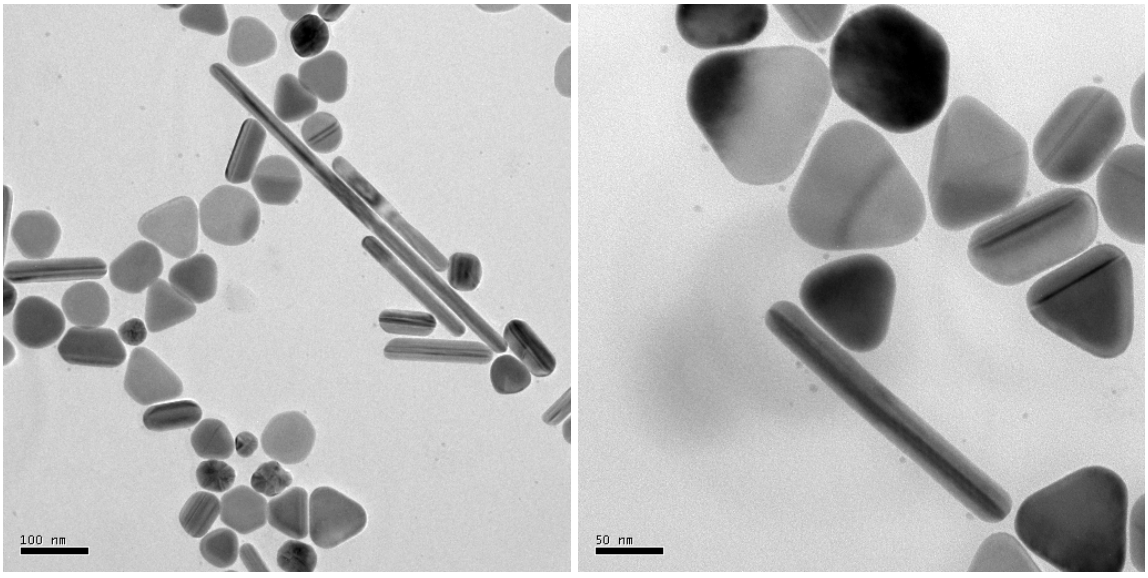

Figure 5-11: HRTEM images of silver particles fabricated using the Murphy method. All the rods observed clear contrast variations down their axes, making the presence of twin planes parallel to the axis apparent. Interestingly, little or no tilting from grid normal was necessary to observe the planes.

All of the nanorods contained contrast lines down their axes, indicating twinning. Little or no tilting from the grid normal was necessary to image most of these twin planes, indicating that the particles were faceted and that there was always a twin plane perpendicular to the face upon which the particle rested on the carbon film. This is not consistent with the silver halide model, because there is no side face exactly perpendicular to a twin plane. Diffraction patterns were taken of rods parallel to the twinning plane, as seen in Figure 5-12.

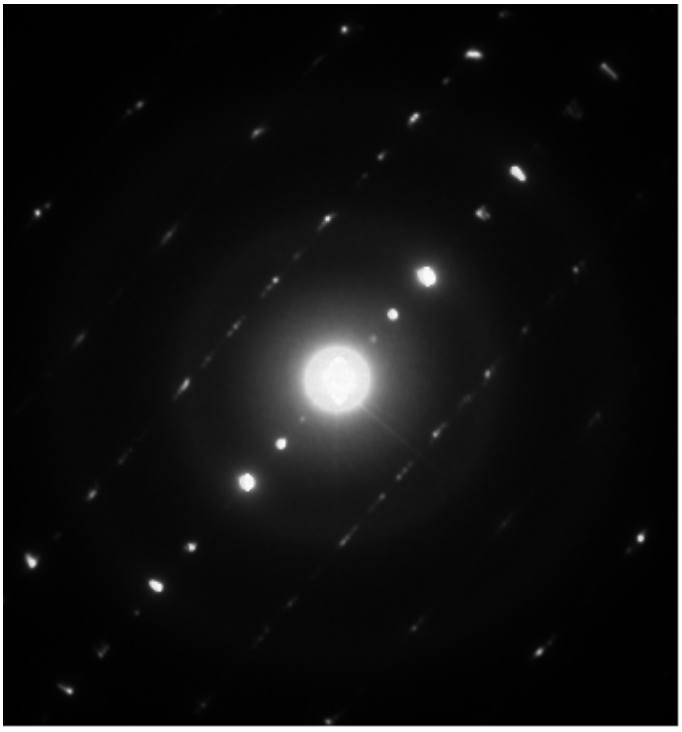

Figure 5-12: Diffraction pattern taken on a particle parallel to a twin plane. The pattern is indexed as a [100] superimposed on a [211] type pattern.

The diffraction pattern was indexed as a [100] superimposed on a [211] type pattern. The 220 spots are superimposed, indicating that this direction is shared by two crystals. This is identical to the silver wires formed by the polyol process when observed parallel to a twin plane. Diffraction patterns were also taken when the rods were tilted approximately 18° from the twin plane. At this angle, two superimposed zone axes were imaged, as seen in Figure 5-13.

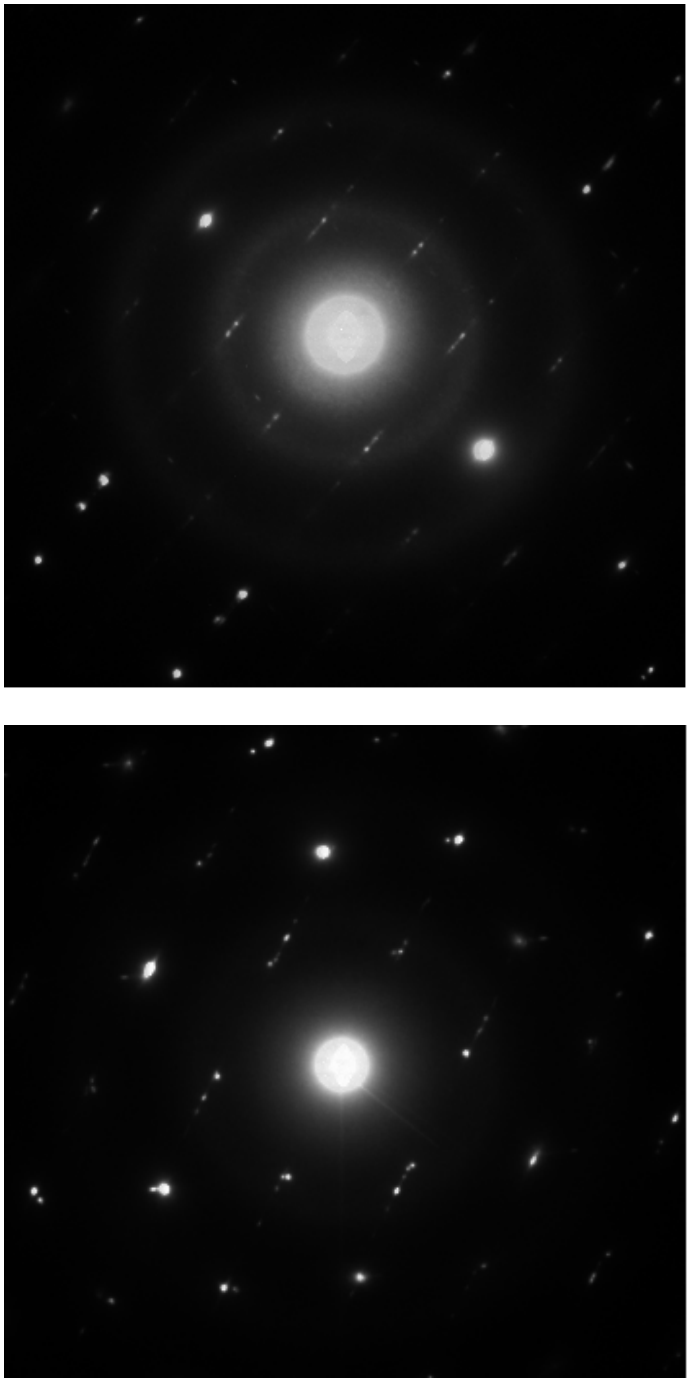

Figure 5-13: Diffraction patterns taken from different silver rods by tilting away from the twin plane approximately 17°. The two patterns can be indexed as a [110] pattern superimposed on [111] pattern.

In each case, [111] and [110] patterns are seen superimposed on each other. Like the silver wires from the polyol process, they have superimposed 220 spots. This

indicates a [110] type axis direction shared by one or more crystal variants. As with the polyol silver wires, this data does not support the silver halide model.

Gold Rods from the Polyol Method

Gold rods were one of the products of reducing gold chloride in EG. The rods were much larger in diameter than those formed by any other method. The rods were generally 500nm to 1μm in diameter and several micrometers in length. Like the silver wires formed in the polyol process, clear five-fold symmetry was observed in cross-section.

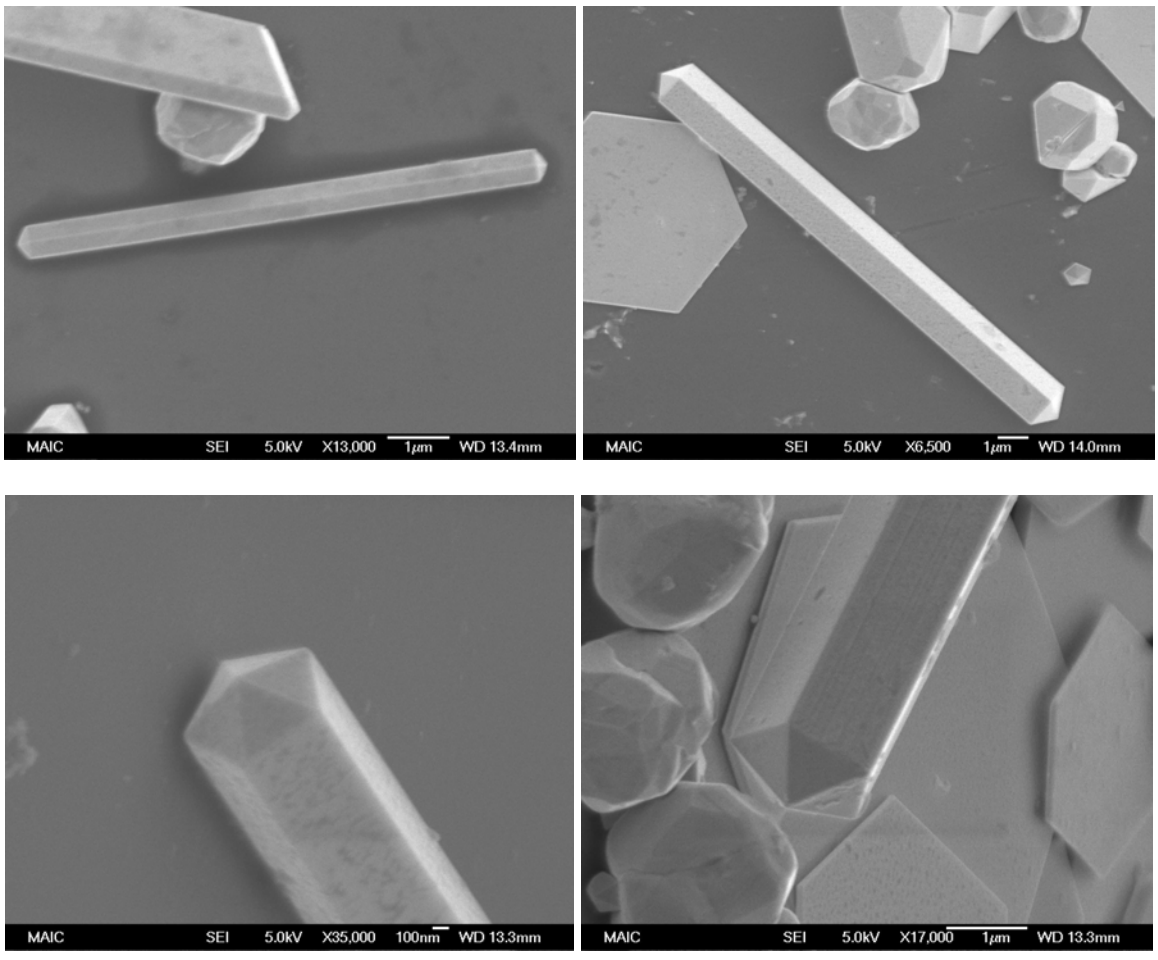

Figure 5-14: SEM images of gold rods formed by the polyol process. As in the silver wires, these rods have clear five-fold symmetry down their axis.

TEM of gold rods was difficult due to the thickness of the rods. As seen in Figure 5-15, the rods were nearly electron opaque and twin planes could not be observed. Diffraction

patterns were difficult to obtain because the image had to be exposed for a long period of time to image the spots outside of the main beam.

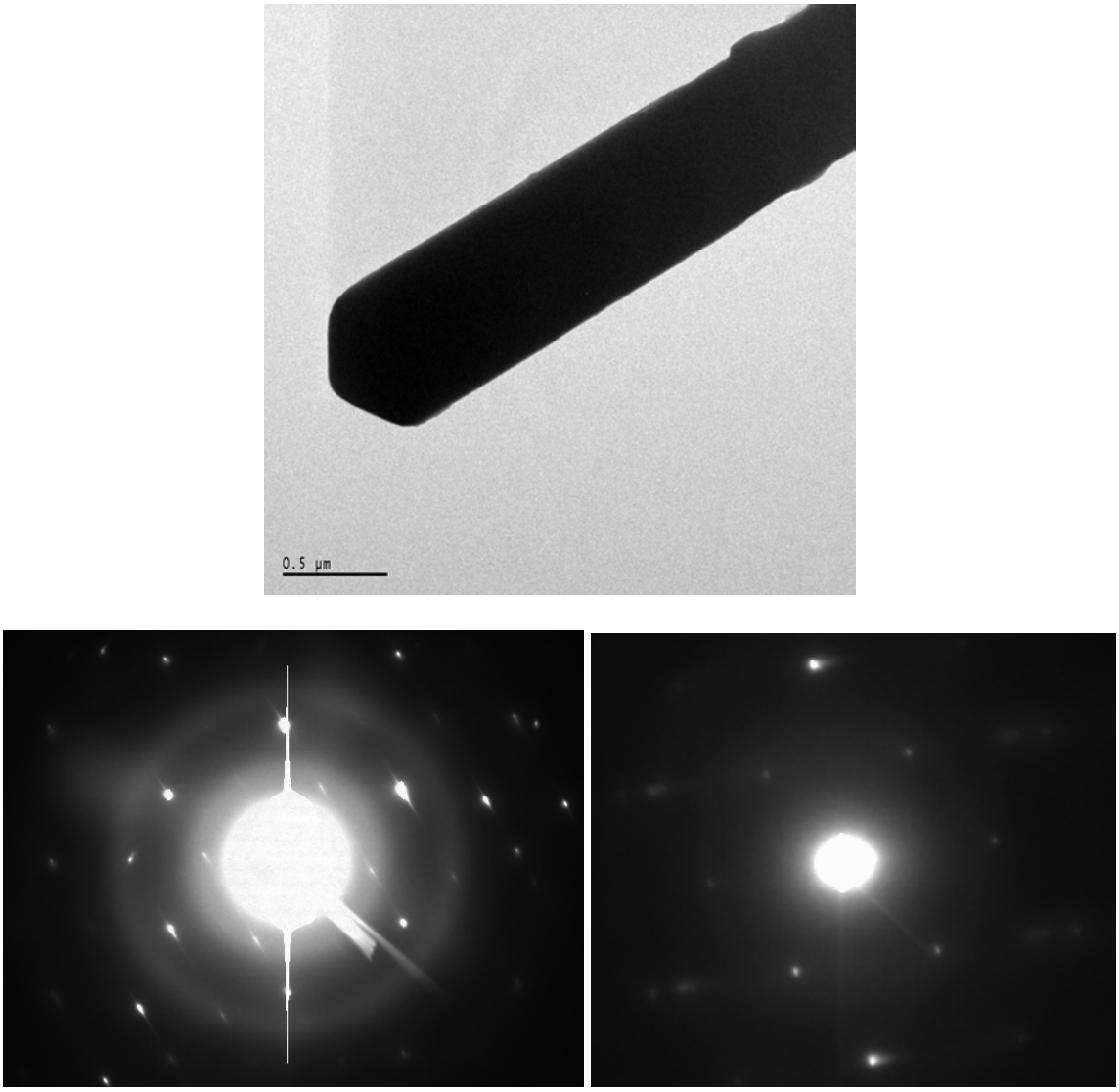

Figure 5-15: TEM data for gold rods formed by the polyol process. The top image shows the tip of a gold rod. The bottom image on the left is a diffraction pattern showing the superposition of a [111] pattern on a [110]. On the right is another example from a different rod.

The diffraction patterns can be indexed as superimposed [111] and [110] patterns identical to that observed in the silver samples. This data again indicates that a new model of the internal structure of the metal rods needs to be developed.

Gold Nanorods from Aqueous Reduction on Seeds

HRTEM was used to investigate gold nanorods synthesized in aqueous solution following Murphy's method of forming seeds capped with citric acid followed by additional gold reduction in concentrated CTAB. The product was a mixture of rods, triangular prisms and multiply twinned particles. The rods were in the size range of 20 to 40 nm in diameter with lengths of a 100 to 200 nm. A gold rod is shown in Figure 5-16.

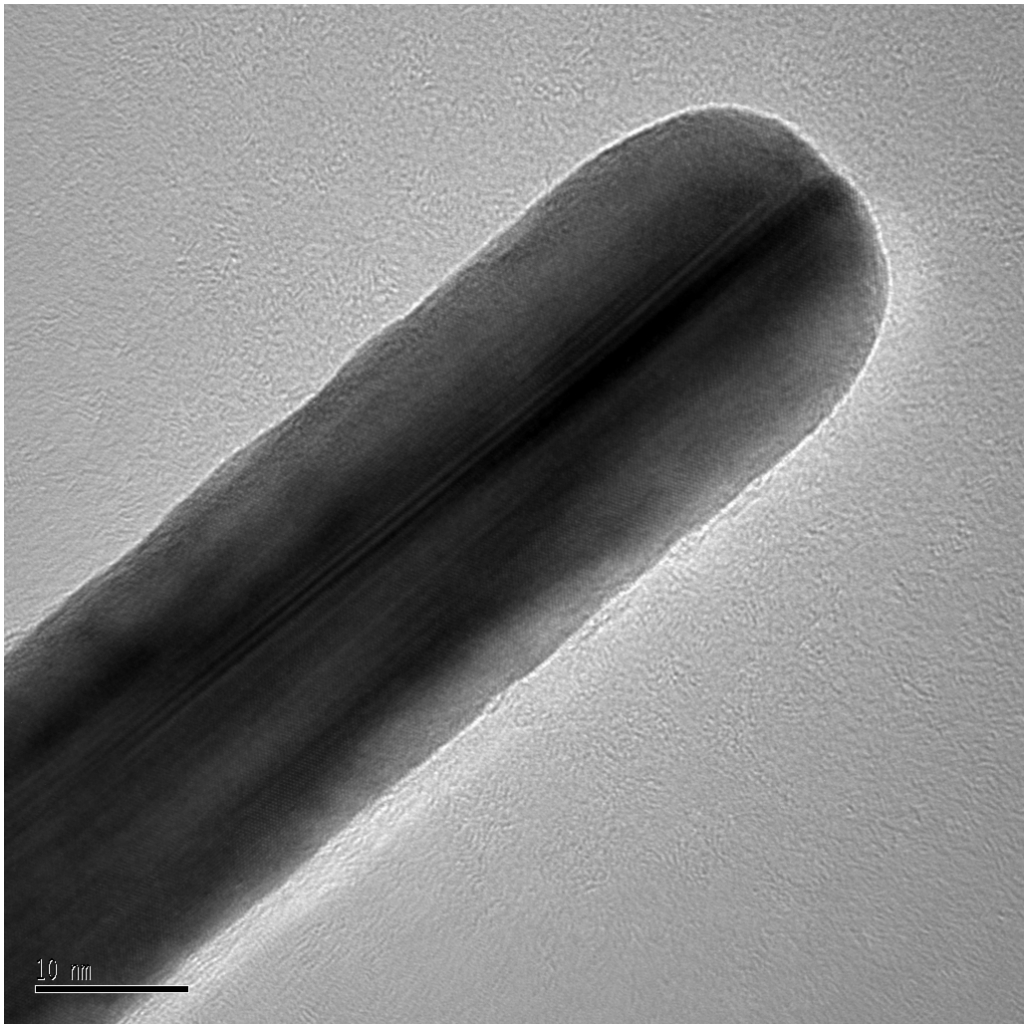

Figure 5-16: Gold rods produced according to the Murphy method in aqueous solution. Widely spaced contrast lines, larger that lattice planes, can be seen down the central axis of the rod. These may arise from double diffraction or Moiré fringes from multiple crystal variants intercepted by the beam in the rod center.

Unlike the silver rods formed by the same process, twin planes could not be observed as easily and were often not perpendicular to the grid. The latter issue is likely due to less faceting and a more circular cross-section. When atomic resolution could be obtained along a <100> axis, (111) lattice lines could be seen near the edges of the rod. Towards the center of the rod, the lattice lines became much larger than the (111) spacing. These could possibly arise from double diffraction or Moiré fringes created by multiple crystal variants.

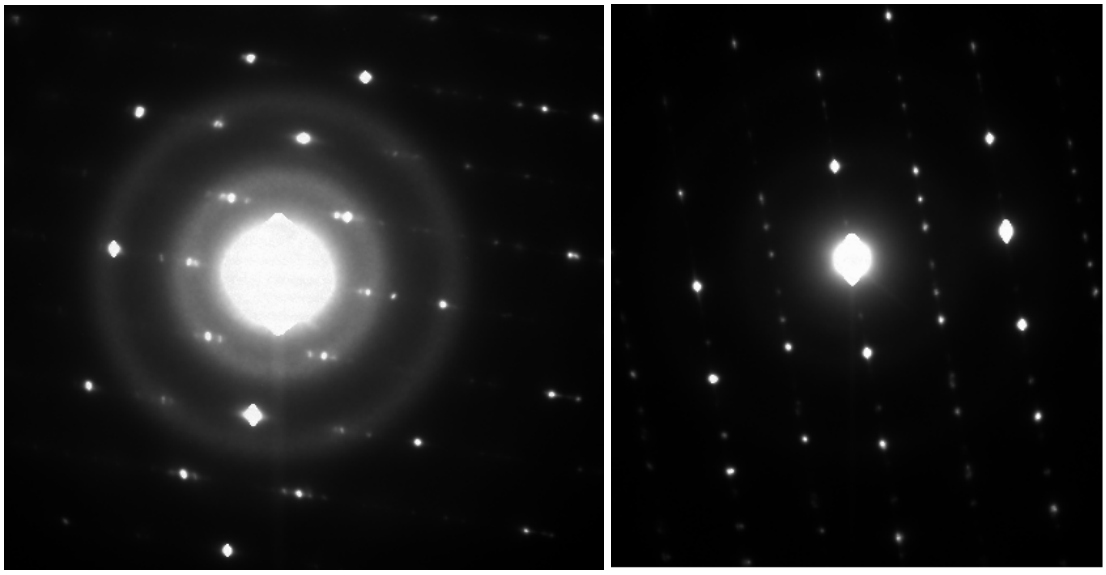

Figure 5-17: Diffraction patterns of gold rods. The pattern on the left was taken on a rod tilted so as to obtain a [111] pattern superimposed on [110]. No twinning was observed at this angle in bright field mode. The right images was taken on a rod tilted down a contrast line showing a [100] pattern on a [211].

The diffraction patterns of gold nanorods showed the same superimposed patterns observed in silver. Parallel to twinning, [100] and [211] patterns were observed, while [111] on [110] patterns were observed when twinning could not be seen in bright field mode. This system is identical to the previously described systems.

Gold Nanorods from Electrochemical Reduction

Gold rods were synthesized using electrochemical reduction with a gold anode and a platinum cathode. The gold was oxidized from the sacrificial anode and reduced as nanoparticles coated by amine surfactants near the cathode. This process generally produced spherical particles, but some batches had large numbers of rods. The diameter of the rods varied from approximately 20 to 60 nm, but was very uniform within batches. The length of the rods varied significantly within batches and between batches.

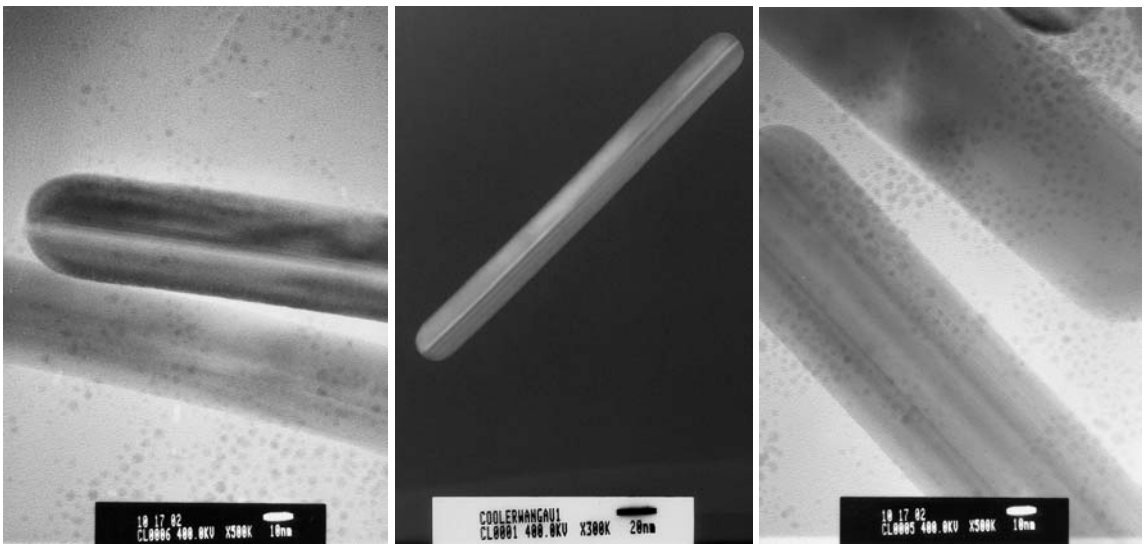

Figure 5-18: Gold nanorods formed through electrochemical reduction. The left and center images clearly show twin planes. The image on the right shows the larger contrast fringes observed in the gold rods formed in the Murphy method.

HRTEM of the rods reveal twin plane contrast down the axes of the rods. Depending on tilting of the rods, twinning or contrast fringes were observed. The fringes were similar in nature to those in the gold rods formed by the Murphy method and only appeared in the center of the rod.

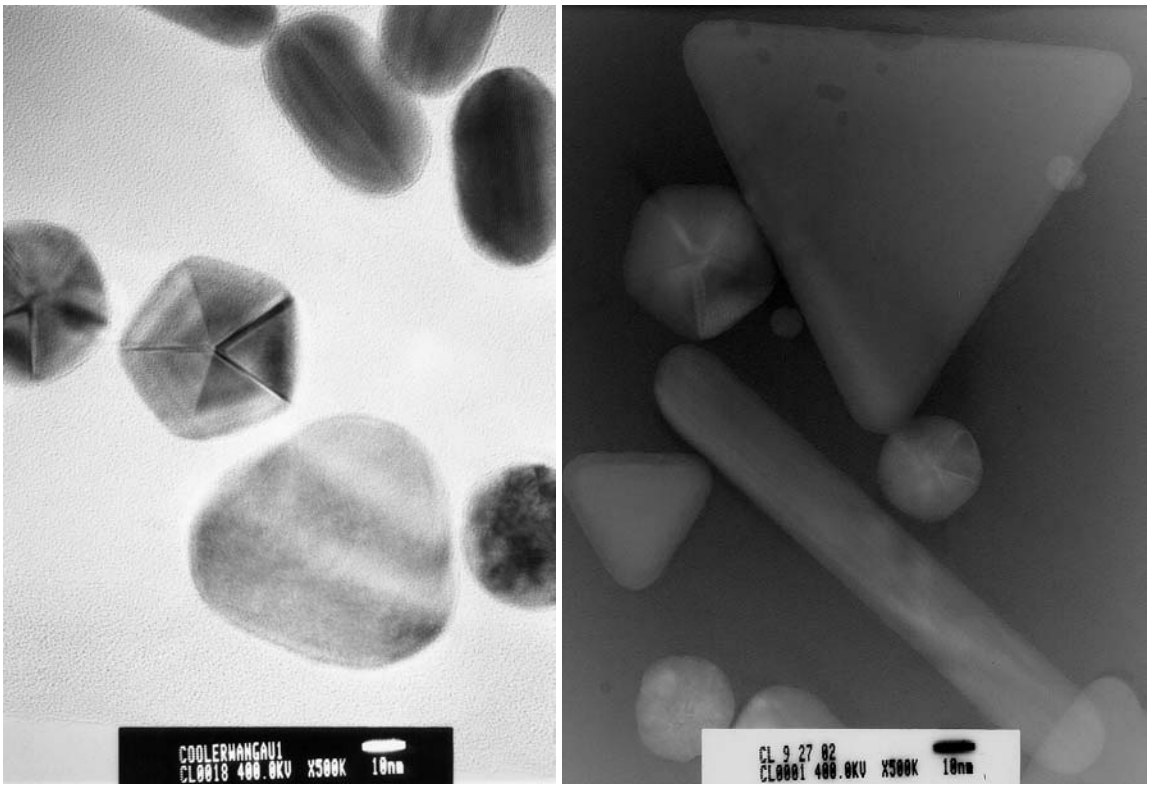

Figure 5-19: Particles with five-fold twinning. These particles were occasionally observed in the samples. They have the same profile as the ends of the silver and gold particles made by the polyol process.

In each batch, a limited number of particles were observed with five-fold twinning identical to the cross-sections of the silver and gold particles made by the polyol process. The shape and orientation of these particles could not be determined.

Copper Nanorods from Reduction in a Sugar Solution

Copper rods were synthesized by reducing copper (I) oxide in a heated sugar solution. The rods were all approximately 1 μm in diameter and several micrometers in length. They were mixed with prisms, isotropic particles and unreduced copper oxide.

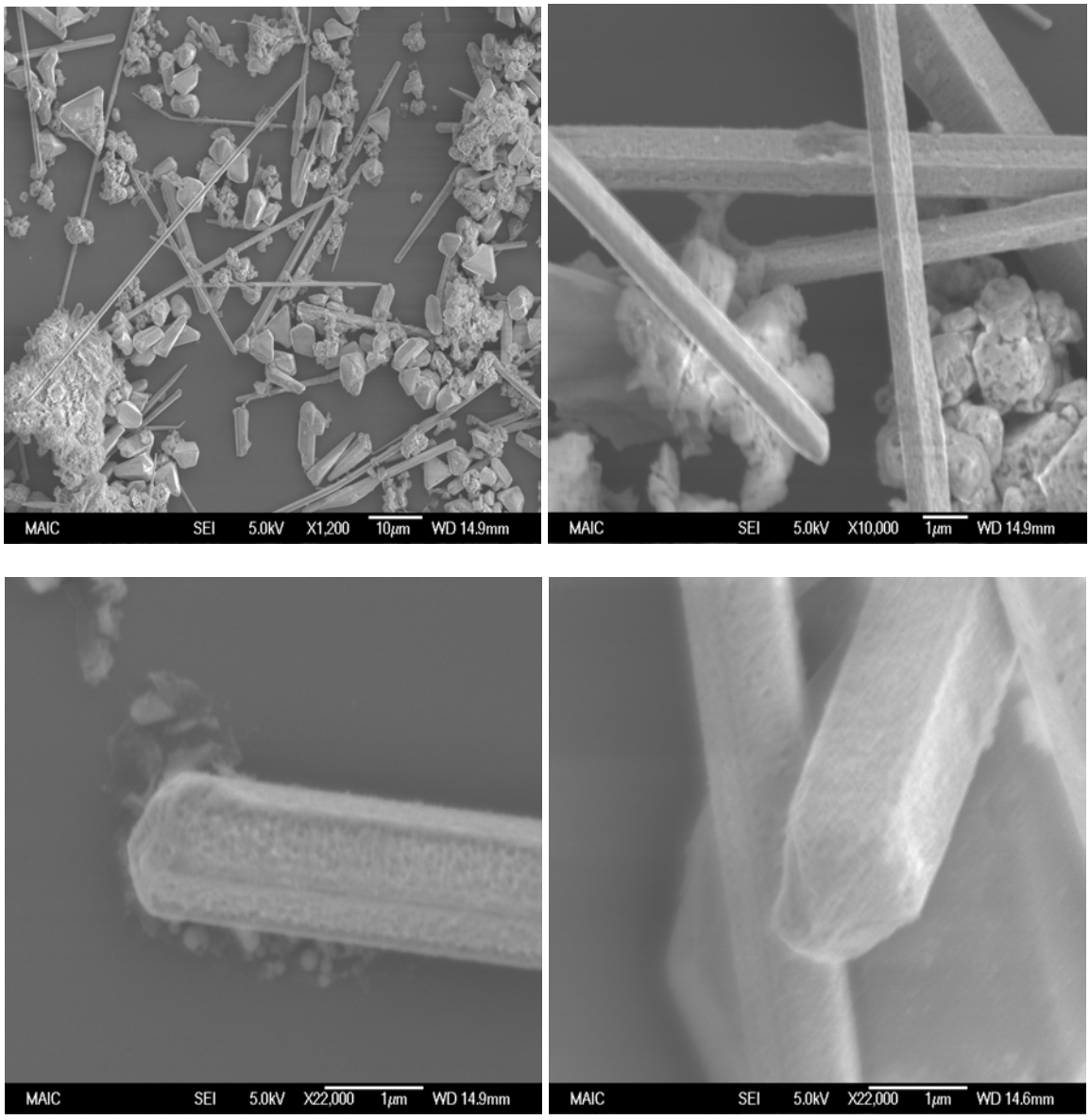

Figure 5-20: Copper rods formed by the reduction of copper (I) oxide in a heated sugar solution. Although the rods often appeared pitted, clear five-fold symmetry was visible on the rods.

As can be seen in Figure 5-20, the rods were highly faceted, but also heavily pitted. This may indicate that oxidation took place locally in the solution after the formation of the rods. Five-fold symmetry was still clearly visible for most of the rods. The thickness of the rods made diffraction very difficult, although with very long exposure times, patterns could be obtained. The patterns are shown in Figure 5-21, and are [100]

superimposed on [211] type patterns. This again follows the data collected for the other one-dimensional particles.

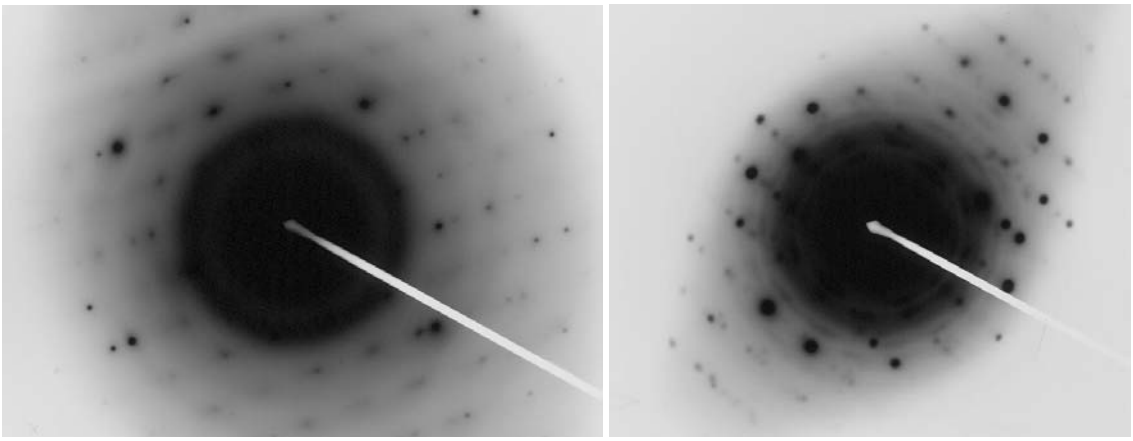

Figure 5-21: TEM diffraction patterns taken from a copper rod showing superimposed [100] and [211] patterns.

Cross-Section Analysis

In order to better evaluate the internal structure of the one-dimensional particles, samples were cross-sectioned using two methods and observed using HRTEM. In the first method, silver wires from the polyol process were deposited on a silicon wafer. Two such wafers were bonded using epoxy, and a stack of wafers was made. The stack was cut into thin slices and circular samples were cored out of the slices. These TEM grid sized samples were polished, dimpled and ion milled at a low angle in a Precisions Ion Mill (PIPS). In the HRTEM, some of the wires were found to be nearly parallel to the beam and were thin enough to observe their cross-section. Images from these samples are shown in Figure 5-22.

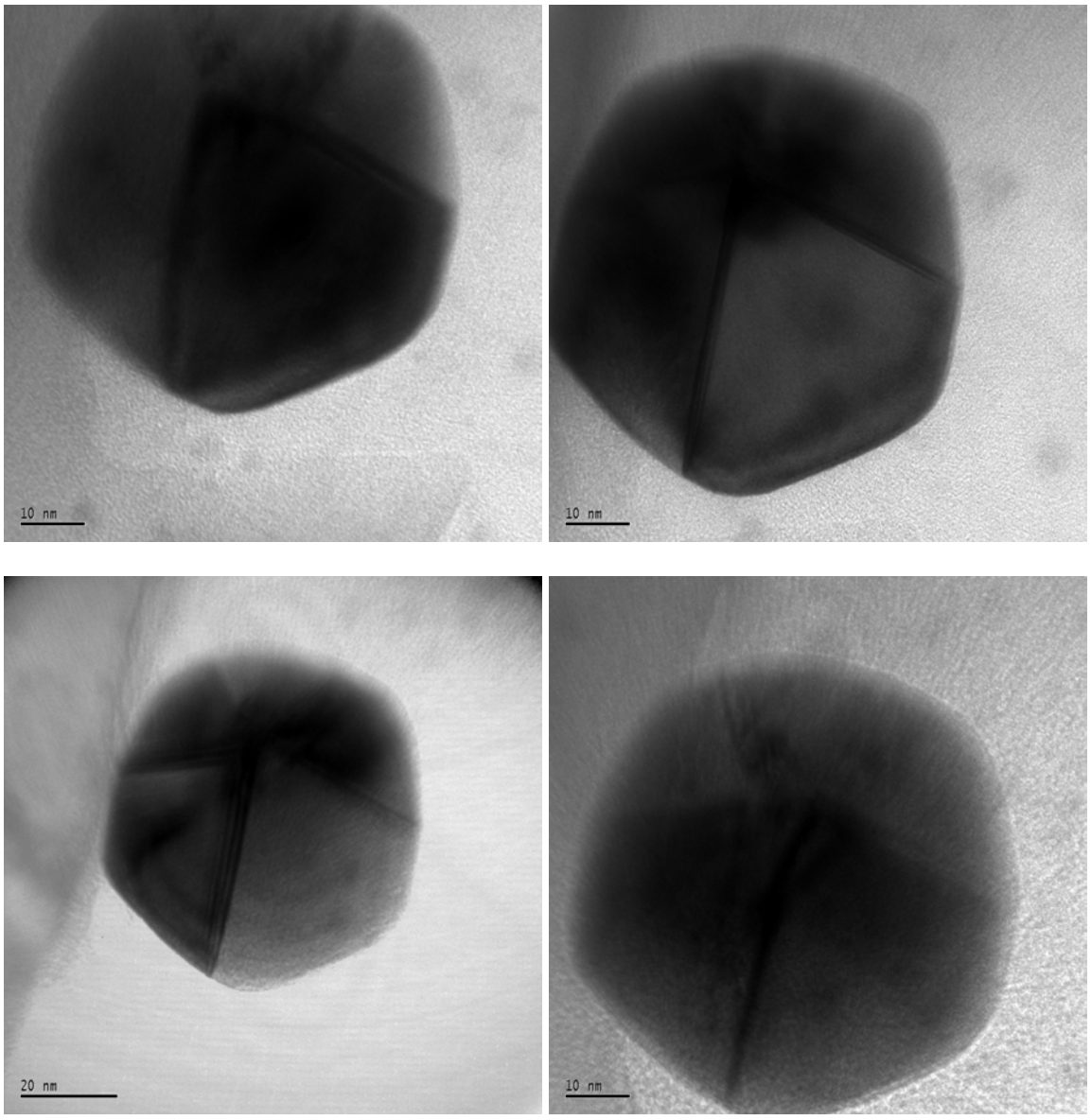

Figure 5-22: TEM images of silver wires cross-sectioned by deposition on a wafer, followed by polishing, dimpling and PIPS ion milling. The cross-section on the wires appears to contain a five fold axis.

Imaging proved difficult due to some what uneven milling of the samples. Imaging the lattice was not possible due to organic contaminance on the silver cross-sections deposited during milling. Five-fold twinning was nevertheless visible in the cross-sections when tilted correctly. This five-fold twinning is nearly identical to that observed

in the electrochemically produced gold particles. It also is useful for explaining the five-fold symmetry of the silver wires and gold rods.

The second method used for making cross-sections was to microtome embedded samples. The most successful technique was to mix silver wires, dispersed in a small amount of ethanol, in an epoxy designed for biological samples. After curing, microtoming produced thin slices of polymer with slices of silver wires from random orientations. The HRTEM of these samples are shown in Figure 5-23.

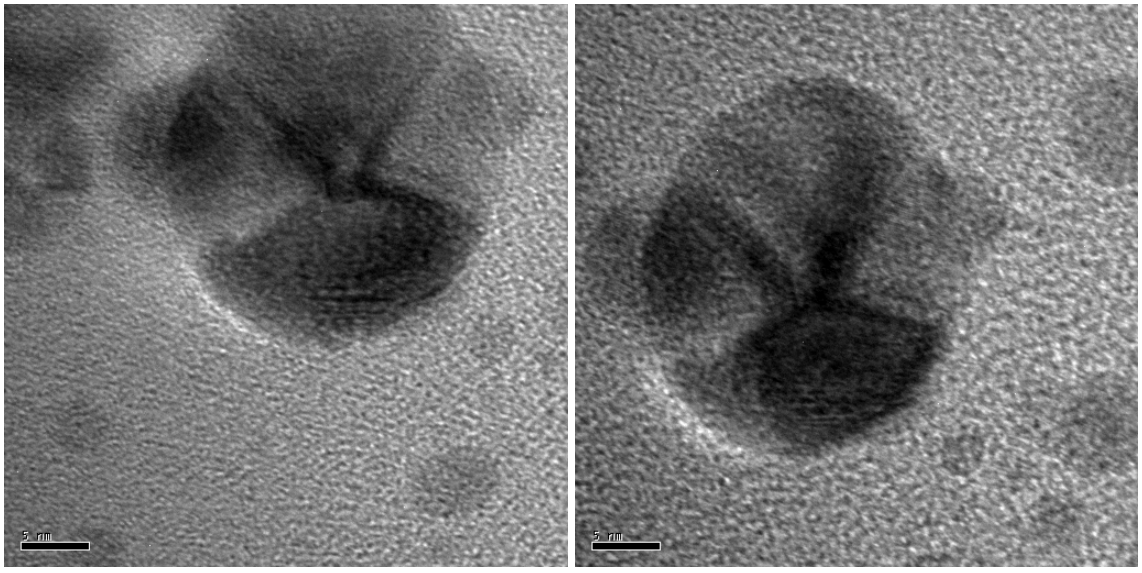

Figure 5-23: Silver wires embedded in epoxy and cross-sectioned with a microtome. The presence of five-fold twinning in the wire is apparent.

There was concern that the microtoming process would damage the slices or introduce extensive deformation as was seen in the gold platelet samples. Although the images were not of the highest quality, and the lattice could not be imaged, what appears to be five-fold twinning was again observed. Two of the five variants appear connected, but the angles measured out by each variant correspond well with the 72° need to make a full circle. The dark contrast region at the bottom of the particles may be two variants

oriented in nearly the same direction. Clearly the presence of five twins in the sample contradicts the silver halide model, and a new model will need to be used.

Quenched Silver Wire Specimens

Samples of the growing silver wires were taken from the reaction vessel and injected into ten times excess acetone at six points during growth. This resulted in rapid cooling and the precipitation of the PVP, which is insoluble in acetone. Both of these actions have the effect of quenching the reaction at that stage. In the reaction scheme used, silver nitrate and PVP containing EG solutions were injected into hot EG at a constant rate over five minutes. The samples were removed after 6 minutes of reaction (one minute after final reactant addition), 10 minutes, 16 minutes, 21 minutes, 32 minutes and 75 minutes. These samples were cleaned of excess PVP, dissolved silver ions and ethylene glycol and observed using the SEM or TEM. The images taken were intended to both represent the samples as a whole, as well as focus on particles of particular interest. Many particles could not be characterized due to their orientation.

At six minutes into the reaction (one minute after the final reactant addition), only a small portion of the silver nitrate had been reduced, leading to a transparent yellow solution characteristic of isotropic silver nanoparticles. The particles were in the size range of approximately 4 nm is diameter, as seen in Figure 5-24.

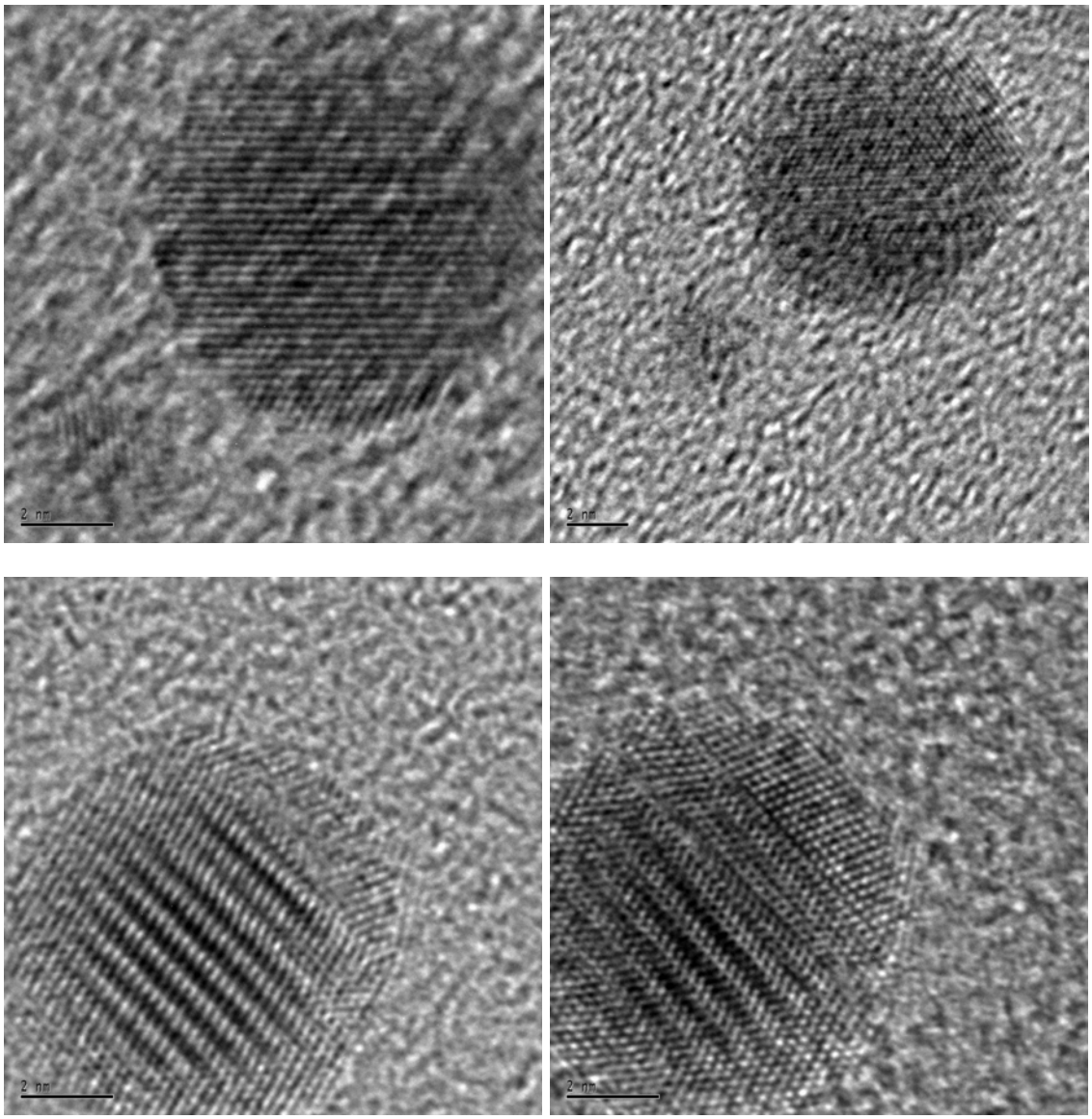

Figure 5-24: Polyol process silver wire reaction samples quenched at six minutes into the reaction (one minute after final reactant addition). The top images show single crystal particles, while the bottom images appear to be twinned particles.

The top images in 5-24 show single crystal silver nanoparticles. The lower images appear to contain twins as can be deducted from the Moiré fringes. In the bottom images, a change in the lattice orientation can be seen in the upper right of the particle. All the particles observed were either single crystals or showed signs of having two or more crystals joined by a twin plane. No five-fold twining was observed in any of the

particles. Some of the particles were oriented such that they could be view nearly parallel to a twin plane. In the case of Figure 5-25, a particle appears to have "V" shaped contrast with three crystallites join together by two twin planes. As can be seen, the lattice fringes change directions in the area where contrast changes. The angle that the "V" sweeps out is approximately 70°, possible indicating that the twin planes are on {111} planes oriented 70.5° apart.

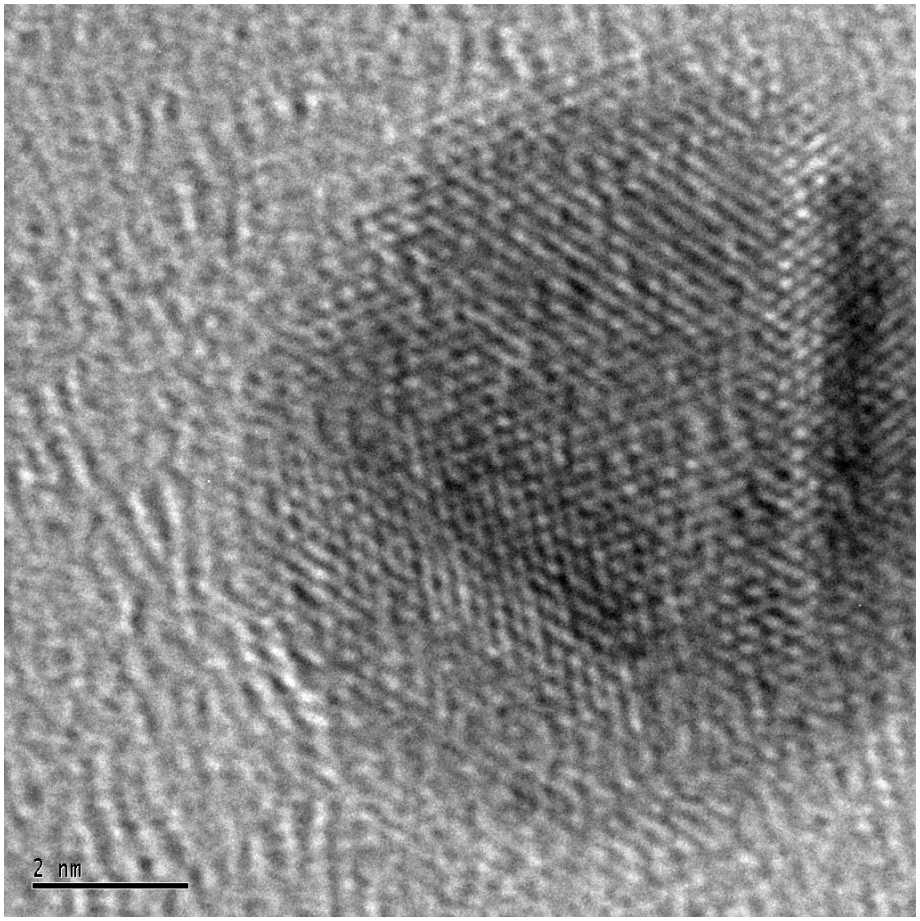

Figure 5-25: Silver particles quenched at 6 minutes containing "V" shaped contrast. The angle of these contrasting regions cut out an approximately 70° angle.

Interestingly, all the particles were spherical, and the twinned particles had not formed into hexagonal or triangular prisms. The very low concentration of silver in the sample either indicates that the EG had not reduced a significant amount of the silver, or that the

growth kinetics at this stage of the reaction did not allow for the zero-valent silver to attach to the nuclei. Given observations of other reaction batches, the former explanation seems unlikely. In some batches, the solution turned an opaque tan color within minutes of the reactants being added. The solution contained a large amount of submicron silver spheres. The total amount of reduced silver in these batches was far in excess of that in these silver wires sample at the same point in the reaction, in the range of two orders of magnitude more. This indicates that the EG solution is capable of reducing a far larger amount of silver than was observed in the 6 minute wire sample. The reason for large discrepancy is not clear, but may indicate that the nuclei from which silver wires grow have a kinetic disadvantage in growth early in the reaction. The internal structure of the samples that form large silver spheres was more difficult to determine because they grew very rapidly to an electron opaque size. An example of a smaller particle quenched after reactant addition is shown in Figure 5-26. Unlike the sample that would form wires, this particle is larger, and contains multiple crystalline boundaries oriented in different directions. These boundaries may have formed from multiple particles aggregating together in the early stages of reaction. This internal structure may create sites of kinetic advantage for adatom attachment that leads to rapid growth. The single and bicrystalline nature of the silver wire samples appears to limit grow at the early stages.

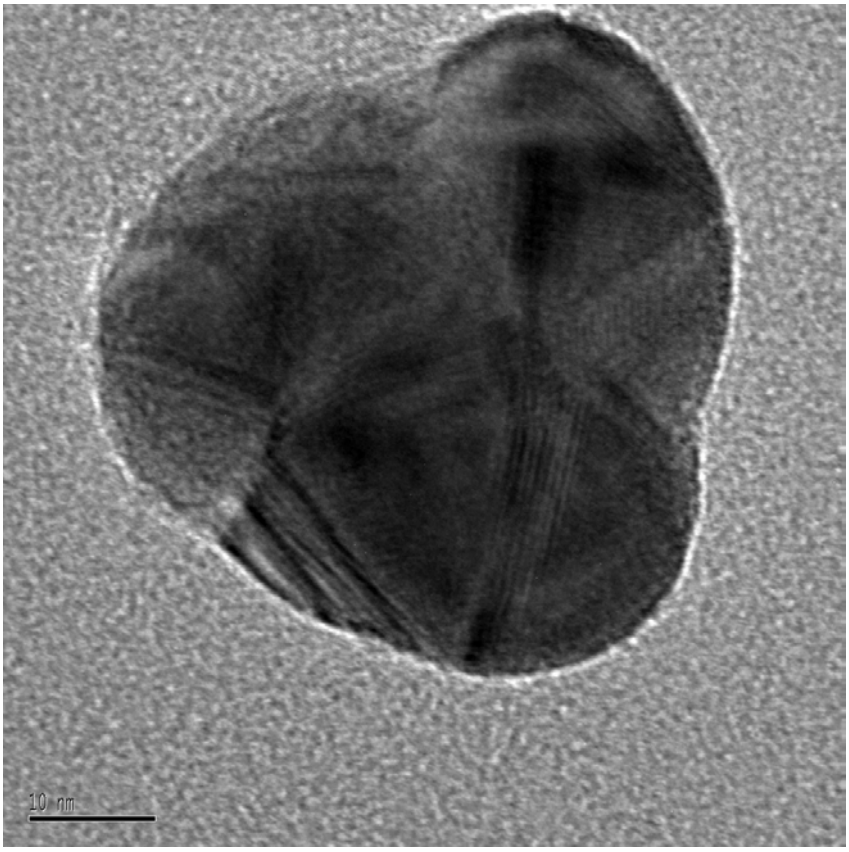

Figure 5-26: HRTEM image of a particle from a silver sphere forming batch quenched immediately after reactant addition. The presence of multiple, randomly oriented crystal boundaries is apparent.

At ten minutes into the reaction, the solution has taken on a darker, yellow-orange color, but is still semi-transparent. The particles have grown larger to approximately 20 nm in diameter and many now contain two or three twins or grain boundaries. None of the particles are elongated at this point. In comparison to the non-wire forming samples, the amount of reduced silver was still much lower. The twined structure of the particles was more easily observed at this magnification. Figure 5-27 shows several images from a particle containing two twin planes approximately 70° apart.

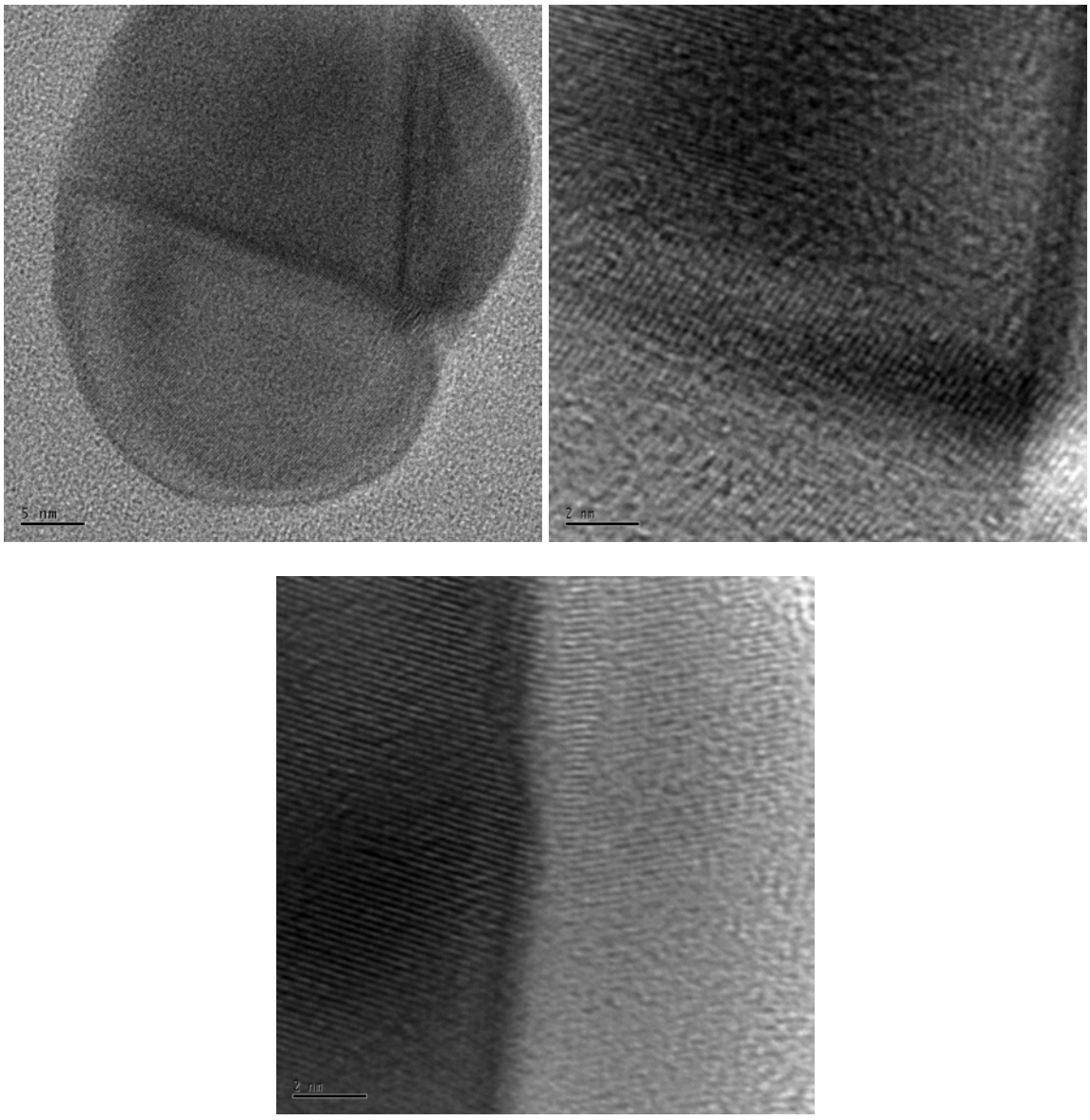

Figure 5-27: Polyol process silver wire reaction sample quenched at ten minutes into the reaction (five minute after final reactant addition). The top image left is magnified in the other two images. The top left shows a typical particle with two twins planes oriented approximately 70° apart. The top right image shows a close up of the lower twin boundary and the bottom image a close up of the upper boundary.

Figure 5-28 shows a particle in which the twin plane is viewed from an angle.

Overlap of the lattice of two crystallites leads to Moiré fringes.

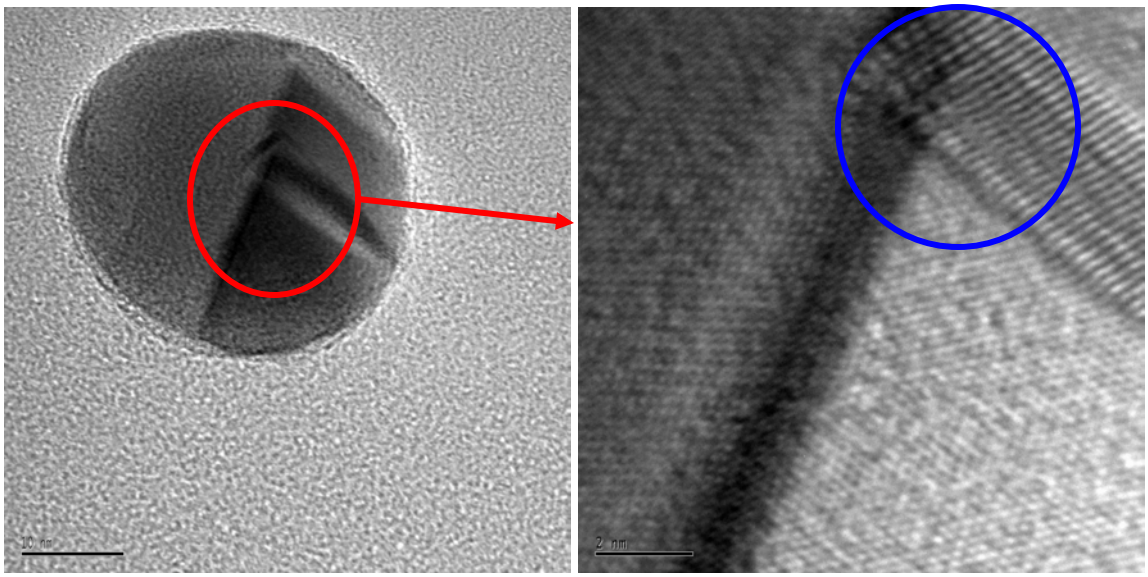

Figure 5-28: Two magnifications of a two twin boundary of a silver particle quenched at 10 minutes. The red circle indicates the area of magnification. The upper boundary is observed from a direction where two variants overlap, leading to Moiré fringes (blue circle).

Another interesting feature was observed in particle that contained three twins that sweep out approximately 140°. These particles contained a region of unusual contrast where it appears that the lattice is strained. Figure 5-29 shows this feature. The strained region is in the right side of the particle at the intersection of the three twin planes.

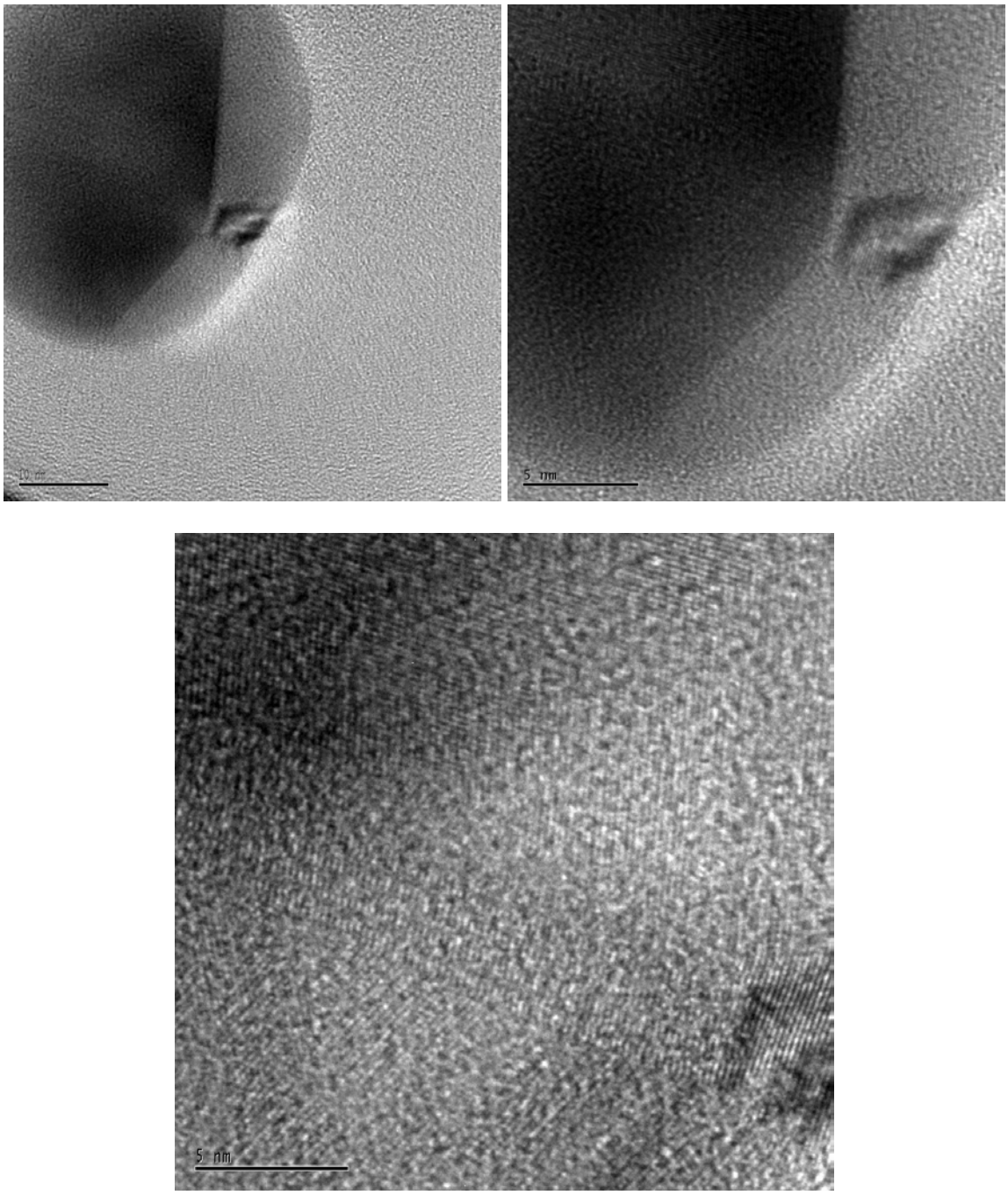

Figure 5-29: A particle containing four crystallites joined by three twins. In the top left image, a darker region sweeps out approximately 140°, and a ring shaped region of contrast is visible on the right side of the particle. The top right image shows a close up of the ring contrast, which is at the intersection of the twin planes. The bottom image shows the lattice fringes in the dark region, making it clear that this dark region is, in fact, two crystallites. The lattice fringes in the ring contrast area (lower right corner) are distorted slightly, indicating strain.

Given the dominance of the (111) type twin plane in FCC structures, the structure of particle in Figure 5-29 appears to be four crystallites joined by three twin planes oriented 70.5° apart. This is similar to the five-fold twinned wire cross-sections and the five-fold gold particles formed through electrochemical reduction. If this arrangement plays a determining part in wire and rod growth, the type of particle in Figure 5-29 could be a step in the formation of the five-fold symmetric structure. Because five (111) planes oriented 70.5° apart cannot fill a circle without a strain of 7.5°, the lattice or one or more of the crystal variants must be strained. From the HRTEM of the 6 minute particles, it appears that the variants are not forming simultaneously, but sequentially. This would favor the occurrence of strain in only the variants formed latter in growth. This could explain the strained region in Figure 5-29, which appears not to be located in the two center variants. These two variants may have formed first, followed by variants on either side of them. The strained region may indicate the initial formation of the fifth variant which would close the circle of twin planes. The strain, and therefore the additional energy, associated with forming this final variant may explain the small size of this region and the fact that no elongation parallel to the twin planes is observed.

Between ten and sixteen minutes of reaction, the solution rapidly becomes darker to a tan color, before a metallic shimmering begins to appear. The effect is attributed to the formation of the wires, which align according to shear field in the stirring solvent. The total amount of reduced silver increases by at least one order of magnitude between 10 minutes and 16 minutes of reaction. The quenched solution is shown in Figure 5-30. As can be seen, high aspect ratio wires have formed, in addition to cubes and a large number of particles containing multiple twins. Most of the wires are in a narrow range of

diameters around 30 nm. The longitudinal changes in contrast are attributed to bending in the wires. As can be seen in the right image of Figure 5-30, several of the isotropic particles have twin planes oriented 70.5° apart. These may later form the five-fold twinning that appears necessary for wire growth.

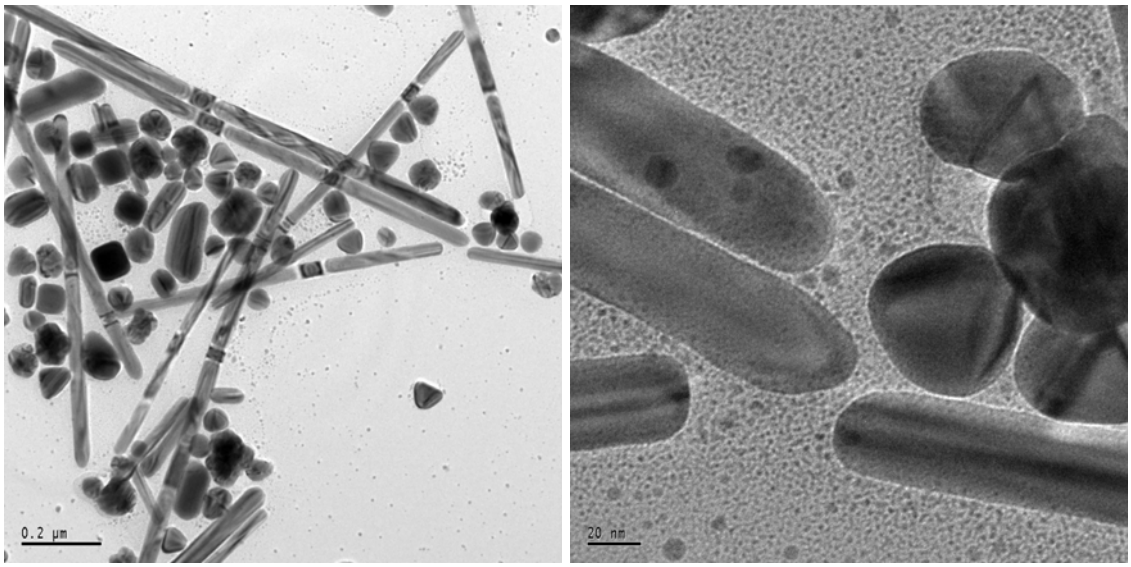

Figure 5-30: Silver wires quenched at sixteen minutes into the reaction (eleven minute after final reactant addition).

The rapid increase in the amount of metallic silver present in the solution, and the sudden appearance of high aspect ratio particles in the six minutes between sample 2 and sample 3, indicates that the kinetics of particle growth have changed significantly. It follows that once the nuclei have advanced to the stage were wire growth is possible, the rate at which adatoms can attach to the wire increases many fold.

Samples quenched at latter points in the reaction are shown in Figures 5-31, 5-32 and 5-32. The general trend is towards an increase in length and diameter, with a reduction in the amount of isotropic particles and an improvement in the degree of faceting. At 21 minutes, the wires are less than 100 nm in diameter, while at 32 minutes some start to approach 100 nm. At 75 minutes, only a very few large isotropic particles

remain, and some of the wires have grown to 200 nm in diameter. The total concentration of metallic silver does not change appreciably after 21 minutes, meaning that further growth of the wires must come from silver that was dissolved and reprecipitated in an Ostwald type process. The silver source for this Ostwald ripening probably comes from the isotropic particles that become less prevalent as the reaction continues. It does not appear that this alone is a sufficient source of silver, requiring that some of the less stable silver wires dissolve.

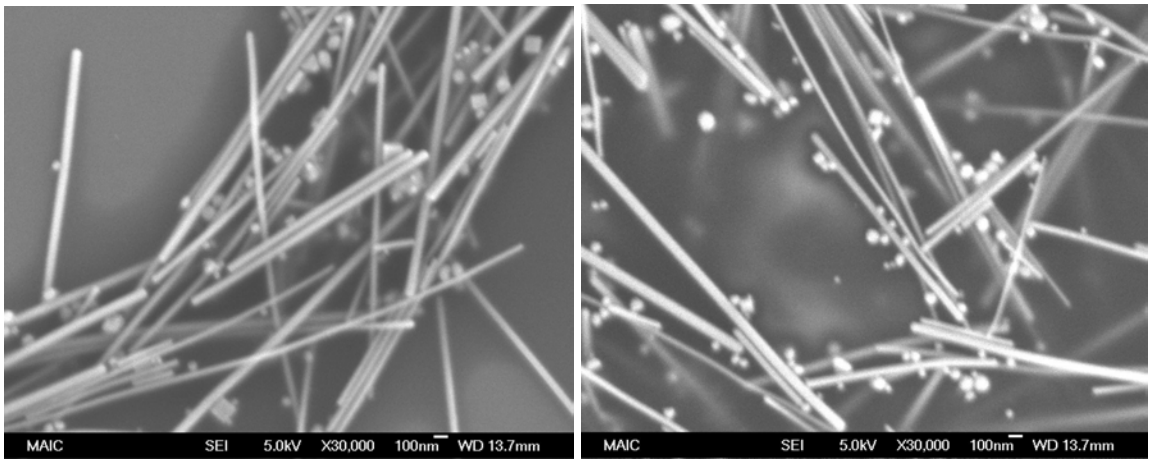

Figure 5-31: Silver wires quenched at 21 minutes

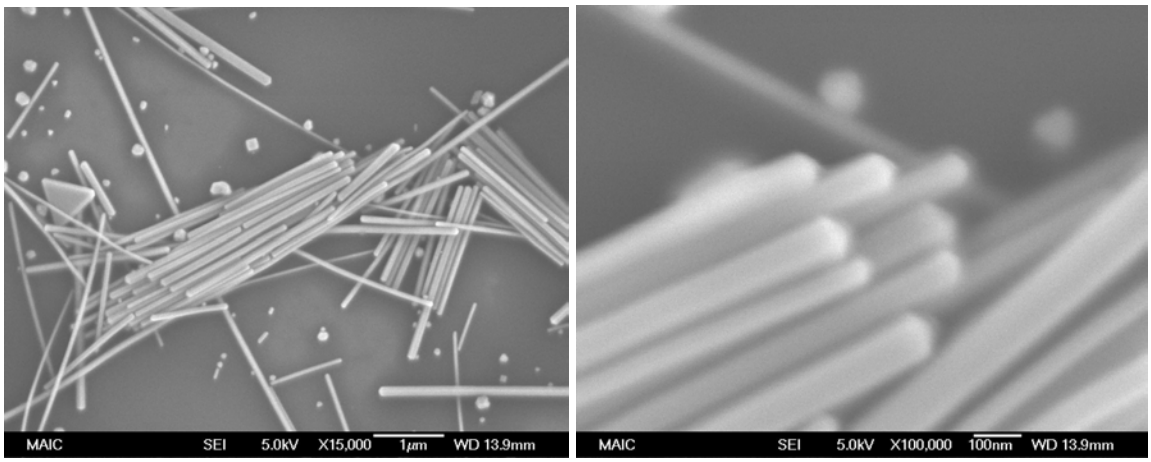

Figure 5-32: Silver wires quenched at 32 minutes.

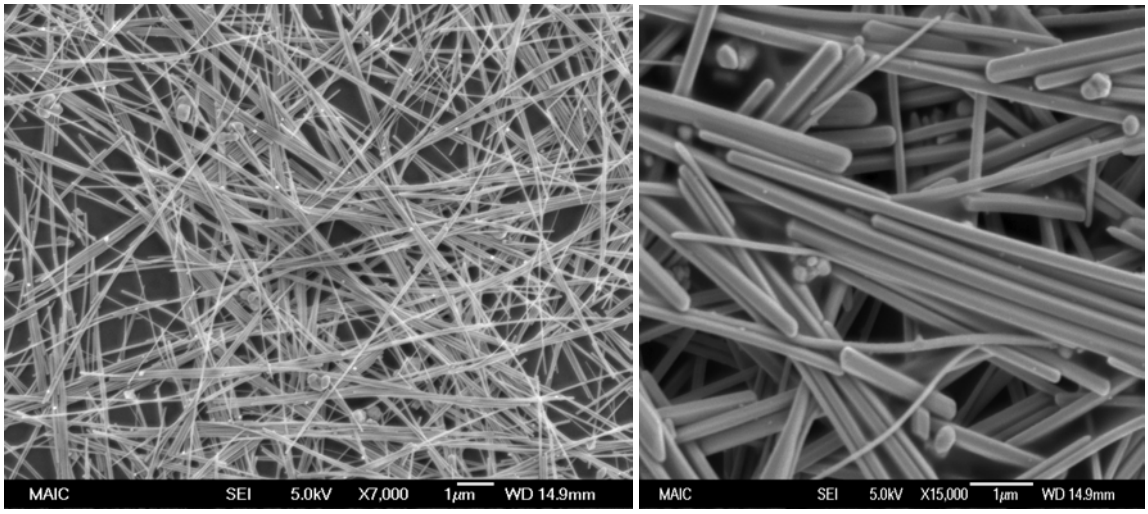

Figure 5-33: Silver wires quenched at 75 minutes.

Proposed Structure and Growth Model of Rods and Wires

All of the data collected from the wires and rods synthesized by each method indicate that the silver halide model cannot be applied to noble metals. The superimposed diffraction patterns cannot be reconciled with any crystallographic directions in the silver halide model. The cross-section analysis in SEM and TEM is not consistent with the three twins and six faces in the silver halide model. The data does indicate that rods and wires have a unique internal structure that appears to lead to a major increase in growth kinetics over particles without this structure. The five-fold symmetry observed in faceting and in the cross-section analysis leads to a new proposed explanation of rod formation. As seen in Figure 5-34, five crystal variants joined by twin (111) twin planes construct a rod cross-section. As mentioned before, (111) planes can be oriented at 0°, 70.5° or 109.5° degrees apart. If each variant was twined on two planes 70.5° degrees apart, a full circle could be created if 7.5° strain were introduced. A decahedral particle, composed of five tetrahedra sharing two {111} faces with two neighbors and sharing one

edge between all five, would have such a cross-section. Such a particle is likely what is seen in Figure 5-19.

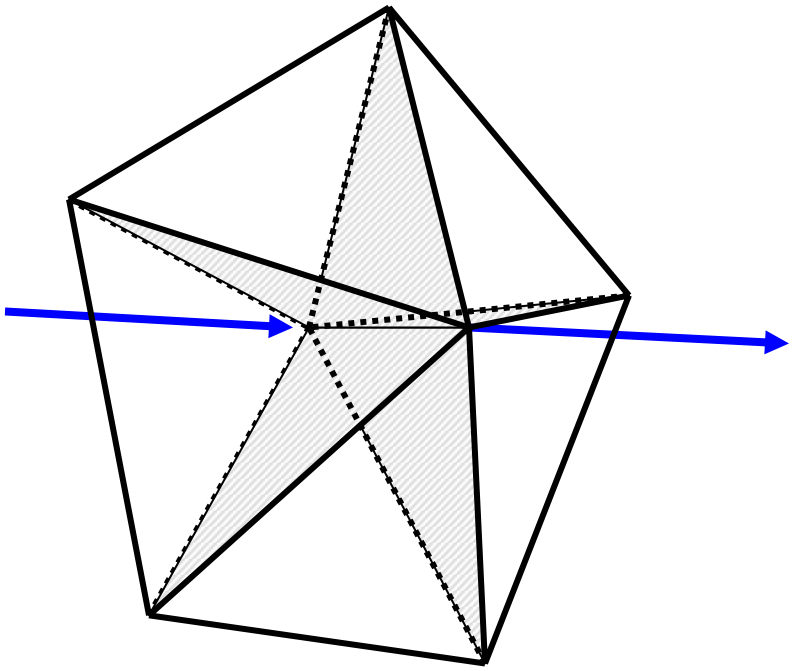

Figure 5-34: A decahedral form constructed of five tetrahedra joined by five twin planes (grey planes) and having a joint axis along a [110] direction (blue lines).

In fact, Cleveland et al. used computer simulations to show that five-fold twinning was favorable for small gold cluster sizes in the range of hundreds of atoms [83]. If this particle were to elongate parallel to the twin boundaries, a rod with five-fold symmetry would form. Such a rod would have a [110] type axis, which is consistent with the diffraction patterns obtained.

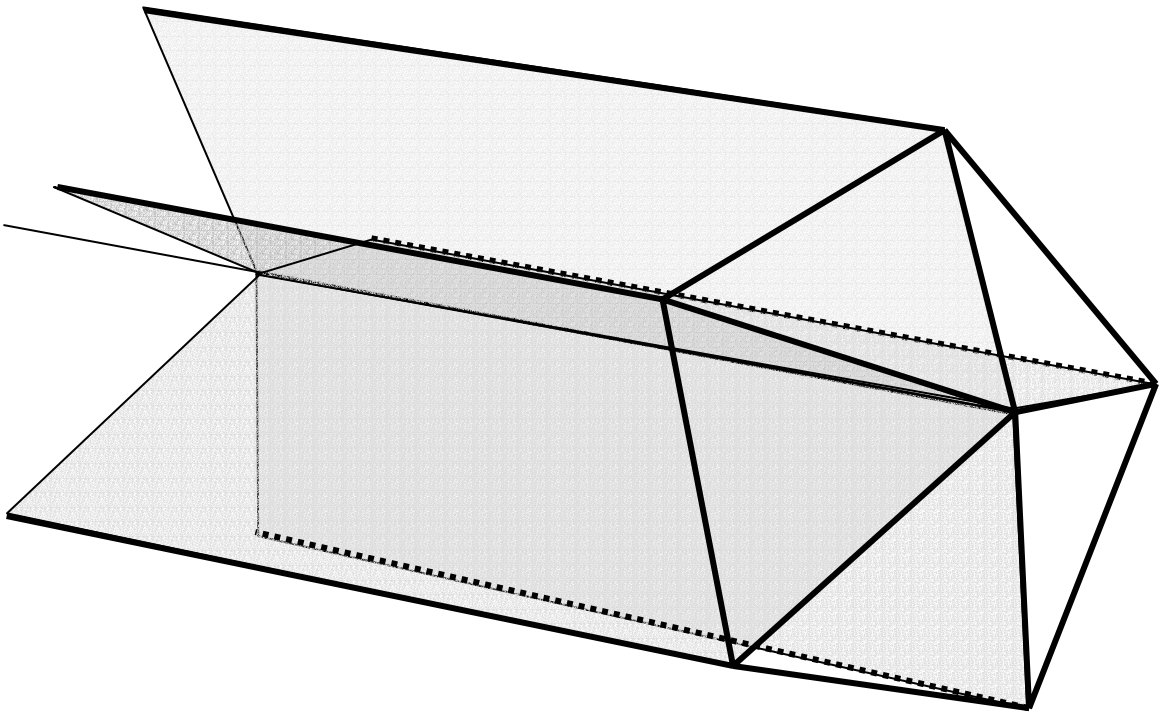

Figure 5-35: Elongation of the twin planes (grey planes) of a decahedron to form a rod. New side faces are created parallel to the [110] direction.

Furthermore, if a electron beam were to pass through the rod parallel to one of the twin planes, two of the variants would produce [211] diffraction patterns and one would produce a [100] pattern. By tilting approximately 18° away from the twin plane, two variants would be aligned to produce a [111] pattern and one would produce a [110] pattern. Both of these directions would explain why these patterns were seen together repeatedly in the rods.

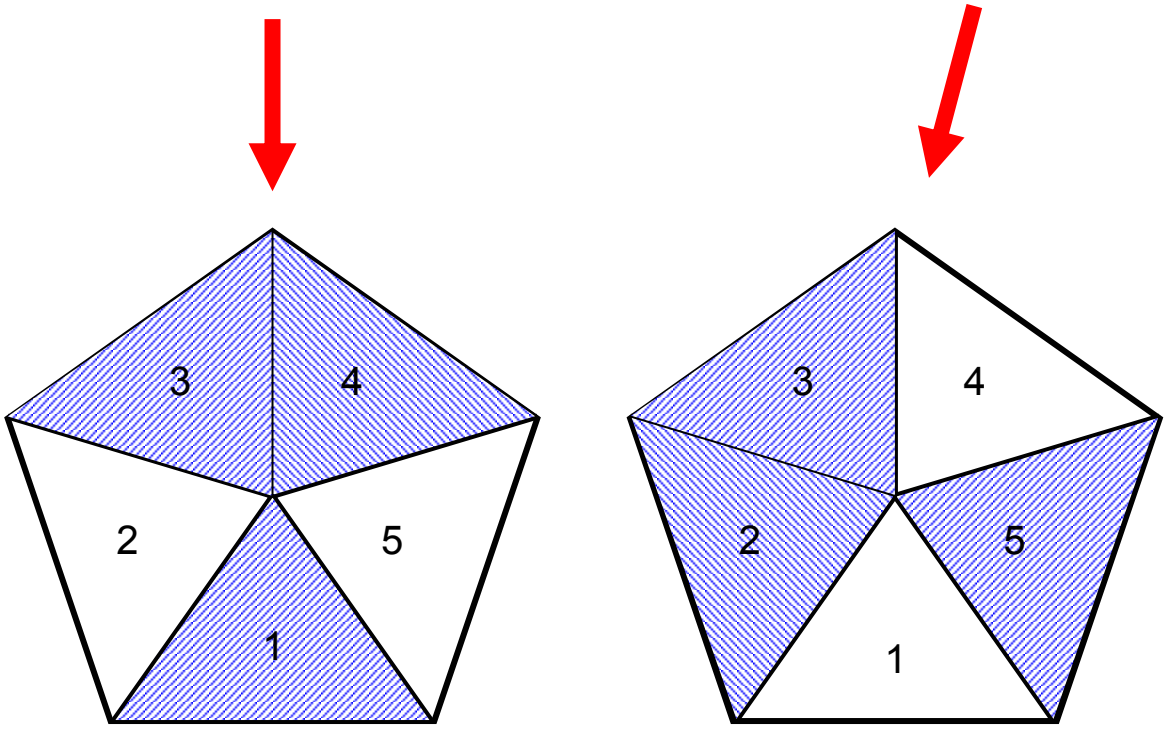

Figure 5-36: Proposed explanation for superposition of zone axes angles in metal wires. The red arrows indicate the direction of the beam. On the left, variant 1 will all be aligned in [100] directions, while the variants 3 and 4 will be in the [211] direction. In this direction, one twin plane is visible. On the right, the variants 2 and 3 will be in the [111] direction and variant 5 in the [110] direction. No twin plane is aligned with the beam in this direction.

From this model of the internal structure of the rods, a model of the faceting can be constructed. Figure 5-37 shows the proposed crystal habit of rods and wires. The end facets are consistent with the rod originating as five tetrahedra joined together by twins, while the side faces are consistent with the orientation of the twin planes and the [110] type axis of the rod.

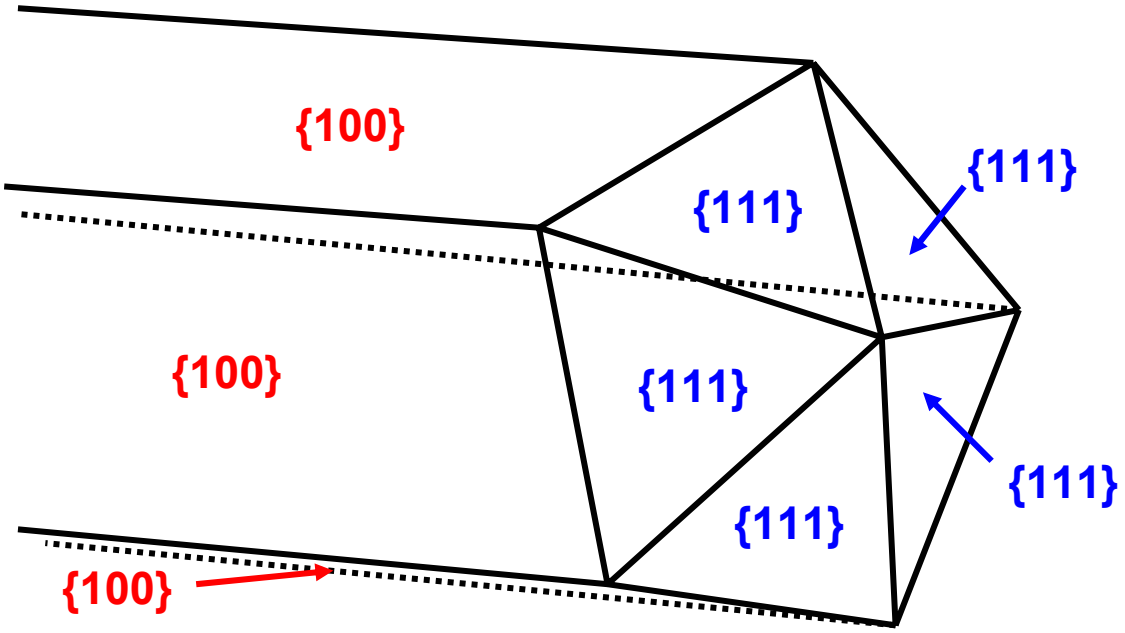

Figure 5-37: The proposed faceting of metal rods with pentagonal profiles. The side faces are (100) and the end faces are (111).

How does the five-fold symmetry develop initially? As was seen in Figure 5-19, decahedron exist in the aqueous solutions containing gold rods. The seed particles for all the aqueous silver and gold syntheses, however, do not have this five-fold symmetry, rather being single crystals or containing a single twin. Likewise, the quenched silver wire specimens contained particles without five-fold symmetry before or after the formation of wires. This demonstrates that, in spite of stability of small decahedron, one-dimensional particles originate from other sources. Two routes for the conversion of single crystal particles into five-fold symmetric particles exist; the sequential twining of a seed particle on {111} faces, or the collision and fusion of particles along {111} surfaces. It is difficult to determine which route is correct because no real time observation of the particles was made. Only snap shots of the growth process are available for analysis. The sequential twining route has difficulty in explaining why five twins would form with the same angle between them and why they would each share a common axis. The

collision and fusion route is also problematical because of the dispersion forces pushing particle away from one another. Yagi et al. reported that multiply twinned particles could form from the coalescence of tetrahedra or by sequential formation of twin planes. [84]. Perhaps the particles in the quenched silver samples containing two twin planes 70.5° apart fused together to form the five-fold cross-section.

The proposed structural model is consistent with the structural data, but cannot yet explain the preferential growth parallel to the twin planes. In the silver halide model, "A" type sides were present at the end of the wire to propagate the wire growth. In the above model, the twin planes intersect the end of the wire on slow growing "B" type sides. Thus, there are no reentrant grooves like those in silver halide wires. Furthermore, while the work of Cleveland et al. states that such a five fold twinning is favorable for small particles, this structure becomes increasingly unfavorable as the size increases. The energetic cost of the 7.4^{o} strain will no doubt hinder the attachment of adatoms on the side faces, restricting lateral growth. Some mechanism may exist to relieve the strain in particles. This may involve edge dislocations radiating out form the central axis, as seen in Figure 5-38.

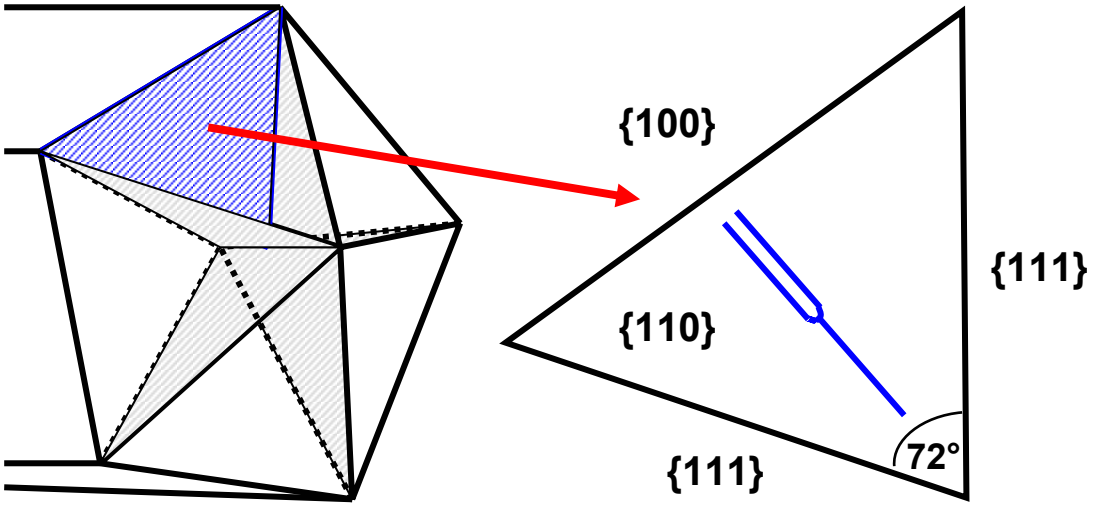

Figure 5-38: Lateral restriction of growth of a pentagonal wire. The cross-section of a wire with five (111) twins will have a strain in the lattice due to variants being 7.5° short of closing a circle. This could lead to an extra plane being inserted perpendicular to the {100} face.

In fact, the added plane need not necessary be perpendicular to the {100} faces to relieve the strain. An added plane could be a {111} plane. Evidence that such extra planes are added into the variants as they grow away from the central axis could not be found in the wire cross-sections due to problems imaging the lattice. Evidence, however, was found in the image from Figure 5-29. In Figure 5-39, an area of one variant is magnified until the lattice is visible. As can be seen by the red lines in the bottom image, an extra plane is clearly seen as one looks from the intersection of the twin planes, towards the left edge of the particle.

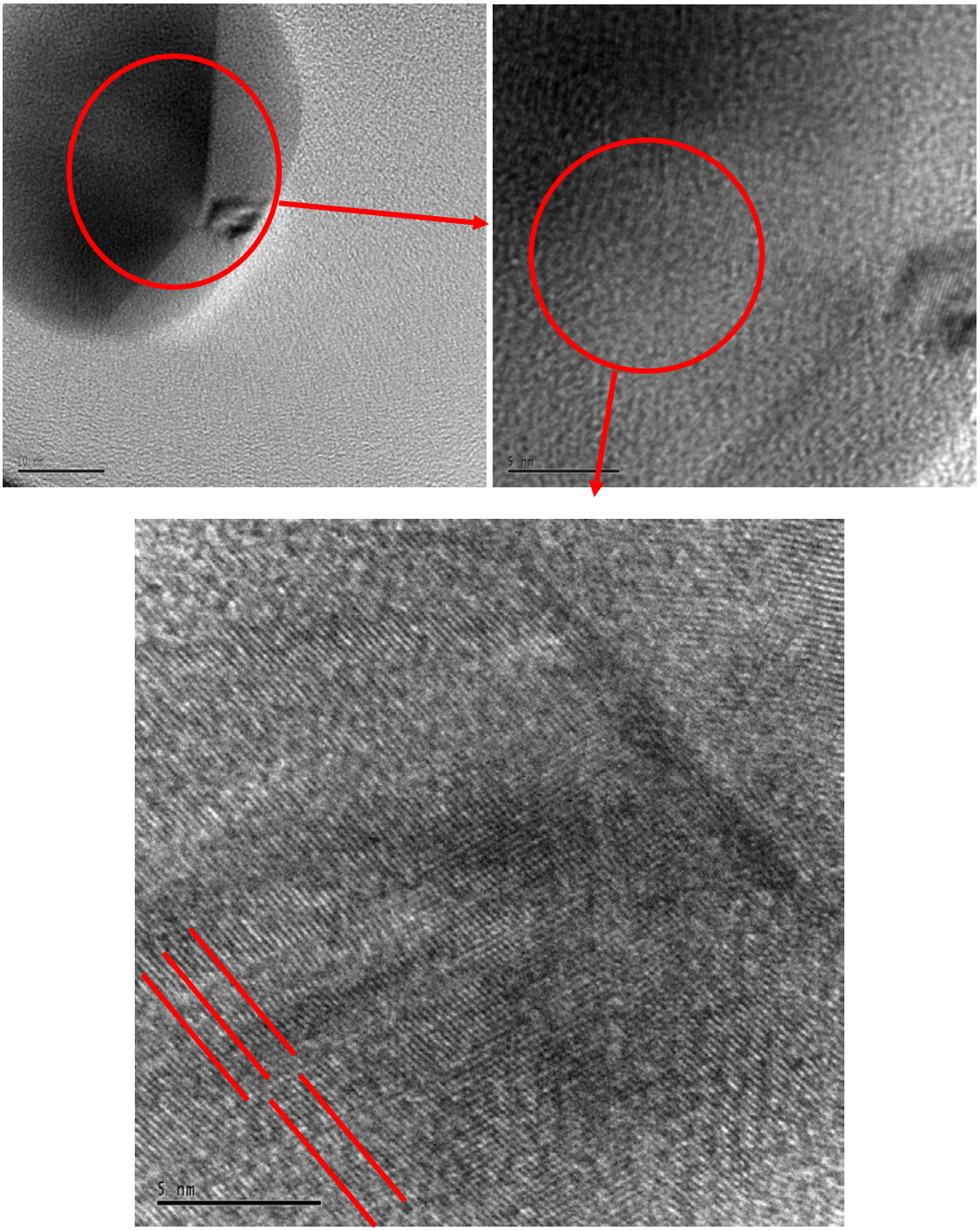

Figure 5-39: Possible evidence of edge dislocations in silver nanoparticles quenched in growth during synthesis of wires. Upper left image shows a silver particle quenched at 10 minutes into the reaction. The area in the red circle is observed at a higher magnification in the upper right image. Magnifying still further, the lattice becomes visible for one of the variants in the lower image. The lattice is not perfect, but contains at least one dislocation, as indicated by the red lines running parallel to the lattice fringes. This plane with the edge dislocation is a {111} type plane.

The planes imaged in this image are {111} planes, and are thus not radiating out directly from the center, but are parallel to one of the twin planes. It is clear that an edge dislocation exists which could stabilize the particle. Without a doubt, if the side faces of a rod were under strain due to the five variants not fitting together properly, this would increase the energy of adding an adatom to that face, reducing the rate of growth of a rod perpendicular to the axis. This would explain the conversion of a decahedron to a rod: As a decahedron grew, the edges would become strained, causing the formation of {100} faces. Because of the strain, adatoms would attach to these {100} faces more slowly than unstrained faces, while they would simultaneously grow in size laterally by the addition of material to the {111} end faces. The restricted growth of {100} side faces would limit the diameter of the rod until a nuclei containing an extra plane were to form on the face. This arresting of wire growth laterally would explain why only certain diameter wires were observed, and why wire diameters were very uniform within batches.

The requirement of strain to close the space between the variants has interesting consequences when considering the apparent sequential twinning of the seed particles into the five-fold symmetry. If the appearance of each twin was completely unrelated to the presence of any previous twins, one would expect that the first four variants would be unstrained and the final variant would contain all the strain. The edge dislocations in Figure 5-39 argue that some strain is present in the particle event through the five-fold symmetry is not observed. The ring shaped strained area at the intersection of the three twin planes may indicate that a site is already present that is straining the four variants. This could possibly transform at a later stage into two more twins and complete the

particle cross-section. Why such a particle would transform cannot be speculated upon at this point.

If edge dislocations are being created on {111} planes, one would expect that some evidence of stacking faults emerging on the side faces. Striations, which could possible be such features, where observed on some of the rods, as seen in Figure 5-40. Such features were observed on only a limited number of rods, and only on some faces, making it difficult to determine if they are actual stacking faults, or merely artifacts.

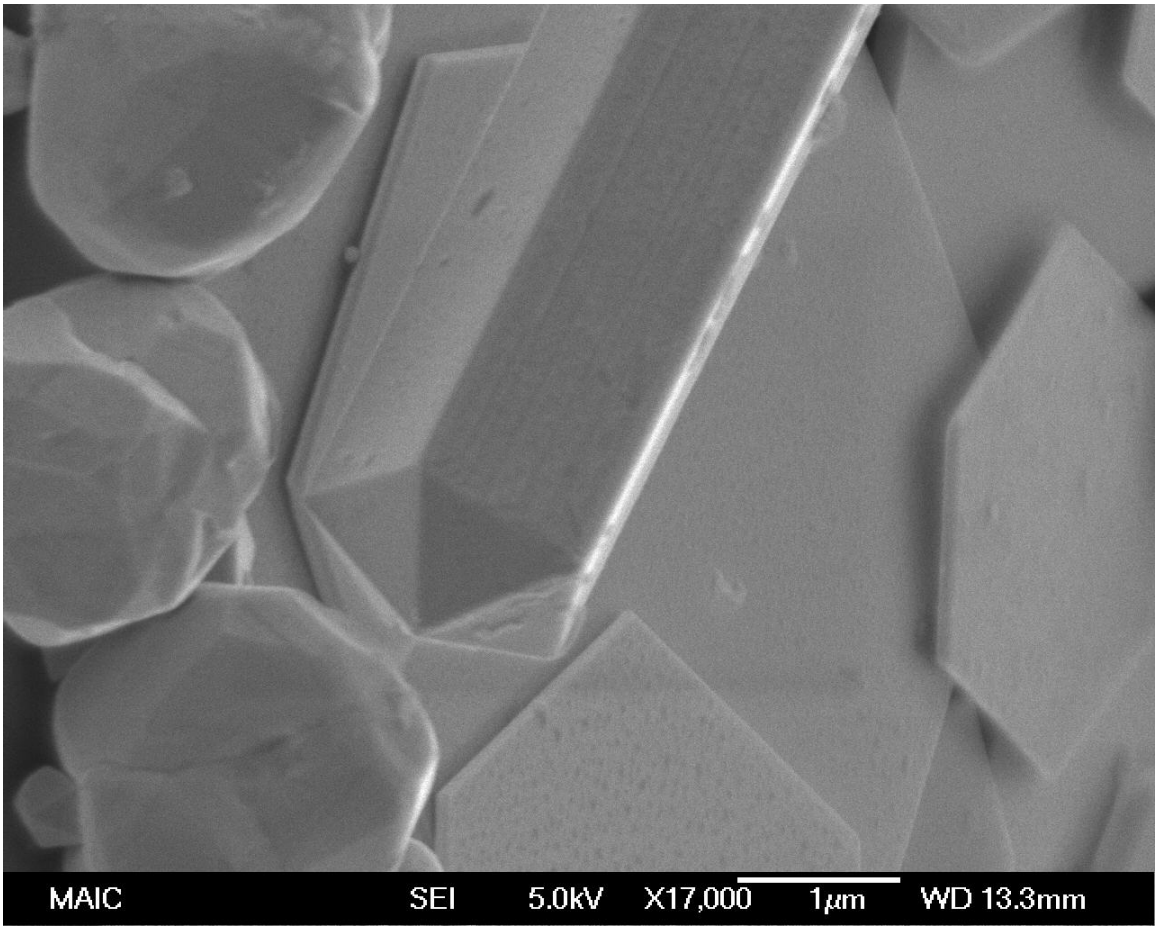

Figure 5-40: Possible evidence for immergence of edge dislocations along the sides of a gold rod particle. The striations visible along the axis may be due to the stacking faults created by an extra plane inserted into the lattice to relieve the stress associated with the joining of the five twins.

As is seen in the quenched samples, the transition between isotropic particles and high aspect ratio wires can take place very rapidly. In this growth, the surface area on which adatoms can attach remains nearly constant, because all the side surface area is under strain and the attachment of adatoms is slowed. This raises the question of whether the linear growth is due only to a slow down in the attachment of adatoms to the sides, or if some mechanism is accelerating growth on the end faces. As was mentioned, the edges joining the end faces are all "B" type side without reentrant grooves. A possible mechanism for accelerated growth of these end faces could be the emergence of the edge dislocations at the end faces. As was described by Ming, The emergence of a pure edge dislocation produces a self perpetuating step on a free surface [19-21].

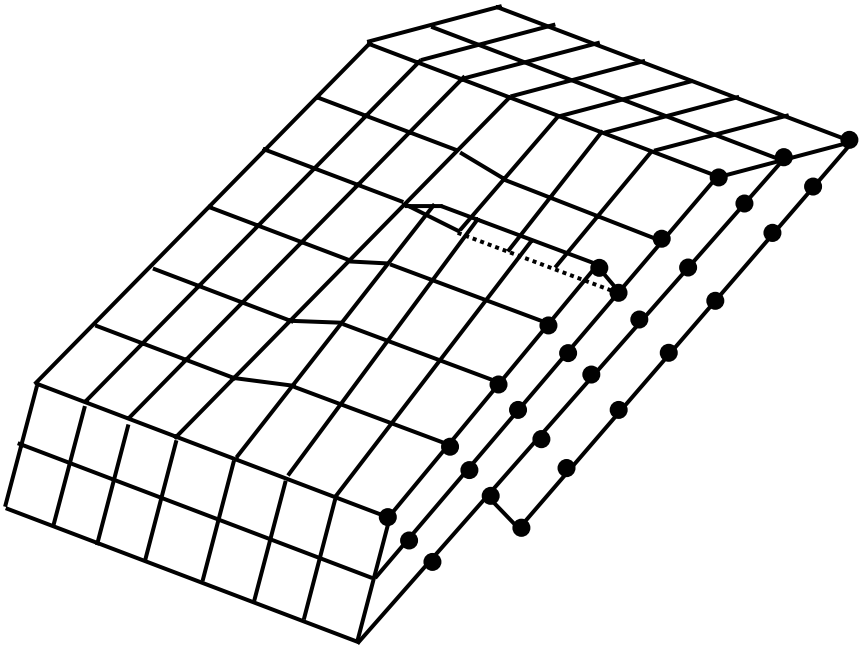

Figure 5-41: The emergence of an edge dislocation on a surface producing a self perpetuating step that can act as a site for accelerated adatom attachment.

This step increases the number of nearest neighbors of an adsorbing adatom from 3 to 5 over a flat surface. This increase in nearest neighbors increases the stabilization energy to the adatom and reduces the chance of dissolution. According to Ming, all the free

surfaces of a crystal that do not belong to the zone of the Burger's vector of the dislocation will have such a step. Because the radial dislocations formed by the lattice strain must be parallel to the axis of the rod, and the {111} end faces are neither parallel nor perpendicular to the axis, the end faces do not belong to the Burger's vector of the dislocation and must contain such a self perpetuating step. Thus, the lattice strain produced by the 7.5° five-fold symmetry mismatch generates a strain on the side faces, which in turn generates edge dislocations to relieve the strain and also provide sites for accelerated growth of the end faces. Such a mechanism cannot be proven because these step were not directly observed, however, the mechanism appears to fit with the data collected.

CHAPTER 6
CRYSTAL HABIT OF ADDITIONAL NONSPHERICAL METAL NANOPARTICLES

Ribbons

In this chapter, four other shapes observed in metal nanoparticle synthesis will be discussed. The existence of these particles supports the proposal that twin planes are the dominant factor in anisotropic metal colloid growth.

Thin ribbon or belt-like structures were formed during the reduction of gold chloride in the polyol process along with rods, platelets and isotropic particles. Most of the ribbons were characterized by angular ends, forming 60° and 120° angles with the sides. The ratio of thickness to width varied greatly in the ribbons. Most of the ribbons had flat top faces, although, the ribbons with nearly equal thickness to width ratios had an edge running down the length of the ribbons, joining two faces of slightly different angles.

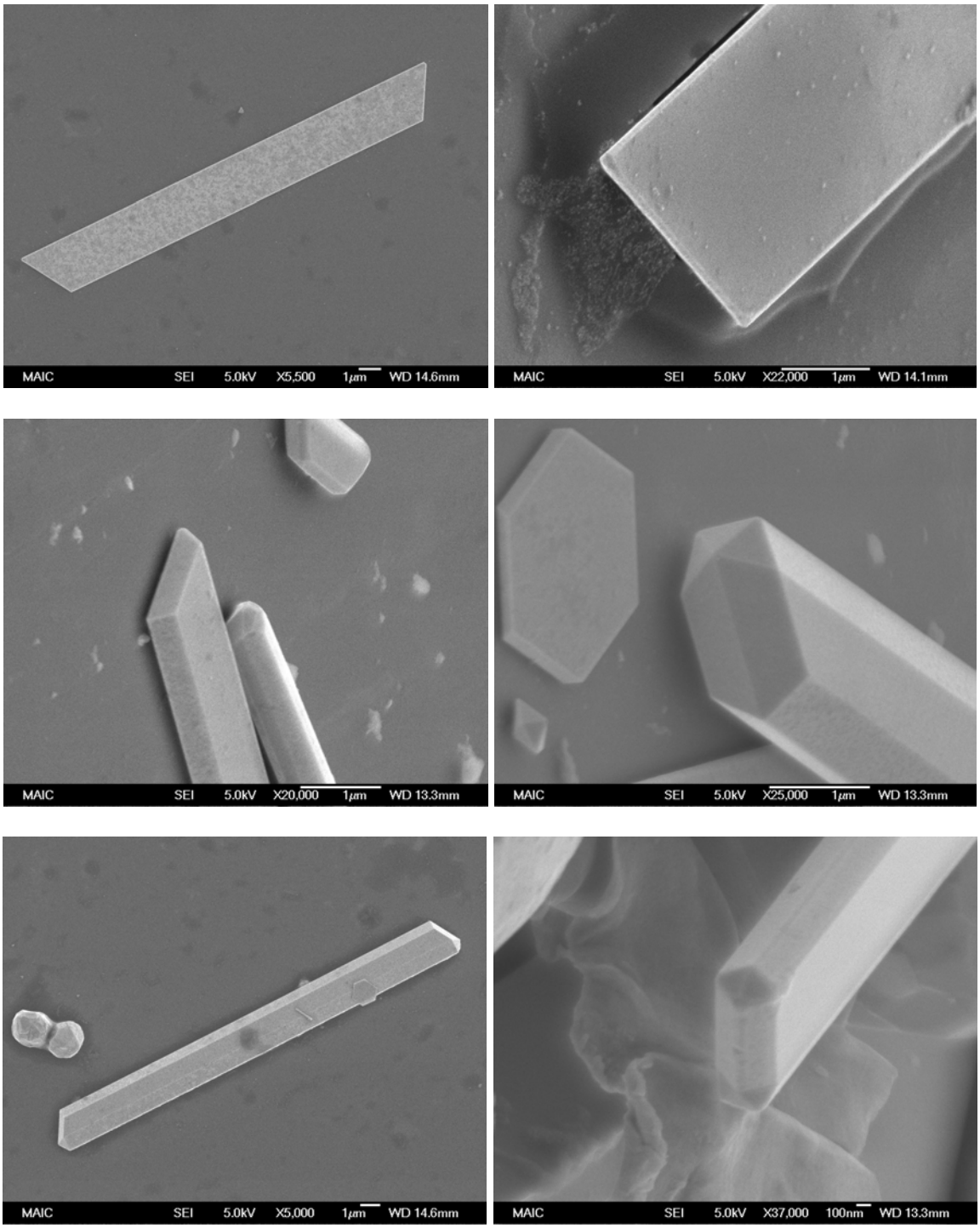

Figure 6-1: Six different gold ribbons formed by the polyol process. A) The most common shape of ribbons; thin (<100nm) with angled ends. B) A less common square end ribbon. C) A thicker ribbon (~200nm) with angled ends. D) A thick ribbon with faceting dividing the main face into two faces at slightly different angles. Notice the five end faces radiating out form a central point. E) A top view of a ribbon similar to D. F) A ribbon with five triangular end faces and two rectangular faces.

Diffraction on the ribbons proved difficult in many cases, due to the thickness of the particles. Diffraction patterns were taken near the edge of the ribbons, where they were not as thick and a larger amount of electrons could penetrate the sample. Only the thinnest, most high aspect ratio ribbons could be analyzed. As seen in Figure 6-2, a [111] pattern was obtained perpendicular to the main face of the ribbon, identical to metal prisms and platelets.

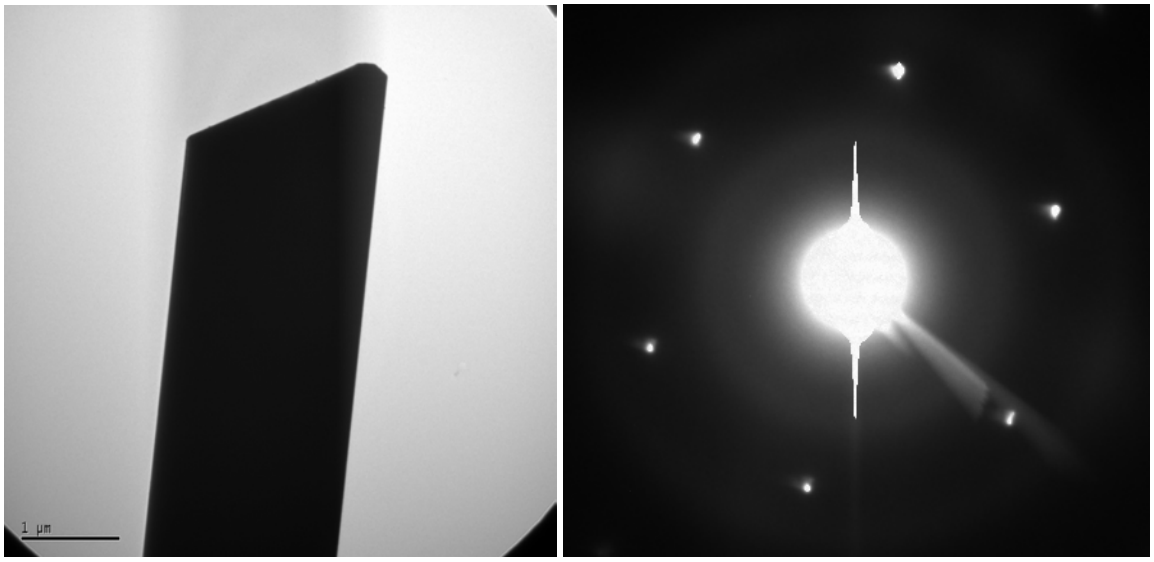

Figure 6-2: A TEM image of a gold ribbon and the corresponding diffraction pattern taken near the left edge where the ribbon was thin enough to obtain a pattern. The pattern indicates that the top face of the ribbon is (111). Notice the shape of the right side of the ribbon end.

As seen in Figure 6-3, this slightly electron transparent ribbon produced a [111] pattern with faint (1/3)[422] forbidden spots, indicating one or more twin planes parallel to the main face. Interestingly, the forbidden spots are angled slightly off from their expected positions.

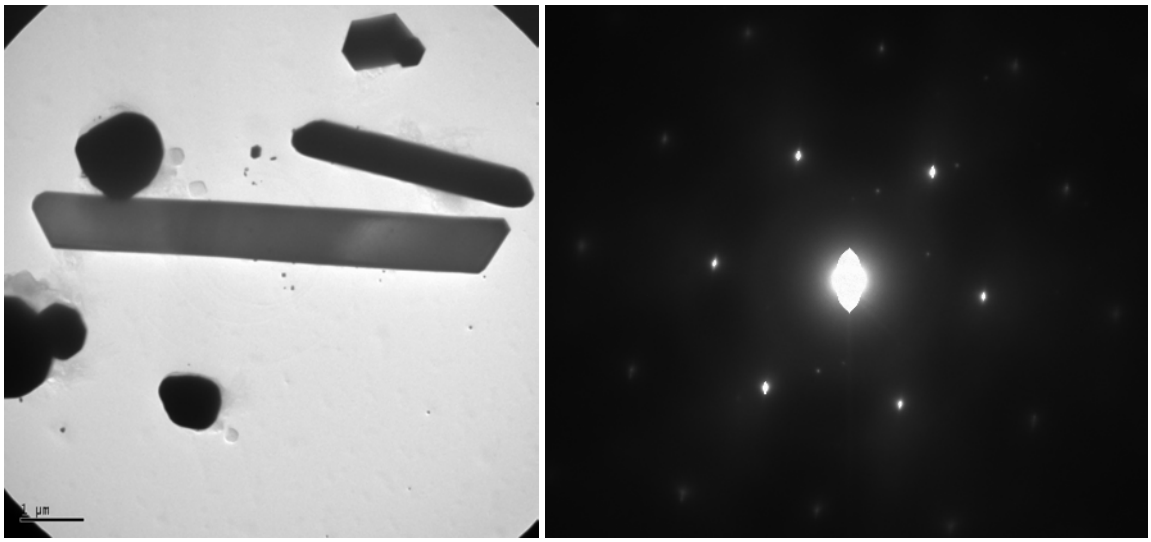

Figure 6-3: TEM image of a thin ribbon with a diffraction pattern taken on a large section of the width. The pattern is [111] and contains the forbidden (1/3)[422] reflections (faint spots inside the ring of six bright [220] spots). Notice again the faceting at the ribbon ends.

Both high aspect ratio platelets and ribbon type structures were not observed to form in silver systems, and their simultaneous formation in gold systems may be linked. The ribbons appear to be a cross between a platelet and a rod. The faceting at the end of the ribbons is very similar to the five-fold faceting of rods and wires, expect that on of the twin planes is elongated relative to the others. For the thin, high aspect ratio ribbons, this elongation is exaggerated. As was proposed in Chapter 4, hexagonal prisms of high aspect ratio can form when two twins form parallel to one another. The six sides have fast growing "A" type reentrant grooves, and slow growing "B" type convex faces. If one side face were to form the five-fold twined structure of a wire, the growth on this face would be halted. Such a particle would have accelerated growth on the remaining faces, and would thus form a hexagon shape elongated in one direction. This would also explain the 60° and 120° angles at the ends of the ribbon and the (1/3)[422] spots observed in the perpendicular to the main face. It is unclear where the two parallel twins

form first and the growth of the platelet is arrested in one direction, or if the five-fold symmetry from sequentially, with two of the five variants forming with two twin planes separating them instead of one. It is clear from the quenched silver wire samples that nuclei without twins can form the five-fold twin structure sequentially or by particle fusion. The shear number of hexagon platelets formed in this process makes it seem probable that the ribbons start out as platelets which later develop the five-fold twinning.

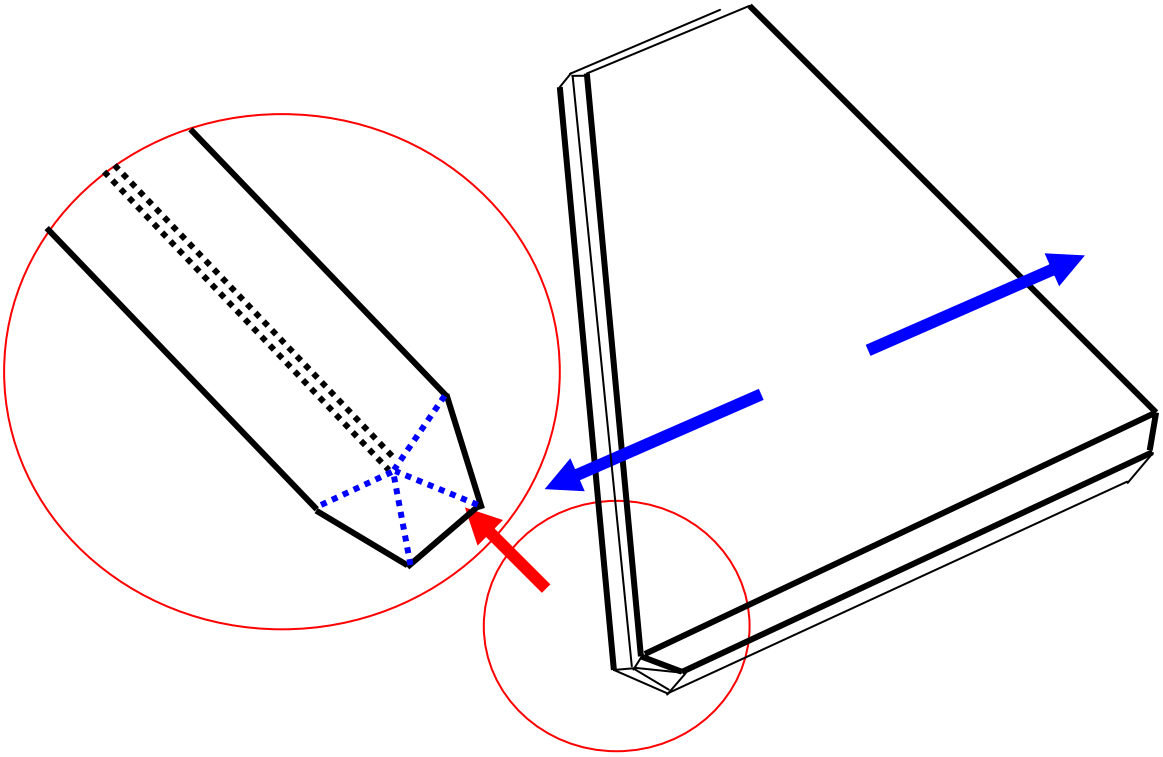

Figure 6-4: Proposed internal structure of gold ribbons. The black dashed lines indicate two parallel twin planes that generate the large faces of the ribbon. The four blue dashed lines are the four remaining twin planes that generate the five-fold symmetry. These block the growth of the parallel twins in this region and cause the elongation of the platelet in one direction.

Tetrahedra

Tetrahedra were observed in small quantities in highly faceted silver samples made by the polyol process. They were also observed in gold samples made by the polyol process and copper samples made in aqueous sugar solutions. These particles were

generally present in all samples, but in very low quantities. Figures 6-5, 6-6 and 6-7 show SEM images of these tetrahedra.

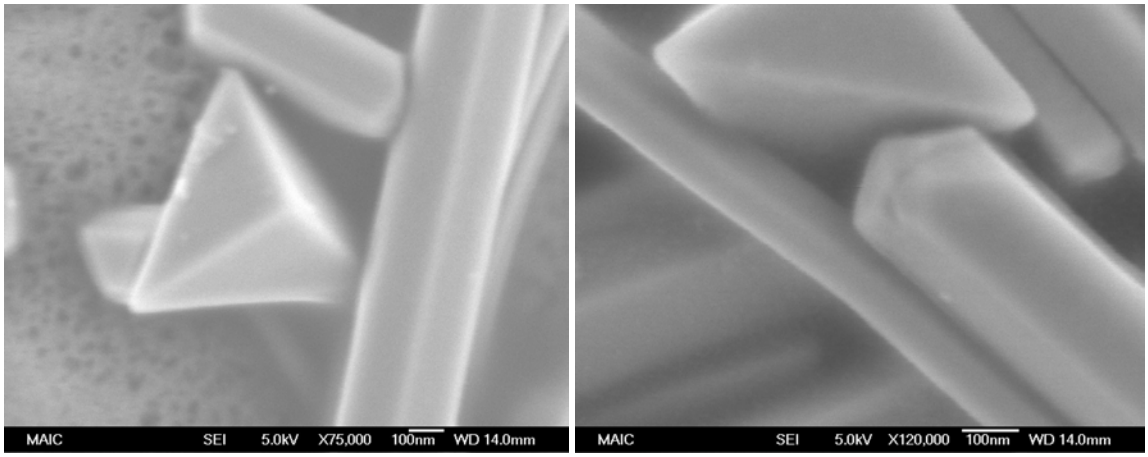

Figure 6-5: SEM images of silver tetrahedral amongst silver wires formed by the polyol process.

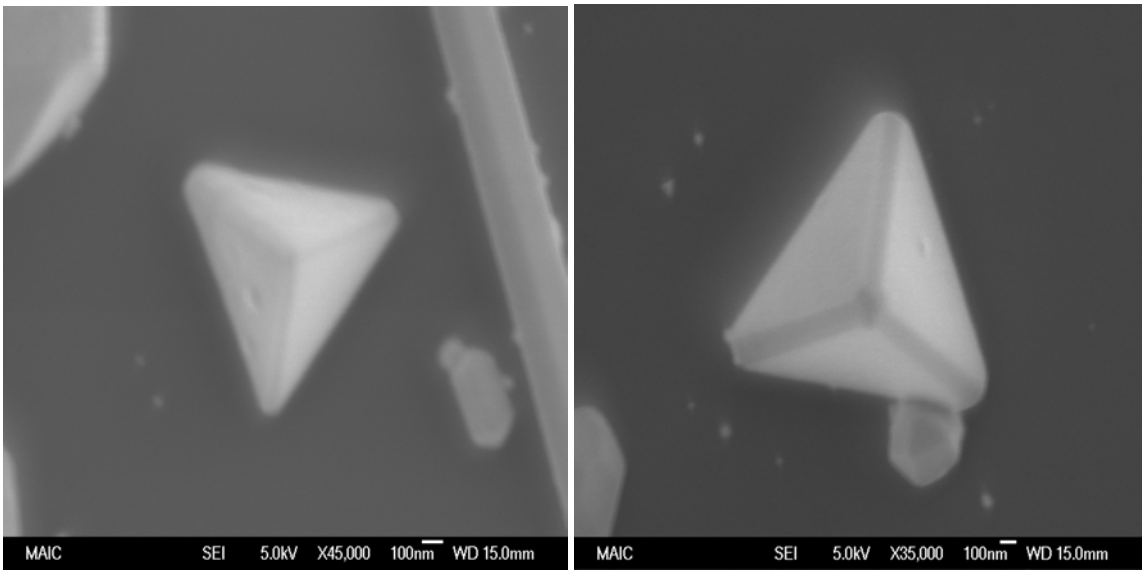

Figure 6-6: Gold tetrahedra formed by the polyol process with platelets, rods and isotropic particles.

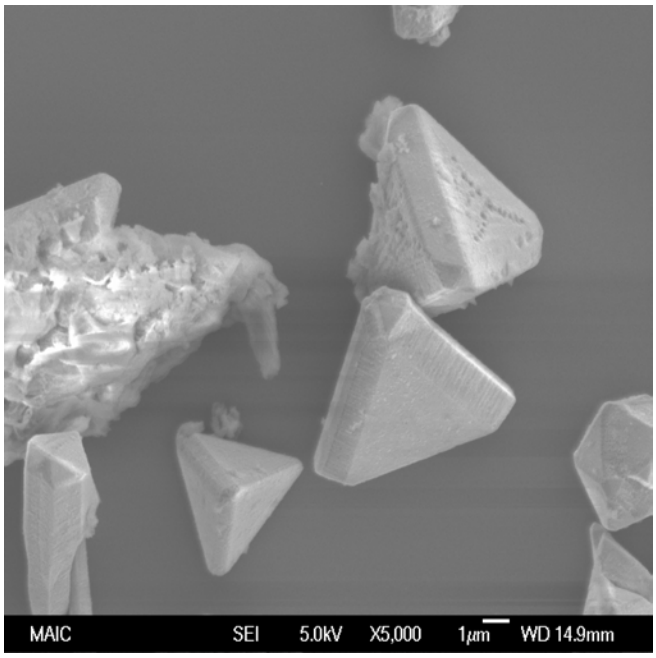

Figure 6-7: Copper tetrahedra made in an aqueous sugar solution along with rod, platelet and isotropic particles. Notice that one the edges of each tetrahedron is more blunt than the others.

Diffraction patterns could not be obtained for gold or copper tetrahedra due to their size. When tilted away from a tip, silver tetrahedra were found to have one observable twin plane parallel to one of the faces. A pattern obtained from a silver tetrahedra while looking down a twin plane is shown in Figure 6-8. This pattern is indexed as a [211] type pattern. This is direction is contained within a {111} plane.

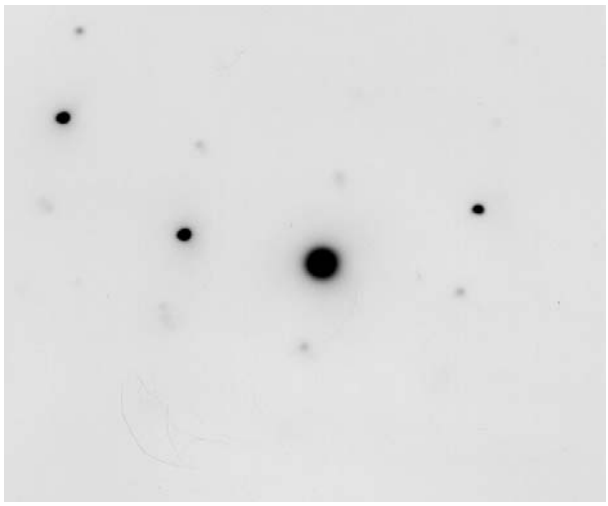

Figure 6-8: A [211] diffraction pattern from a silver tetrahedron taken parallel to a twin plane.

The shape and internal structure of the metal tetrahedra is consistent with that described for silver halide tetrahedra [26]. In the event of a twin plane forming in a FCC particle, the growth at the reentrant grooves causes the fast growing "A" type sides to grow themselves out, leaving only slow growing "B" type faces with {111} faces joined together in a convex fashion, 219° apart. The formation of a second twin plane on one of these faces forms a 70.5° angle with the first twin plane, creating a new reentrant groove. As seen in Figure 6-9, when the reentrant groove grows out, a tetrahedra has formed. One of the edges of the tetrahedra is more blunt that the other due to the intersection of the two twin planes. The final particle contains three crystal variants.

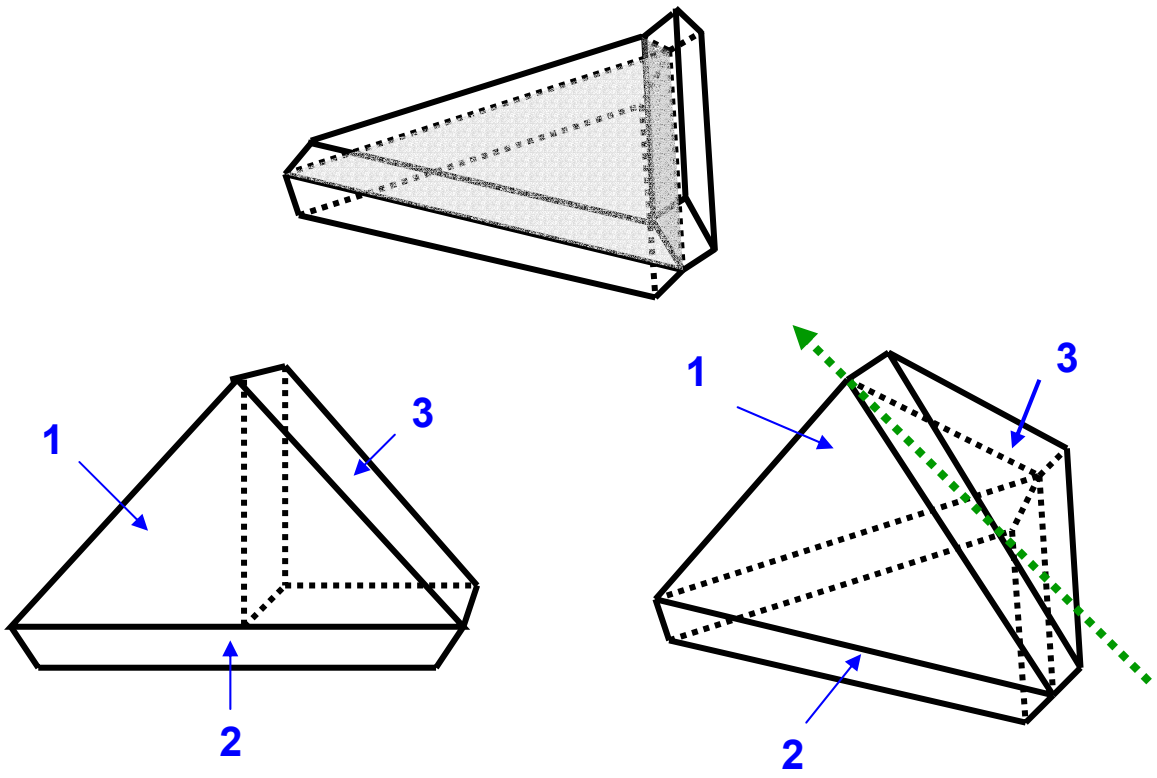

Figure 6-9: Proposed structure of tetrahedral silver crystals. At the top is a triangular prism in which a second twin plane (dark grey) has formed on a "B" type side, forming a 70.5° angle with the first (light grey). The final particle is shown in the bottom two pictures. Each of the three variants is identified in blue. Between each variant is a twin plane. On the left is a view perpendicular to the twin plane separating variant 1 and 2. On the right is another view showing the [211] direction observed parallel to the twin plane in the TEM investigation.

Submicron Size Decahedra

Decahedra are ten sided particles with five fold symmetry in one direction and two fold symmetry perpendicular to this direction. They were observed in small quantities in gold particles produced using the polyol process with gold chloride and PVP. These size decahedra were not observed in any other synthesis system. Several reports have described five-fold symmetric decahedron and icosahedron in nanosize gold clusters in experiment and in modeling [84-86]. In clusters of gold containing on the order of a few hundred atoms, the energetic importance of surface energy becomes important enough to

make multiply twinned particles the favored form. The decahedron and icosohedron shapes have all close-packed {111} faces the minimize surface tension, over coming bulk strain [87]. These shapes become unfavorable as the cluster size increases, and the largest gold decahedron previously reported was 13 nm in diameter [84].

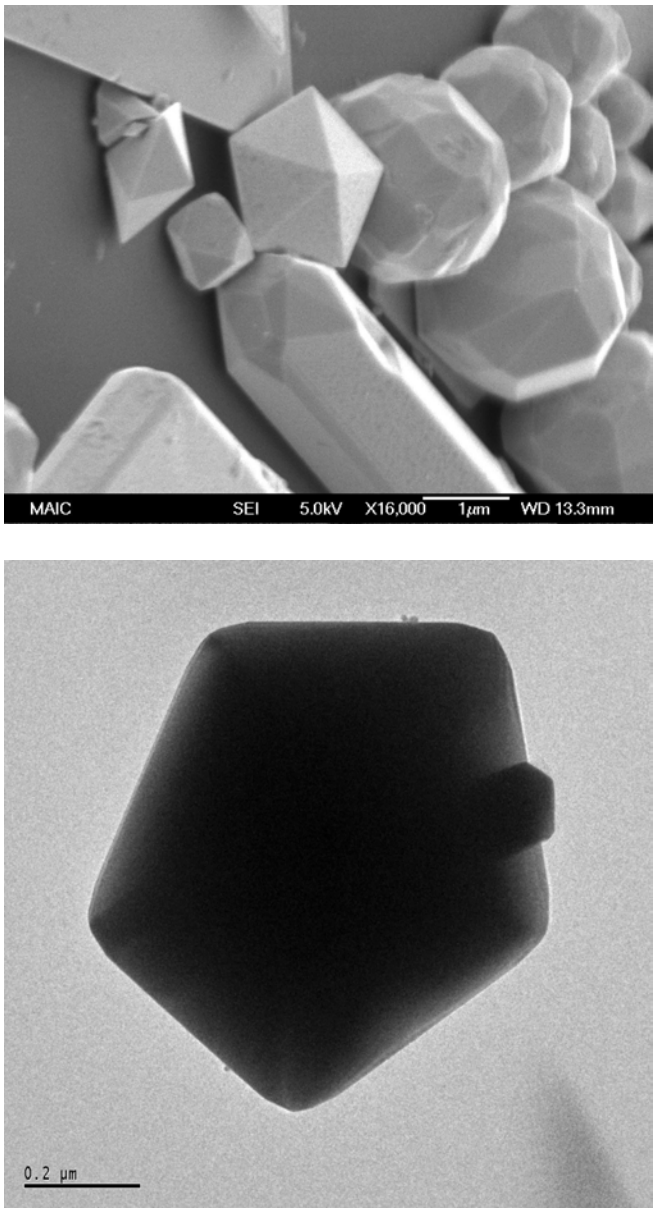

Figure 6-10: Images of gold decahedra produced through the polyol process. A) Shows two decahedra, one showing the five-fold symmetry, and the other, next to it, in a side view. B) A decahedra nearly parallel to the five-fold symmetry. Note the lower contrast of the middle of the edges where the crystal becomes thin. A small particle rests below the upper right corner.

The five-fold symmetry is not a normal shape because no five-fold symmetry exists in the FCC system, although the triangular facets suggest {111} faces. The structure can be described as five tetrahedra meeting along a line with one of their edges, and joined to two others by their triangular faces. In this event, the common edge between the tetrahedra would be a [110] direction. This is confirmed through diffraction in Figure 6-11, where a [110] pattern is obtained parallel to the five-fold axis.

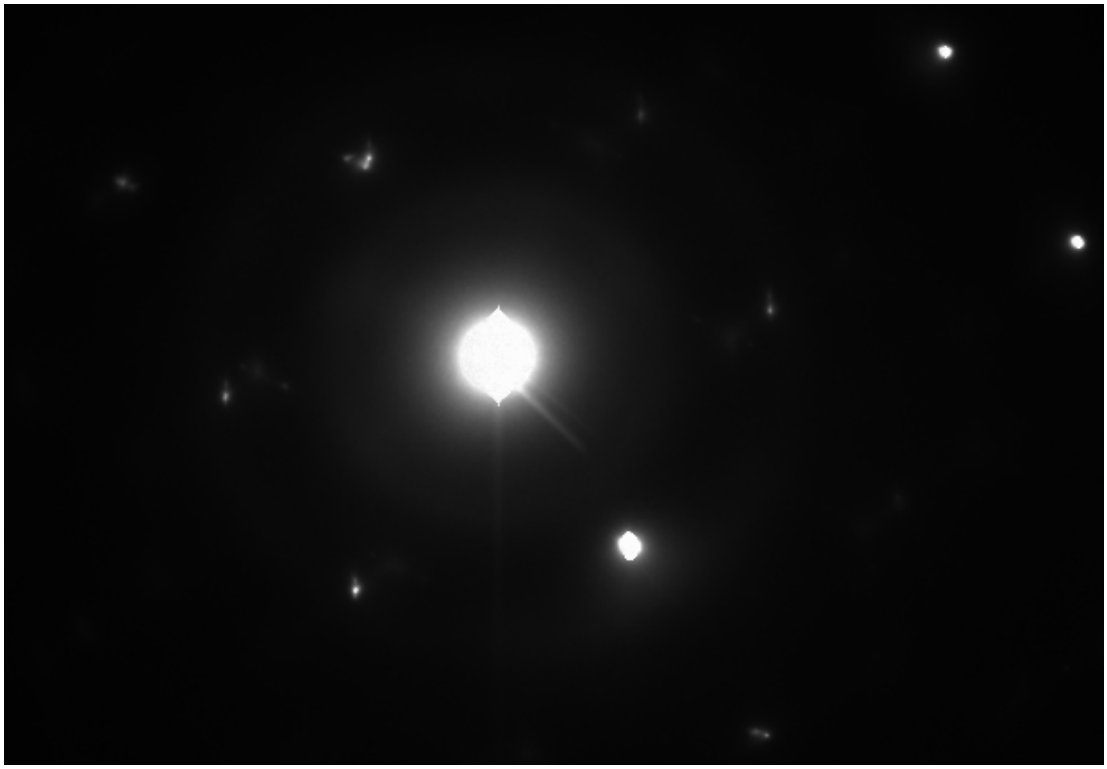

Figure 6-11: Diffraction pattern of a gold decahedra taken parallel to the five fold axis showing a [110] direction.

A tetrahedron formed by four {111} faces has an angle of 70.53^{o} between faces, while five-fold symmetry about a line requires $360^{o}/5 = 72^{o}$ for each section. Thus, the five tetrahedra could comprise a decahedron, but a strain of $\sim 7.4^{o}$ is necessary to close the gap between them. This structure is identical to that of the nanometer size nuclei observed in gold and silver systems, as well as metal wires and rods without elongation parallel to the

twin planes. Each twin plane is a equilateral triangle identical to a twinned prism where the fast growing "A" side have grown out. Thus, the edges between each variant are "B" sides which have formed from fast growing "A" sides that have grown themselves out. This means that the angle between each end face is 109.5°.

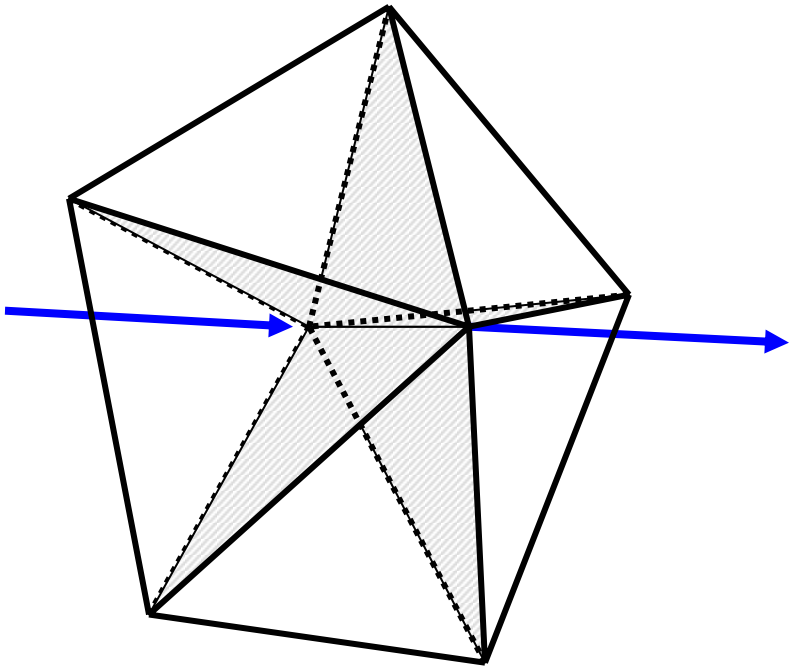

Figure 6-12: Diagram of a decahedral particle. The shaded regions indicate twin planes between each of the five variants. The blue line is the five-fold axis in the [110] direction. The edges where the twin planes intersect the surface are "B" type sides.

Figure 6-13 shows an undeveloped decahedron. The five {111} faces are visible with sharp edges between them. The tip of the particle is undeveloped and there are obtuse grooves at the outside edges of the particle where each variant meet another. The location of these undeveloped regions exactly corresponds to where the "A" sides of a twin plane would generate reentrant grooves. Thus this particle appears to have been arrested in a state where these "A" sides had not completely grown out.

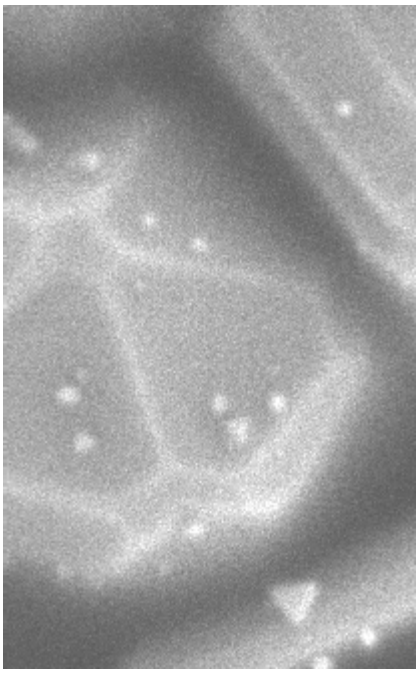

Figure 6-13: Magnified view of a decahedron in an undeveloped state. Notice the well developed edges between the five {111} faces and undeveloped tip and obtuse grooves at the outside edges where the variants meet.

It is unknown why these decahedra do not elongate as most of the gold rods in the solution with the same five-fold symmetry do. Nor is it clear if they were originally small decahedra that grew through the successive formation of edge dislocations, or if their twin planes formed sequentially. The fact that all the visible sides of the particle in Figure 6-13 are undeveloped indicates that all five variants are growing at the same time, and not sequentially. The existence of these decahedra in the same solution as gold rods also argues against the first possibility. The sequential formation of twins would imply that the strain is not shared equally between the variants, but that the last to form would adsorb the complete 7.4° strain. This could occur through the formation of some other type of twin interface, such as a (441) type twin plane, which would fill the remaining 7.4° with much less strain. On the other hand, the silver wires where able to form the five-fold twinning sequentially or through the fusion of smaller particles, so such a

mechanism may be possible for these large decahedron. Direct observation of the crystal lattice, however, was not possible with the size of the decahedra in the gold polyol samples. It is quite possible that some essential structural difference exists between decahedron and rods that was not observed and could explain why decahedron do not elongate and why they are observed less often than rods.

Wulff Shapes

Cubes were observed in significant quantities in samples of highly faceted silver made by the polyol process. In reference 49, Sun and Xia reported that their synthesis of silver wires could be converted to silver cubes by increasing the concentration of silver nitrate by a factor of 3 and reducing the ratio of silver to PVP from 1 to 6 to 1 to 1.5. Attempts to repeat these results proved unsuccessful, instead producing silver wires in high yield. Silver cubes only appeared as a minor product in silver wire synthesis.

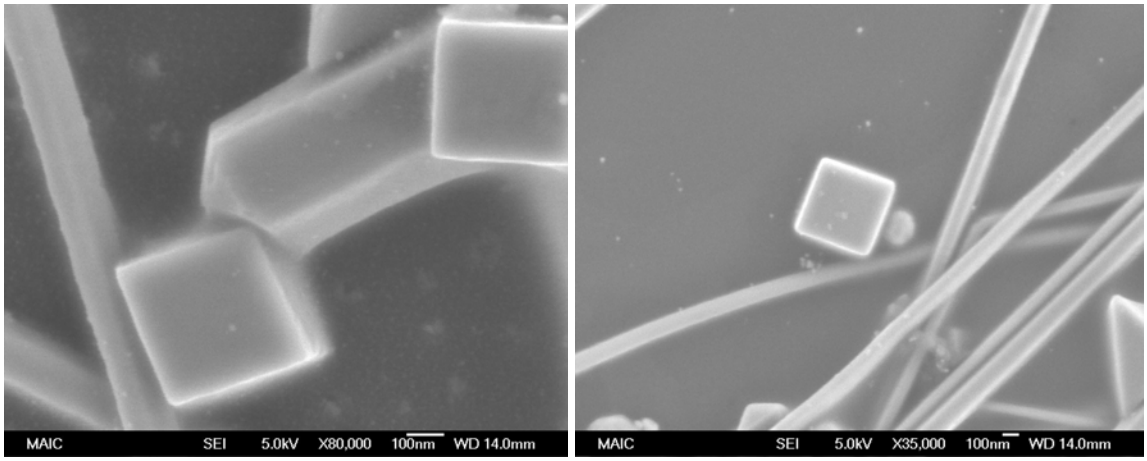

Figure 6-14: SEM images of silver cubes made as a minor product in silver wire polyol synthesis.

A cube is the favored shape of a FCC crystal when the {100} faces have dominance. In TEM analysis shown in Figure 6-15, these cubes were confirmed to have {100} faces. No twin planes were observed in any cubes. The presence of cubes in silver samples

likely indicates that the {100} face is a slow growing face which develops when fast growing faces that it bounds grow themselves out. This could indicate that without a structure breaking twin plane, the particles form a truncated octahedron containing {111} and {100} faces. The {111} faces grow faster and would disappear, leaving the {100} faces of a cube. The fact that cubes coexist with wires indicates of the mixture of nuclei that grow to form particles, some do not have twins. They are limited in size, however, because they do not have reentrant grooves.

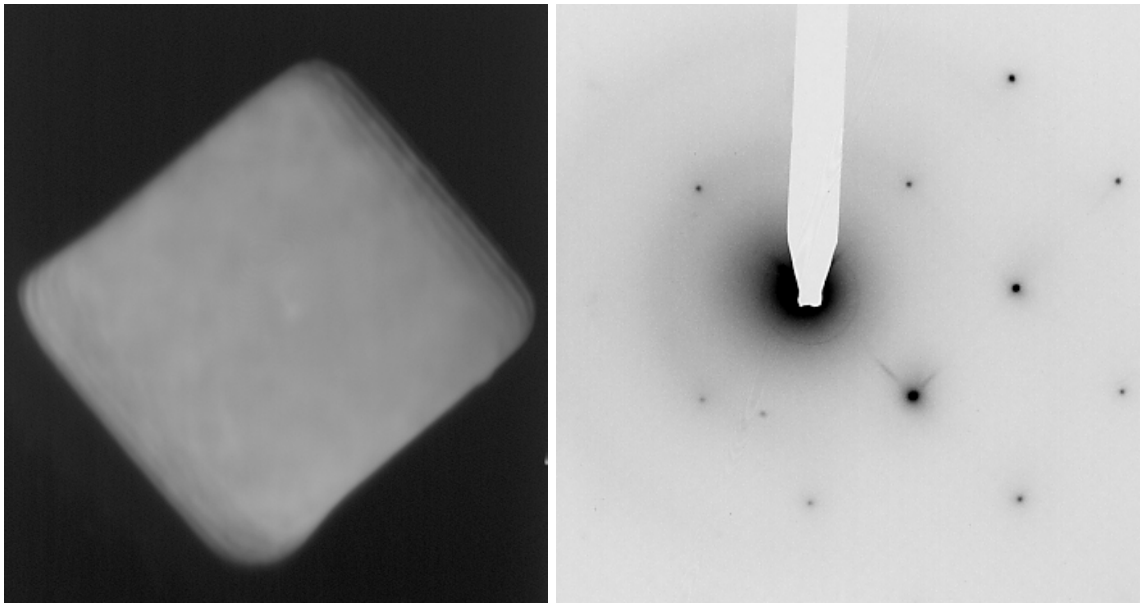

Figure 6-15: TEM of silver nanocubes. An image of a silver cube taken perpendicular to one of the faces, and the corresponding diffraction pattern, indexed as [100].

In addition to cubes, truncated octahedron and truncated rhombic dodecahedron were observed rarely in gold samples made by the polyol process. These Wulff shapes did not contain twins, and indicated that the natural form of single crystal noble metal particles is a simple, symmetric shape.

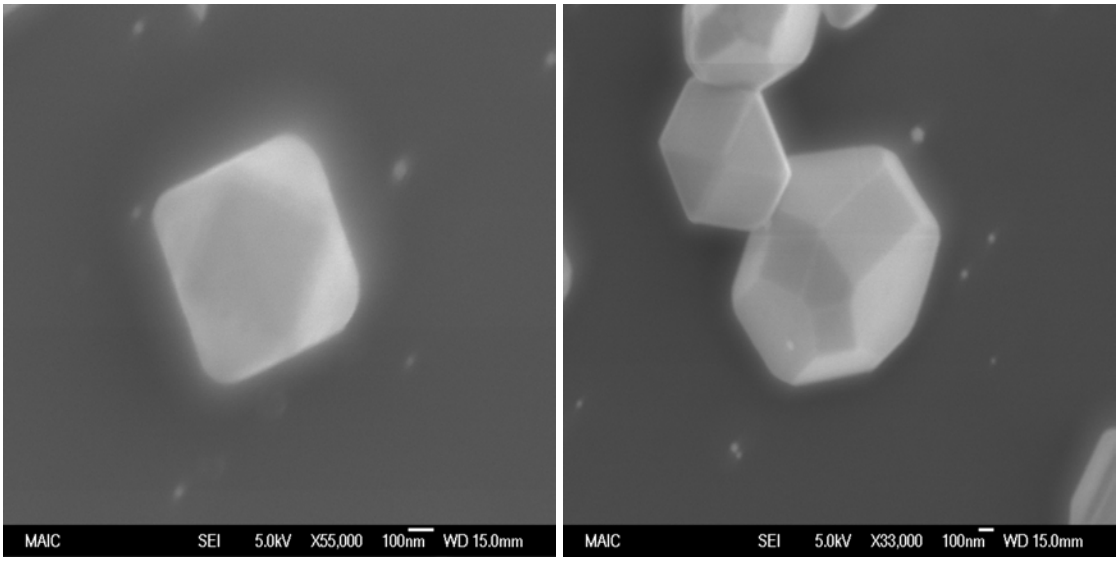

Figure 6-16: A truncated gold octahedron and a truncated gold rhombic dodecahedron made by the polyol process.

CHAPTER 7
CONCLUSIONS

The hypothesis of this dissertation stated that anisotropic particles of gold, silver and copper grown in solution were the result of the preferential attachment of adatoms to reentrant grooves formed by the (111) twin planes, and that the number and orientation of twin planes determines the final shape of the particle. In order to confirm this hypothesis, several methods of synthesizing colloids from literature, as well as modified and original techniques, were used to make samples of gold, silver and copper. These samples were analyzed using SEM and TEM to determine if their external habit and internal structure corresponded to that predicted by the growth theory. It can now be concluded that this hypothesis was partially correct. For two-dimensional prisms and platelets, as well as for tetrahedra, this mechanism is well supported by the data collected. The structure of untwined particles such as cubes, truncated octahedra and truncated rhombic dodecahedra also supports this conclusion. The structure of rod and wires, however, does not follow the expected structure, indicating that a mechanism other than reentrant grooves causes their anisotropy. The critical nature of twinning in breaking the symmetry of the FCC structure for all the particle shapes is apparent.

The formation of particles with symmetry lower than the FCC system requires some structure breaking factor during growth. In the formation of metal particles from the solution reduction of a metal salt, a mixture of different morphologies results even from a highly homogeneous reaction environment. Highly anisotropic particles such as wires or platelets form and grow concurrently with faceted isotropic particles. The

products from batch to batch are inconsistent even when great care is taken to repeat the synthesis conditions. Furthermore, identical morphologies appear from reactions in different chemical environments and with different surface active agents. The structure of the particles is largely independent of the type of synthesis procedure used. The current theories on the mechanism for anisotropic metal particle growth are inadequate to explain these observations. The similarities between the observed morphologies and those of silver halide crystals suggests that the growth mechanism that works for the silver halide system should also be applied to noble metal particles.

As predicted by the theory, untwined particles developed into Wulff shapes with symmetric forms and close-packed crystal faces with low Miller indices. Cubes were the most common untwined shape observed in silver systems, while truncated octahedral and truncated rhombic dodecahedra were observed in gold samples. The plate morphology, observed in all three metal systems and with all methods of synthesis, shows a consistent {111} main face with a triangular, hexagonal, or intermediate main face. This is consistent with one or more twin plane on a (111) plane parallel to the main faces. The orientation of the main face is confirmed with electron diffraction and the presence of the twin planes by the forbidden reflections in the diffraction pattern. When the twin planes intercept the edges of the platelet, reentrant grooves are generated on alternating sides around the platelet. These grooves can be observed under high magnification in a SEM. The reentrant groove is a channel formed by two {111} edge planes intersecting the twin plane, forming a atomic step like region where adatoms can receive extra stabilization by increasing the number of nearest neighbors, making dissolution of the adatom back into solution unlikely. The presence of a single twin plane causes alternating sides of the

hexagonal plane to have reentrant grooves. These sides with the grooves grow themselves out rapidly, forming a triangular prism or platelet. This type of platelet was observed for silver and copper systems. It the event of a second twin plane forming parallel to the first, the reentrant grooves of the second twin plane are on the non-grooved sides of the first twin plane, leading to each of the sides regenerating the others and preventing the reentrant grooves from growing out. This allows for the very highly aspect ratio gold platelets with their hexagonal shape. The fact that the gold platelets are of the high aspect ratio, double twinned variety, while the silver and copper particles appeared to contain only one twin plane is not understood. The shape and structure of tetrahedra also follows the hypothesis. The particles were found to contain two twin planes oriented 70.5° apart. Surface evidence of the site of twin plane intersections was also observed.

The structure of rods, wires, ribbons and decahedra did not follow the expected structure from silver halide particles. The evidence indicates that the expected three radial twins do not occur in one-dimensional metal particles. The wires and rods had five-fold symmetry when observed in the SEM instead of six side faces. The diffraction data also contradicted the expected results, instead showing consistent superimposed [100] and [211] type patterns when the particle were observed along a twin plane, and superimposed [110] and [111] zones when rotated approximately 18°. This data can be explained by the particles consisting of five crystal variants joined by five (111) twin planes. The five variants meet on a central axis along a [110] direction. Cross-sectional data also supports this proposed structure. Quenching of silver wires during nucleation and growth indicates that the wires do not originate as five-fold symmetric particles, but

instead begin as particles with one or two twin planes. The completion of the cross-section may occur by sequential twining, or by collision and fusion of particles. Once the five-fold symmetry is established, rapid growth takes place parallel to these twin planes. The arrangement of the twin planes indicates that reentrant grooves should not form, and thus the anisotropic growth must be explained with another mechanism. The angles required for the five (111) twin planes are not sufficient to close the circumference of the wire without a 7.5° strain. The strain caused by this effect may make addition of adatoms to the side faces of the rod less favorable, favoring axial growth. The strain may be relieved by edge dislocations which could potentially generate self-perpetuating steps on the end faces of the wires. This could be another mechanism for accelerated axial growth of the wires. The speculations are difficult to correlate with the existence of submicron size decahedra. These particles have the same internal structure as rods and wires, but have not elongated parallel to their twin planes. The existence of these particles in the same solution as rods cannot be explained.

Ribbon or tape shaped gold particles were observed from the polyol process. The main face of these particles was found to be {111} like that of gold platelets, however the main face of the ribbons was trapezoidal instead of hexagonal. The faceting at the ends of these particles resembled the five-fold twinning of rods and wires with one of the twin boundaries being elongated. From diffraction data and crystal habit, it was deduced that these particles had the five radial twin planes of rods, but with one variant being separated by two parallel twins. This provides the width of the ribbon, while the five-fold symmetry generates the length of the ribbon.

The data collected clearly demonstrates the validity of a new mechanistic explanation for the growth of noble metal colloids. The shape of metal particles is dictated by the number, orientation, and time of formation of twin planes during particle growth. Ideally, this work will contribute both to the understanding of metal particle structure and to creating robust and reproducible schemes for synthesizing high yields of shape selected colloids.

LIST OF REFERENCES

1. Nikhil R. Jana, Latha Gearheart and Catherine J. Murphy, "Wet Chemical Synthesis of Silver Nanorods and Nanowires of Controllable Aspect Ratio," Chemical Communications, 617-618 (2001)

2. Isabel Pastoriza-Santos and Luis M. Liz-Marzán, "Synthesis of Silver Nanoprisms in DMF," Nano Letters, Vol. 2, (2002)

3. P. Kamat, "Photophysical, Photochemical and Photocatalytic Aspects of Metal Nanoparticles," Journal of Physical Chemistry B, Vol. 106, 7729-7744 (2002)

4. P. Kamat, M. Flumiani and A. Dawson, "Metal-Metal and Metal-Semiconductor Composite Nanoclusters," Colloids and Surfaces A: Physicochemical and Engineering Aspects, Vol. 202, 269-279 (2002)

5. Younan Xia, Peidong Yang, Yugang Sun, Yiying Wu, Brian Mayers, Byron Gates, Yadong Yin, Franklin Kim and Haoquan Yan, "One-dimensional Nanostructures: Synthesis, Characterization, and Applications," Advanced Materials, Vol. 15, 353-389 (2003)

6. G. Wulff, Zeitschrift fur Kristalographie, Vol. 34, 449 (1901)

7. Z. L. Wang, M. B. Mohamed, S. Link and M. A. El-Sayed, "Crystallographic Facets and Shapes of Gold Nanorods of Different Aspect Ratios," Surface Science, Vol. 440, L809-L814 (1999)

8. S. Chen and D. Carroll, "Synthesis and Characterization of Truncated Triangular Silver Nanoplates," Nano Letters, Vol. 2, 1003-1007 (2002)

9. I. Lisiecki, A. Filankembo, H. Sack-Kongehl, K. Weiss, M.-P. Pileni and J. Urban, "Structural Investigations of Copper Nanorods by High-Resolution TEM," Physical Review B, Vol. 61, 4968-4974 (2000)

10. C. J. Johnson, Erik Dujardin, Sean A. Davis, Catherine J. Murphy and Stephen Mann, "Growth and Form of Gold Nanorods Prepared by Seed-Mediated Surfactant-Directed Synthesis," Journal of Materials Chemistry, Vol. 12, 1765-1770 (2002)

11. Franklin Kim, Jae Hee Song and Peidong Yang, "Photochemical Synthesis of Gold Nanorods," Journal of the American Chemical Society, Vol. 124, 14316-14317 (2002)

12. Yugang Sun and Younan Xia, "Large-Scale Synthesis of Uniform Silver Nanowires Through a Soft, Self-Seeding, Polyol Process," Advanced Materials, Vol. 14, 833-837 (2002)

13. Y. Sun, B. Mayers, T. Herricks and Y. Xia, "Polyol Synthesis of Uniform Silver Nanowires: A Plausible Growth Mechanism and the Supporting Evidence," Nano Letters, Vol. 3, 955-960 (2003)

14. U.S. Patent 6306736: "Processing for Forming Shaped Group III-V Semiconductor Nanocrystals, and Product Formed Using Process" (2001)

15. D. Evans and H. Wennerstrom, The Colloidal Domain, VCH Publishers, New York (1994)

16. A. Van Hook, Crystallization, Reinhold Publishing Corporation, New York (1961)

17. V. La Mer and R. Dinegar, "Theory, Production and Mechanism of Formation of Monodispered Hydrosols," Journal of the American Chemical Society, Vol. 72, 4847- (1950)

18. D. Kashchiev, Nucleation: Basic Theory With Applications, Butterworth Heinemann, Boston (2000)

19. N. Ming, "Defect Mechanisms of Crystal Growth and Their Kinetics," Journal of Crystal Growth, Vol. 128, 104-112 (1993)

20. N. Ming and H. Li, "Twin Lamella Mechanism of FCC Crystal Growth: The Monte-Carlo Simulation Approach," Journal of Crystal Growth, Vol. 115, 199-202 (1991)

21. N. Ming and I. Sunagawa, "Twin Lamella as Possible Self-Perpetuating Step Sources," Journal of Crystal Growth, Vol. 87, 13-17 (1988)

22. R. W. Berriman and R. H. Herz, "Twinning and the Tabular Growth of Silver Bromide Crystals," Nature, Vol. 180, 293-294 (1957)

23. J. F. Hamilton and L. E. Brady, "Twinning and Growth of Silver Bromide Microcrystals," Journal of Applied Physics, Vol. 35, 414-421 (1964)

24. D. R. Hamilton and R. G. Seidensticker, "Propagation Mechanism of Germanium Dendrites," Journal of Applied Physics, Vol. 31, 1165-1168 (1960)

25. C. Goessens, D. Schryvers, J. Van Landuyt, A. Millan and R. De Keyzer, "Electron Microscopical Investigation of AgBr Needle Crystals," Journal of Crystal Growth, Vol. 151, 335-341 (1995)

26. C. Goessens, D. Schryvers, J. Van Landuyt and R. De Keyzer, "Electron Microscopical Investigation of Tetrahedral-Shaped AgBr Microcrystals," Journal of Crystal Growth, Vol. 172, 426-432 (1997)

27. G. Goessens, D. Schryvers and J. Van Landuyt, "Transmission Electron Microscopy Studies of (111) Twinned Silver Halide Microcrystals," Microscopy Research and Technique, Vol. 42, 85-99 (1998)

28. C. Goessens, D. Schryvers, J, Van Landuyt, S. Amelinckx, A. Verceeck and R. De. Keyzer, "Characterization of Crystal Defects in Mixed Tabular Silver Halide Grains by Conventional Transmission Electron Microscopy and X-Ray Diffractometry," Journal of Crystal Growth, Vol. 110, 930-941 (1991)

29. G. Bögels, H. Meekes, P. Bennema and D. Bollen, "The Role of {100} Side Faces for Lateral Growth of Tabular Silver Bromide Crystals," Journal of Crystal Growth, Vol. 191, 446-454 (1998)

30. R. Zsigmondy, Zeitschrift fur Physik, Vol. 56, 65 (1906)

31. D. Beischer and F. Krause, Naturwissenschaften, Vol. 25, 825 (1937)

32. J. Turkevich, P. C. Stevenson and J. Hillier, "A Study of the Nucleation and Growth Processes in the Synthesis of Colloidal Gold," Discussions of the Faraday Society, Vol. 11, 55 (1951)

33. W. O. Milligan and R. H. Morriss, "Morphology of Colloidal Gold – A Comparative Study," Journal of the American Chemical Society, Vol. 86, 3461 (1964)

34. Y. Zhou, C. Y. Wang, Y.R. Zhu, and Z. Y. Chen, "A Novel Ultraviolet Irradiation Technique for Shape-Controlled Synthesis of Gold Nanoparticles at Room Temperature," Chemistry of Materials, Vol 11, 2310-2312 (1999)

35. N. Malikova, I. Pastoriza-Santos, M. Schierhorn, M. Kotov and L. Liz-Marzán, "Layer-by-Layer Assembled Mixed Spherical and Planar Gold Nanoparticles: Control of Interparticle Interactions," Langmuir, Vol. 18, 3694-3697 (2002)

36. J. S. Bradley, B. Tesche, W. Busser, M. Maase, and M. T. Reetz, "Surface Spectroscopic Study of the Stabilization Mechanism for Shape-Selectively Synthesized Nanostructured Transition Metal Colloids," Journal of the American Chemical Society, Vol. 122, 4631-4636 (2000)

37. Barbara Brüche, "Über sehr dünne Goldeinkristall-Plättchen," Kolloid-Zeitschrift, Vol. 170, 97-104 (1960)

38. Andrew C. Curtis, Daniel G. Duff, Peter P. Edwards, David A. Jefferson, Brian F. G. Johnson, Angus I. Kirkland and Andrew S. Wallace, "A Morphology-Selective Copper Organosol," Angewandte Chemie International Edition, Vol. 27, 1530-1533 (1988)

39. A. I. Kirkland, D. A. Jefferson, D. G. Duff, P. P. Edwards, I. Gameson, B. F. G. Johnson and D. J. Smith, "Structural Studies of Trigonal Lamellar Particles of Gold and Silver," Proceedings of the Royal Society of London A, Vol. 440, 589-609 (1993)

40. R. Jin, Y. W. Cao, C. A. Mirkin, K. L. Kelly, G. C. Schatz and J. G. Zhung, "Photoinduced Conversion of Silver Nanospheres to Nanoprisms," Science, Vol. 294, 1901-1903 (2001)

41. K. Kimoto and Isao Nishida, "An Electron Microscope and Electron Diffraction Study of Fine Smoke Particles Prepared by Evaporation in Argon Gas at Low Pressures (II)," Japanese Journal of Applied Physics, Vol. 6, 1047-1059 (1967)

42. T. Hayashi, I. Ohno, S. Yatsuya, R. Uyeda, "Formation of Ultrafine Metal Particles by Gas-Evaporation Technique. IV. Crystal Habits of Iron and FCC Metals, Al, Co, Ni, Cu, Pd, Ag, In, Au and Pb," Japanese Journal of Applied Physics, Vol. 16, 705-717 (1977)

43. Takanori Tomita, "A Concept for the Growth of Twinned Crystals of FCC Structure," Journal of Crystal Growth, Vol. 24/25, 331-333 (1974)

44. G. Dieter, Mechanical Metallurgy, McGraw Hill, New York (1986)

45. C. Ducamp-Sanguesa, R. Herrera-Urbina, and M. Figlarz, "Synthesis and Characterization of Fine and Monodisperse Silver Particles of Uniform Shape," Journal of Solid State Chemistry, Vol. 100, 272-280 (1992)

46. Yugang Sun, Byron Gates, Brian Mayers, and Younan Xia, "Crystalline Silver Nanowires by Soft Solution Processing," Nano Letters, Vol. 2, 165-168 (2002)

47. Yugang Sun, Yadong Yin, Byron T. Mayers, Thurston Herricks and Younan Xia, "Uniform Silver Nanowires Synthesis by Reducing AgNO3 with Ethylene Glycol in the Presence of Seeds and Poly(Vinyl Pyrrolidone)," Chemistry of Materials, (2002)

48. Y. Yin, Y. Lu, Y. Sun and Y. Xia, "Silver Nanowires Can Be Directly Coated With Amorphous Silica To Generate Well-Controlled Coaxial Nanocables of Silver/Silica," Nano Letters, Vol. 2, 427-430 (2002)

49. Y. Sun and Y. Xia, "Shape-Controlled Synthesis of Gold and Silver Nanoparticles," Science, Vol. 298, 2176-2179 (2002)

50. Isabel Pastoriza-Santos and Luis M. Liz-Marzán, "Formation of PVP-Protected Metal Nanoparticles in DMF," Langmuir, Vol. 18, 2888-2894 (2002)

51. Zongtao Zhang, Bin Zhao, and Liming Hu, "PVP Protective Mechanism of Ultrafine Silver Powder Synthesized by Chemical Reduction Processes," Journal of Solid State Chemistry, Vol. 121, 105-110 (1996)

52. H. Huang, X. Ni, G. Loy, C. Chew, K. Tan, F. Loh, J. Deng and G. Xu, "Photochemical Formation of Silver Nanoparticles in Poly(N-vinylpyrrolidone)," Langmuir, Vol. 12, 909-912 (1996)

53. Brantely D. Busbee, Sherine O. Obare and Catherine J. Murphy, "An Improved Synthesis of High-Aspect-Ratio Gold Nanorods," Advance Materials, Vol. 15, 414-416 (2003)

54. N. Jana, L. Gearheart, S. Obare, C. Johnson, K. Elder, S. Mann and C. Murphy, "Liquid Crystalline Assemblies of Ordered Gold Nanorods," Journal of Materials Chemistry, Vol. 12, 2909-2912 (2002)

55. C. Murphy and N. Jana, "Controlling the Aspect Ratio of Inorganic Nanorods and Nanowires," Advanced Materials, Vol. 14, 80-82 (2002)

56. N. Jana, L. Gearheart and C. Murphy, "Wet Chemical Synthesis of High Aspect Ratio Cylindrical Gold Nanorods," The Journal of Physical Chemistry B, Vol. 105, 4065-4067 (2001)

57. N. Jana, L. Gearheart and C. Murphy, "Seed-Mediated Growth Approach for Shape-Controlled Synthesis of Spheroidal and Rod-like Gold Nanoparticles Using a Surfactant Template," Advanced Materials, Vol. 13, 1389-1393 (2001)

58. B. Nikoobakht and M. El-Sayed, "Preparation and Growth Mechanism of Gold Nanorods (NRs) Using Seed-Mediated Growth Method," Chemistry of Materials, Vol. 15, 1957-1962 (2003)

59. H. Yao, T. Onishi, S. Sato and K. Kimura, "High Aspect Ratio Gold Nanorods Grown Normal to High-Energy Surfaces," Chemistry Letters, Vol. 4, 458-459 (2002)

60. Babak Nikoobakht and Mostafa A. El-Sayed, "Evidence for Bilayer Assembly of Cationic Surfactants on the Surface of Gold Nanorods," Langmuir, Vol. 17, 6368-6374 (2001)

61. S. Chang, C. Shih, C. Chen, W. Lai and C. Wang, "The Shape Transition of Gold Nanorods," Langmuir, Vol. 15, 701-709 (1999)

62. Y. Yu, S. Chang, C. Lee and C. Wang, "Gold Nanorods: Electrochemical Synthesis and Optical Properties," The Journal of Physical Chemistry B, Vol. 101, 6661-6664 (1997)

63. K. Caswell, C. Bender, and C. Murphy, "Seedless, Surfactantless Wet Chemical Synthesis of Silver Nanowires," Nano Letters, Vol. 3, 667-669 (2003)

64. A. Filankembo and M. P. Pileni, "Shape Control of Copper Nanocrystals," Applied Surface Science, Vol. 164, 260-267 (2000)

65. J. Tanori and M. P. Pileni, "Control of the Shape of Copper Metallic Particles by Using a Colloidal System as Template," Langmuir, Vol. 13, 639-646 (1997)

66. M. P. Pileni, T. Gulik-Krzywicki, J. Tanori, A. Filankembo and J. C. Dedieu, "Template Design of Microreactors with Colloidal Assemblies: Control the Growth of Copper Metal Rods," Langmuir, Vol. 14, 7359-7363 (1998)

67. I. Lisiecki, F. Billoudet and M. P. Pileni, "Control of the Shape and the Size of Copper Metallic Particles," Journal of Physical Chemistry, Vol. 100, 4160-4166 (1996)

68. Z. Liu and Y. Bando, "A Novel Method for Preparing Copper Nanorods and Nanowires," Advanced Materials, Vol. 15, 303-305 (2003)

69. M. Y. Yen, C. W. Chiu, C. H. Hsia, F. R. Chen, J. J. Kai, C.Y. Lee and H. T.Chiu, "Synthesis of Cable-Like Copper Nanowires," Advanced Materials, Vol. 15, 235-237 (2003)

70. Z. L. Wang, "Transmission Electron Microscopy of Shape-Controlled Nanocrystals and Their Assemblies," Journal of Physical Chemistry B, Vol. 104, 1153-1175 (2000)

71. Pratibha L. Gai and Mark A. Harmer, "Surface Atomic Defect Structures and Growth of Gold Nanorods," Nano Letters, Vol. 2, 771-774 (2002)

72. Chen-Li Chiang "Controlled Growth of Gold Nanoparticles in Aerosol-OT/Sorbitan Monooleate/Isooctane Mixed Reverse Micelles," Journal of Colloid and Interface Science, Vol. 230, 60-66 (2000)

73. Y. Sun, B. Mayers, Y. Xia, "Transformation of Silver Nanospheres Into Nanobelts and Triangular Nanoplates Through a Thermal Process," Nano Letters, Vol. 3, 675-679 (2003)

74. J. M. Tarascon, F. J. DiSalvo, C. H. Chen, P.J. Carrol, M. Walsh, L. Rupp, "1st Example of Monodispered (Mo3Se3) Infinity-1 Clusters," Journal of Solid State Chemistry, Vol. 58, 290 (1985)

75. J. H. Golden, F. J. DiSalvo, J. M. J. Fréchet, J. Silcox, M. Thomas, J. Elman, "Subnanometer-Diameter Wires Isolated in a Polymer Matrix by Fast Polymerization," Science, Vol. 273, 782 (1996)

76. J. H. Golden, H. Deng, F. J. DiSalvo, J. M. J. Fréchet, P. M. Thompson, "Monodisperse Metal-Clusters 10-Angstroms in Diameter in Polymeric Host – The Monomer-as-Solvent Approach," Science, Vol. 268, 1463 (1995)

77. A. A. Kudryavtsev, The Chemistry and Technology of Selenium and Tellurium, Collet's, London (1974).

78. B. Gates, Y. Yin and Y. Xia, "A Solution-Phase Approach to the Synthesis of Uniform Nanowires of Crystalline Selenium with Lateral Dimensions in the Range of 10-30 nm," Journal of the American Chemical Society, Vol. 122, 12582-12583 (2000)

79. Z. Peng and X. Peng, "Mechanisms of the Shape Evolution of CdSe Nanocrystals," Journal of the American Chemical Society, Vol. 123, 1389-1395 (2001)

80. U.S. Patent 6306736: "Processing for Forming Shaped Group III-V Semiconductor Nanocrystals, and Product Formed Using Process" (2001)

81. V. Puntes, K. Krishnan, A. Alivisatos, "Colloidal Nanocrystal Shape and Size Control: The Case of Cobalt," Science, Vol. 291, 2115-2117 (2001)

82. G. Bögels, J. G. Buijsters, S. A. C. Verhaegen, H. Meekes, P. Bennema and D. Bollens, "Morphology and Growth Mechanism of Multiply Twinned AgBr and AgCl needle crystals," Journal of Crystal Growth, Vol. 203, 554-563 (1999)

83. C. Cleveland, U. Landman, T. Schaaff, M. Shafigullin, P. Stephens, R. Whetten, "Structural Evolution of Smaller Gold Nanocrystals: The Truncated Decahedral Motif," Physics Review Letters, Vol. 79, 1893 (1997)

84. K. Yagi, K. Takayanagi, K Kobayashi and G. Honjo, "In-Situ Observations of Growth Processes of Multiply Twinned Particles," Journal of Crystal Growth, Vol. 28, 117-124 (1975)

85. C. Granqvist and R. Buhrman, "Ultrafine Metal Particles," Journal of Applied Physics, Vol. 47, 2200-2219 (1976)

86. C. Mottet, G. Tréglia, B. Legrand, "New Magic Numbers in Metallic Clusters: An Unexpected Metal Dependence," Surface Science Letters, Vol. 383, L719-L727 (1997)

87. C. Cleveland, U. Landman, T. Schaaff, M. Shafigullin, P. Stephens and R. Whetten, "Structural Evolution of Smaller Gold Nanocrystals: The Truncated Decahedral Motif," Physical Review Letters, Vol. 79, 1873-1876 (1997)

88. A. Millan, P. Bennema, A. Verbeeck, D. Bollen, "Morphology of Silver Bromide Crystals from KBr-AgBr-DMSO-Water Systems," Journal of Crystal Growth, Vol. 192, 215-224 (1998)

BIOGRAPHICAL SKETCH

Charles Martin Lofton III was born in Pittsburgh, Pennsylvania, in 1976. He earned his Bachelor of Science in ceramic engineering from the University of Missouri-Rolla in 1998 and his Master of Science in materials science and engineering from the University of Florida in 2001.